TRANSIENT AND STEADY STATE PHOTOCONDUCTIVITY OF HYDROGENATED AMORPHOUS $Si_{1-x}Ge_x$ FILMS

by

V. Herak

A thesis
presented to the University of Manitoba
in partial fulfillment of the
requirements for the degree of
Master of Science
in
Electrical Engineering

Winnipeg, Manitoba, 1982

June 1982

TRANSIENT AND STEADY STATE PHOTOCONDUCTIVITY OF HYDROGENATED AMORPHOUS $SI_{1-x}GE_x$ FILMS

BY

THEODORE VICTOR HERAK

A thesis submitted to the Faculty of Graduate Studies of the University of Manitoba in partial fulfillment of the requirements of the degree of

MASTER OF SCIENCE

I hereby declare that I am the sole author of this thesis.

I authorize the University of Manitoba to lend this thesis to other institutions or individuals for the purpose of scholarly research.

V. Herak

I further authorize the University of Manitoba to reproduce this thesis by photocopying or by other means, in total or in part, at the request of other institutions or individuals for the purpose of scholarly research.

V. Herak

ABSTRACT

Steady state and transient photocurrents in radio frequency sputter deposited hydrogenated amorphous $Si_{1-x}Ge_x$ films, have been measured as functions of applied bias and light intensity for red and infrared light excitation. The transient photocurrent consists of fast and slow sections, due to trapping effects. Experimental results support a model for the distribution of the density of states similiar to the distribution given in the modified Davis and Mott model.

ACKNOWLEDGEMENTS

The author wishes to thank Professor K.C. Kao for his supervision in this research. Thanks also, to L. Chow and S. Mejia. Special thanks to D. Buchanan for help with the manuscript.

CONTENTS

List of Symbols

A	defined as $\sigma_{ph}(x)/\sigma_0$ cf Eqn. 5.23
A'	radiation recombination probability
B	constant cf Eqn. 2.7
C	capacitance, centigrade
C'	constant cf Eqn. 2.1
d	thickness
d_e	thickness of electrode
D	diffusion coefficient
D_n	diffusion coefficient for electrons
D^+, D^-	positively charged defect, negatively charged defect
e	electronic charge
E	energy level
E_c, E_v	conduction band edge, valence band edge
E_{dn}, E_{dp}	electron demarcation level, hole demarcation level
E_g	bandgap energy
E_t	energy of a trap level
E_{te}	effective trap depth

E_p	mobility activation energy
E_{p1}, E_{p2}, E_{p3}	mobility activation energy at different temperature regions
E_x	defined in Fig. 6.5
E_A	activation energy of photoconductivity
E_F	Fermi level
E_{Fn}	quasi-Fermi level for electrons
E_L	energy level of lowest localized state
E_M	midgap energy level cf Fig. 5.4
E_P, E_Q, $N_1(E)$, $N_2(E)$	parameters defined in Fig. 5.4
f	frequency
f_e	Fermi factor
F	electric field
F_e	probability for carrier injection into an insulator from a metal contact over a barrier
g	generation rate of electrons from traps
g_{op}	volume-photogenerated rate of carriers
G_{ph}	photoconductance

G_I	total conductance
G_0	thermal equilibrium conductance
h, hf	Planck's constant, photon energy
h_t	incident photon flux (incident light intensity)
I	incident photon flux (incident light intensity)
I_0	pre-exponential factor, $I(x) = I_0 \exp(-\alpha x)$
j	total current
j_0	photoinjected current at a metal-semiconductor interface
j_D	diffusion current
j_F	conduction current
J_{ph}	photocurrent
k	Boltzmann's constant
K	degrees Kelvin
K'	constant cf Eqn. 5.34
K''	constant cf Eqn. 6.7
ℓ	length
ℓ_e	debye or screening length
$\bar{\ell}$	mean free path

m_n^*	effective electron mass
m_0	rest electron mass
n	electron concentration
n'	constant defined by $J_{ph} \propto F^{n'}$
n_0	thermal equilibrium electron concentration
n_r	density of occupied recombination centers (density of trapped electrons in recombination centers)
n_t	density of occupied trapping centers (density of trapped electrons in trapping centers)
n_1	reduced density of states cf Eqn. 5.29
N_d	density of defect states
N_r	density of recombination centers
N_{rc}	density of charged recombination centers
N_c	effective density of states in the conduction band
$N_m(E)$	density of states about the midgap cf Fig. 5.4
N_t	density of trapping centers
N_A, N_B	defined in Fig. 5.4
N_D	density of donors

N_D^+	density of ionized donors
N(E)	distribution of the density of states
p_r	density of unoccupied recombination centers
P_{el}	electroluminescence quantum efficiency
P_{pl}	photoluminescence quantum efficiency
P_{pl0}	photoluminescence quantum efficiency at absolute zero temperature
r	resistance
R	reflectivity
$R_{r,d}$	ratio of the fast portion to total current in the transient photocurrent response. r denotes the rising edge and d denotes the decay. cf Fig. 4.2
R_0	critical distance for separation between photogenerated electron and hole
R_A	separation distance between photogenerated electron and hole
R_{DD}	ratio of drift to diffusion current
s	area
S_h	capture cross section of an occupied center for a hole
S_n	capture cross section of an unoccupied center for an electron

t	time
t_A, t_B, t_{ss}, t_∞(ie. $t \to \infty$)	specific instants in time with respect to the photoresponse cf Eqn. 5.5
$\bar{t}$	mean time between collisions
T	temperature
T_A	annealing temperature
T_s	substrate temperature
T_1	characteristic temperature cf Eqn. 5.41
W	bonding energy of an electron-hole pair
x	space coordinate
α	absorption coefficient
α_e	absorption coefficient of metallic electrode
β	quantum efficiency
Δn	excess electron concentration
Δn_0	pre-exponential factor cf Eqn. 5.10
Δn_x	excess electron concentration as a function of x cf Eqn. 5.10
ε	permittivity
ε_0	permittivity of free space

ε_r	relative permittivity
η	photoconduction quantum efficiency
θ, θ_m	carrier relaxation time constants cf Eqns. 5.6 and 5.7
λ	wavelength
μ	carrier mobility
μ_d	carrier drift mobility
μ_{d0}	pre-exponential factor cf Eqn. 2.8
μ_n	electron mobility
μ_0	electron mobility at E_c
ν	constant cf Eqn. 2.1
ρ	space charge density
σ	conductivity
σ_0	thermal equilibrium conductivity
σ_{ph}	photoconductivity
σ_{ph0}	pre-exponential factor cf Eqn. 2.6
τ	carrier lifetime
τ_a	lifetime associated with a temperatue activated non-radiative process cf Eqn. 2.10

τ_n free electron lifetime

$\tau_{r,d}$ response times of the transient photocurrent response. r denotes the rising edge and d denotes the decay cf Fig. 4.2

τ_t lifetime associated with a temperature independent non-radiative process. cf Eqn. 2.11

τ_R radiative lifetime

τ_1 pre-exponential factor, $\tau_a = \tau_1 \exp(\Delta E/kT)$

υ thermal velocity

Φ_B potential barrier at a metal-semiconductor interface

ω' recombination probability

Chapter I

INTRODUCTION

Increasingly over the past few years, attention has been turned to the understanding of the properties of the amorphous state. Motivation for research in this direction is the fabrication of amorphous as compared to crystalline material, with the hope that amorphous material may be used for device applications such as, for example, solar cells and amorphous thin film transistors, etc.. The translational and, in the case of compounds, compositional disorder in amorphous semiconductors introduce large densities of states within the bandgap. These states can dramatically affect the optical and electronic properties of these semiconductors. Many techniques have been used to study various materials including optical absorption, photoemission, luminescence, space-charge-limited-currents, temperature stimulated currents, and others.

The study of photoconductivity is a promising approach towards a closer understanding of recombination processes in solids. However, the interpretation of the results requires a knowledge of the distribution of localized states in the mobility gap if we are dealing with an amorphous semiconductor. Much theoretical work has gone into finding an appro-

priate model for the distribution of localized states, especially for amorphous Silicon and Germanium. Various models for amorphous semiconductors have been proposed, such as the Cohen, Fritzsche, Ovshinsky (CFO) model, Davis and Mott model, Mott model and the Marshall and Owen model. All these models make use of the idea of a mobility gap and tails of localized states in the bands.

Regarding hydrogenated amorphous Si-Ge alloys, results on optical and optoelectronic properties of glow-discharge produced films [1] and of sputtered films [2], have been reported. In this thesis, we shall report our investigation into transient and steady state photoconductivities of hydrogenated amorphous $Si_{1-x}Ge_x$ alloys prepared by sputtering techniques. Features of the photocurrent such as the magnitude, response time, and general waveshape have been measured as functions of incident photon flux (red and infrared light excitation), and applied electric field for various compositions. Results are interpreted in terms of a distribution of states similiar to the distribution of states in the modified Davis and Mott model.

Chapter II

OPTOELECTRONIC PROPERTIES OF A-SI, A-GE, AND A-SI-GE FILMS

In this chapter we shall review some of the optoelectronic properties of amorphous Silicon, Germanium, and Silicon/Germanium alloys. Almost all the discussion is in regard to a-Si since the literature available on a-Ge and a-Si-Ge alloys is minimal due to the, generally, poor photoresponse of a-Ge.

In the case of a-Si, most of the emphasis is on photoconductivity, however, luminescensce and photoemission are also discussed. The effects of doping on photoconductivity and luminescence are also included. A general discussion on recombination is presented since recombination is obviously strongly related to almost all optoelectronic phenomena. The effects of various fabrication parameters on the properties of amorphous semiconductor films are also presented.

For a-Ge films, the optoelectronic properties are discussed for both evaporated and sputtered films. Various theoretical calculations for the optoelectronic properties of these films are also mentioned. Finally a brief review is given for a-Si-Ge alloys.

2.1 AMORPHOUS SILICON

2.1.1 Photoconduction

A. Factors controlling photoconduction

Suzuki et al. [3] have reported that the photoconductivity of evaporated a-Si films prepared under well defined conditions is strongly dependent on the photon energy of the illuminating light. This spectral dependence is also strongly dependent on the annealing temperature as shown in Figure 2.1. In all samples, the photoconductivity disappears at photon energies below about 0.6 eV. The photoconductivity spectra of the well-annealed evaporated films resembles those of glow-discharge grown a-Si films. The photoconductivity has a rapid rise for photon energies about 1.5 eV. It has been found that the mobility gap of the evaporated a-Si films is approximately 1.4 eV which is 0.1 eV smaller than that of glow-discharge grown a-Si films [4,5].

Photoconductivity for glow-discharge grown a-Si films is shown in Figures 2.2 and 2.3 [5]. The a-Si films produced from either dc or r.f. glow-discharge in silane, in general, have good photoconductive properties in contrast to the a-Si films produced by sputtering or evaporation techniques which show poor photoconductivity. This may be due to the presence of hydrogen in the former case and the absence of hydrogen in the latter case.

Figures 2.2 and 2.3 show the dependence of the $\eta\mu_n\tau_n$ product on photon energy for both r.f. and d.c. glow-dis-

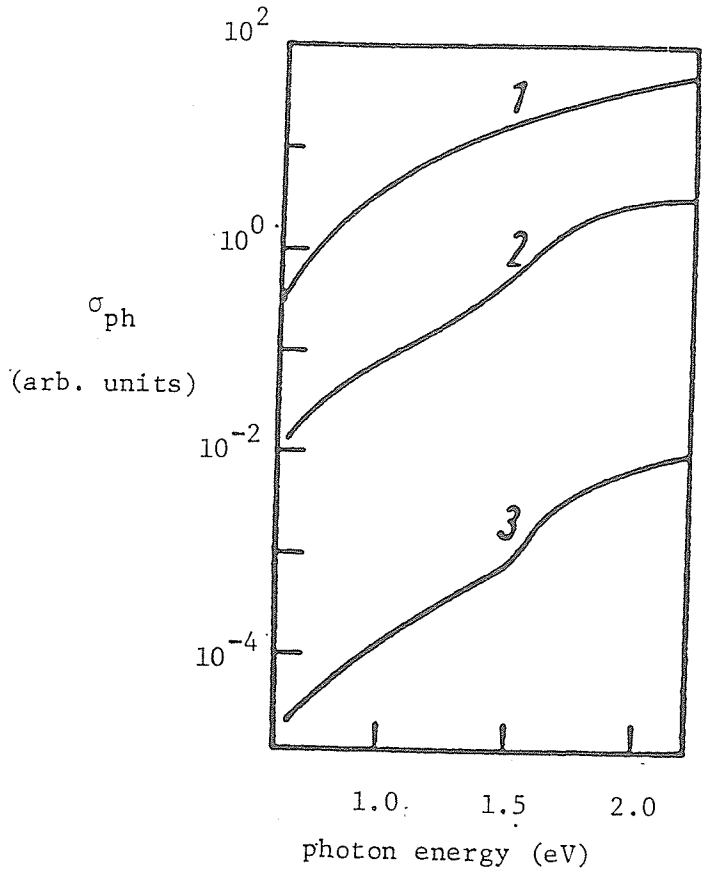

Figure 2.1: Spectral dependence of normalized photoconductivity at 300 K for a-Si films annealed at various temperatures. (1) as-deposited, annealed at (2) 300 and (3) 600 C [3].

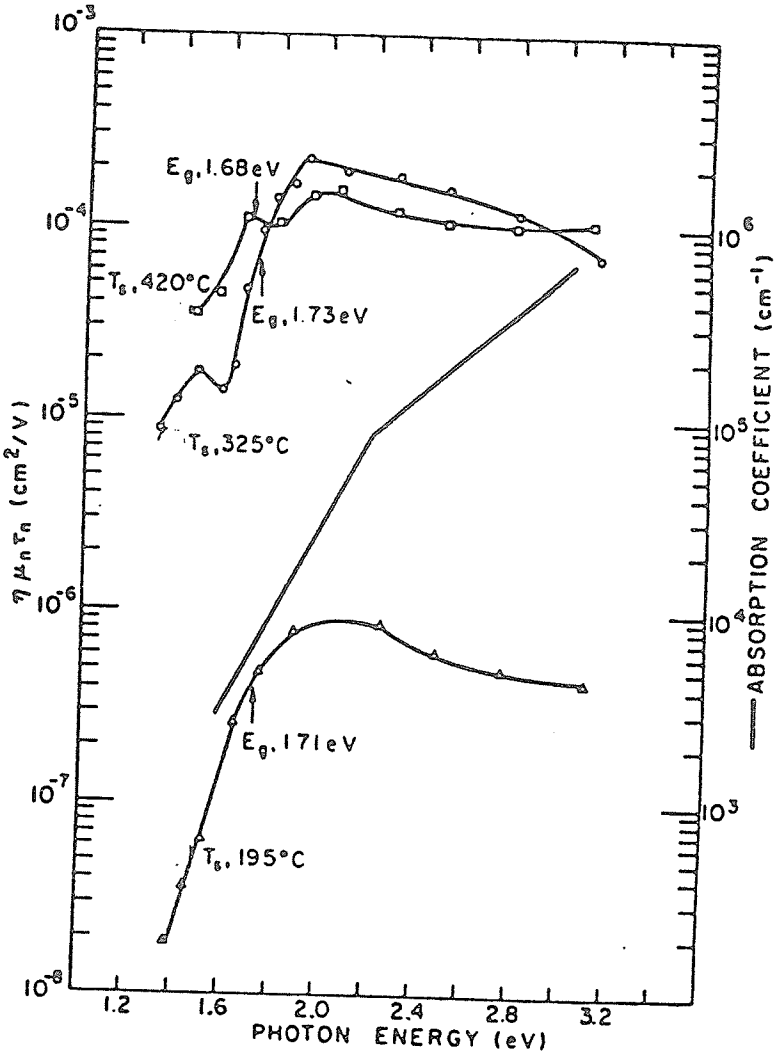

Figure 2.2: Electron mobility-lifetime product as a function of photon energy for r.f. discharge grown a-Si. Data compared to the absorption coefficient for r.f. discharge grown a-Si [5].

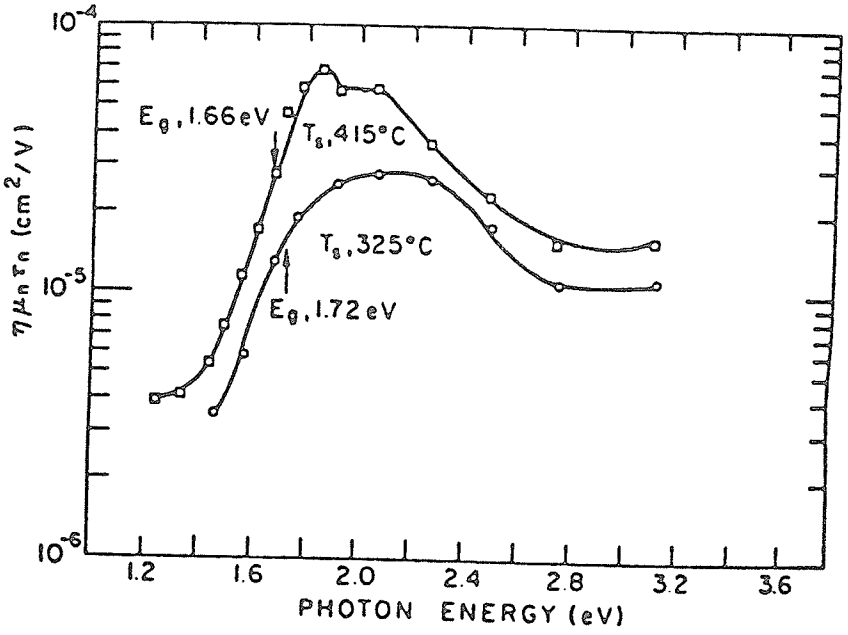

Figure 2.3: Electron mobility-lifetime product as a function of photon energy for d.c. discharge grown a-Si [5].

charge grown films, in which η is the photo-generation efficiency of free carriers, μ_n is the electron mobility and τ_n is the electron lifetime. The wavelength dependence of the photoconductivity for r.f. glow-discharge produced a-Si as shown in Figure 2.2 has an apparent structure at the higher substrate temperatures. There is only about an order of magnitude difference in $\eta\mu_n\tau_n$ for photon energies greater than the optical gap of the film as compared to the value of $\eta\mu_n\tau_n$ for photon energies less than the optical gap for films deposited at substrate temperatures of 325 and 420 C. For films deposited at 195 C, such a difference is much larger. For d.c. glow-discharge grown films, the $\eta\mu_n\tau_n$ values are comparable to those of r.f. glow-discharge films at substrate temperatures of 320 and 420 C as shown in Figure 2.3. Again, there is a decrease of only 10 in the $\eta\mu_n\tau_n$ value for photon energies greater than the optical gap as compared to the value for photon energies less than the optical gap. For energies above the optical gap, the electron lifetime is estimated to be about 10^{-4} s for a substrate temperature of approximately 300 C and about 10^{-6} s for a substrate temperature of approximately 200 C for r.f. glow-discharge produced films (taking $\mu_n = 1$ and $\eta = 1$ since for photon energies above the optical gap $\eta \simeq 1$). The corresponding values for the electron lifetimes are about 10^{-4} and 10^{-5} s, respectively, for d.c. glow-discharge produced films.

In addition, Zanzucchi et al. [5] also have reported the dependence of photoconductivity σ_{ph} on illuminating light intensity for r.f. and d.c. glow-discharge a-Si films. The photoconductivity measurements have been used to study the nature of free-carrier recombination in these films. The photoconductivity of r.f. glow- discharge produced films deposited at substrate temperatures of 195, 320, and 415 C as a function of illuminating light intensity is shown in Figure 2.4.

The photocurrent J_{ph} in these films as a function of illuminting light intensity I is given by [5]

$$J_{ph} = C' \, I^{\nu} \quad , \tag{2.1}$$

where C′ and ν are constants. Over the range of intensities studied, the J_{ph} - I relation has $\nu = 0.9$ for σ_{ph} less than 8×10^{-6} $(\Omega\text{-cm})^{-1}$ as shown in Figure 2.4.

The photoconductivity of d.c. glow-discharge produced a-Si films for the same illumination is shown in Figure 2.5. The volume generated photoconductivities for r.f. glow-discharge produced films, at substrate temperatures of 320 to 420 C, are almost the same, having the value of ν between 0.70 and 0.75. A transition of ν from 0.75 to 0.50 is indicated at the highest illumination light intensity used for the film deposited at 320 C.

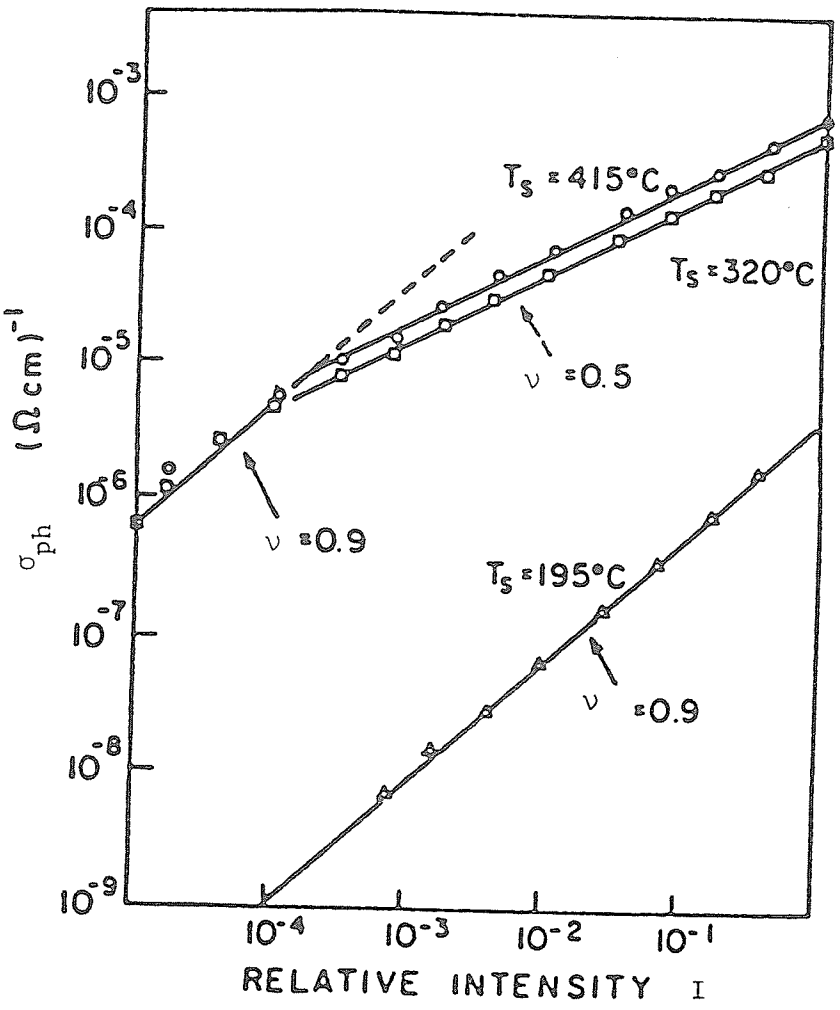

Figure 2.4: Photoconductivity of r.f. discharge-produced a-Si films as a function of illumination for various substrate temperatures at deposition [5].

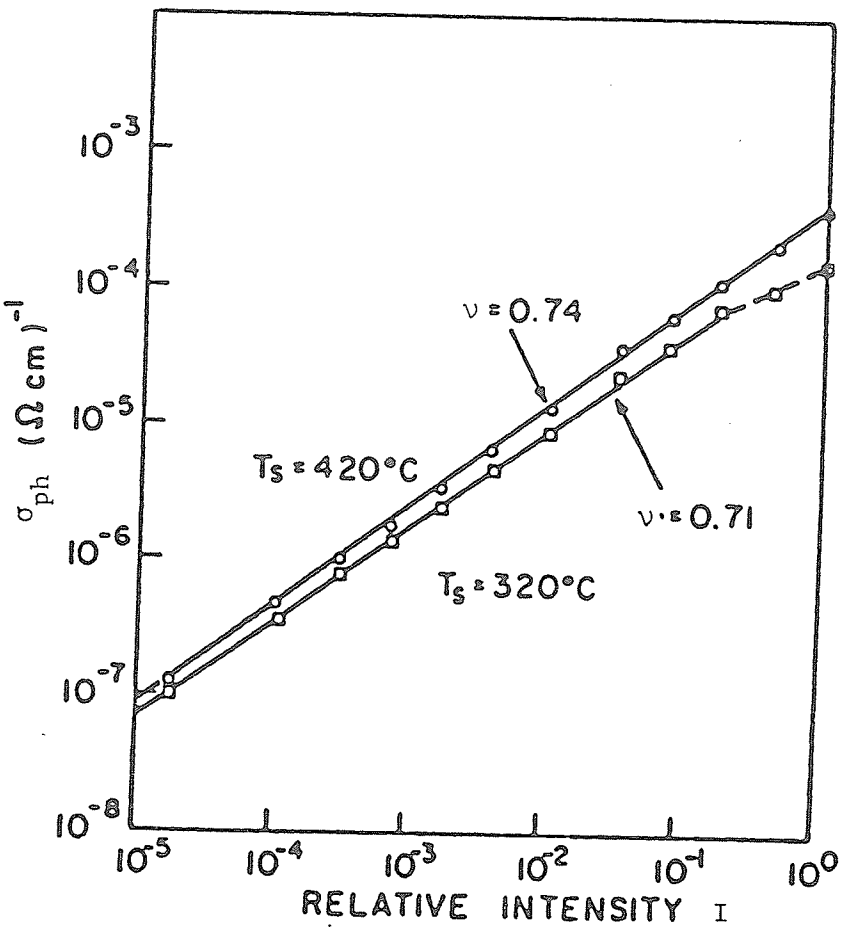

Figure 2.5: Photoconductivity of d.c. discharge produced a-Si films as a function of illumination for various substrate temperatures at deposition [5].

B. Temperature dependence of photoconductivity

Figure 2.6 shows the temperature dependence of the photoconductivity at constant photon energies for evaporated a-Si films [3]. Three activation energies E_{p1}, E_{p2}, and E_{p3}, can be regarded as mobility activation energies at three different temperature ranges and are found irrespective of the exciting photon energy. E_{p1} for $T > 415$ K can be understood as the activation energy of the trap controlled drift mobility. E_{p2} for $165\ K < T < 415\ K$ and E_{p3} for $T < 165$ K are considered to be activation energies for hopping. The value of E_{p2} is close to the mobility activation energy for glow-discharge a-Si films in the same temperature range from 165 K to 415 K.

Fuhs et al. [6] have analyzed the steady state and transient photoconductivity and carrier mobility for glow-discharge grown a-Si films. The steady state photoconductivity can be written as

$$\sigma_{ph} = e\, g_{op}\, \tau\, \mu \quad , \qquad (2.2)$$

where g_{op} is the generation rate, μ the microscopic carrier mobility, and τ the lifetime of the free carriers. The generation rate g_{op} is related to the incident photon flux I, the absorption coefficient α, and the reflectivity, R, by

$$g_{op} = \beta\, I\, (1-R)\, (1-e^{-\alpha d})/d \quad , \qquad (2.3)$$

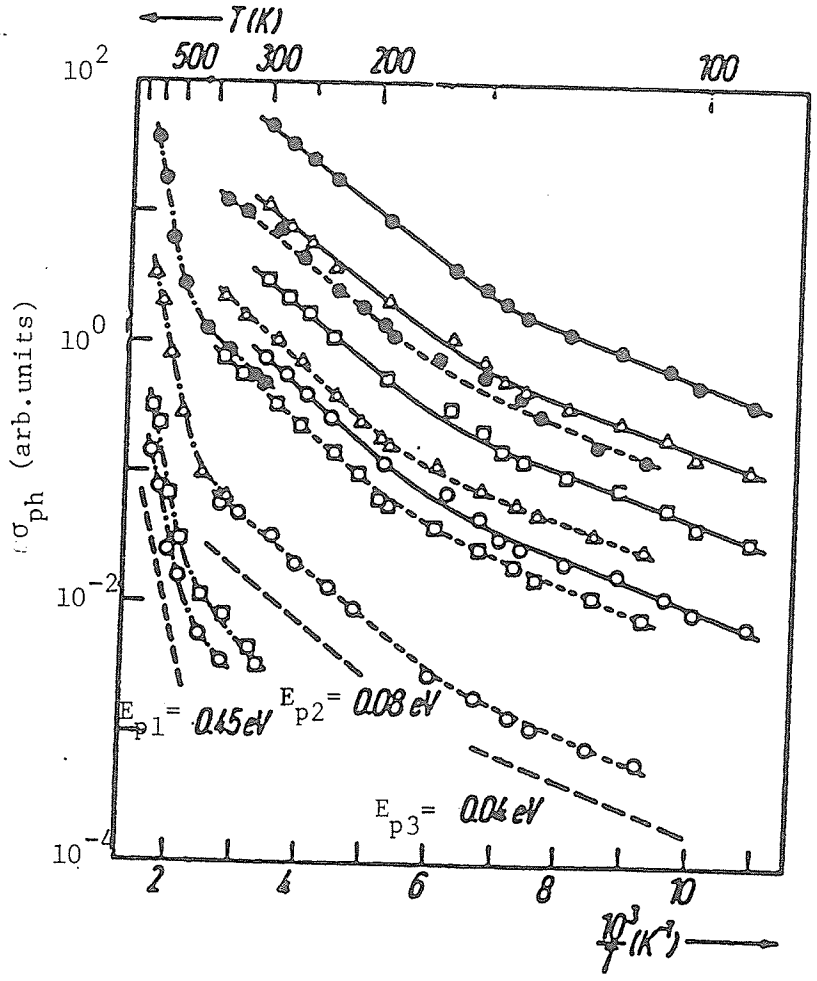

Figure 2.6: Temperature dependence of photoconductivity obtained at constant photon energies hf for a-Si films annealed at various temperatures. ——— as-deposited, ---- annealed at 180 and —·— 500 C; ○ hf = 0.69, □ 0.89, △ 1.24, ● 2.07 eV [3].

where d is the film thickness and β the quantum efficiency, which in the range of intrinsic absorption can be taken equal to unity. The photoresponse time from the decay of the photoconductivity is defined as

$$\tau_r^{-1} = \frac{1}{\sigma_{ph}} \frac{d\sigma_{ph}}{dt}\bigg|_{t=0} \quad . \qquad (2.4)$$

In the presence of traps this response time will be longer than the lifetime of the free carriers by a factor of $(1 + n_t / n)$ [7]. We can write

$$\tau_r = \tau\ (1 + n_t/n) \quad . \qquad (2.5)$$

The response time τ_r may be regarded as a recombination lifetime, the time required for the total recombination of both the free carriers and the trapped carriers, and hence the mobility determined from Equations (2.2)-(2.5) does not represent the microscopic mobility, but the drift mobility.

Fuhs et al. [6] have also reported that the activation energy of the photoconductivity is temperature dependent. At low temperatures the photoconductivity has an activation energy of 0.11 eV, but at temperatures above 250 K the acti-

vation energy becomes 0.08 eV as shown in Figure 2.7. The lower activation energy corresponds to a higher photoconductivity and higher values for the response time τ_r.

The drift mobility, μ_d, is defined by activation energies of 0.16 and 0.13 eV at high and low temperatures, respectively. Figure 2.7 illustrates that this change in the slope of the mobility occurs near $10^3/T = 4\ K^{-1}$ ($T = 250\ K$).

Fuhs et al. [6] have also observed that the photoconductivity decreases rapidly and the temperature dependence changes after long exposure to light of band gap energy as shown in Figure 2.8. The weaker temperature dependence dominates at $T > 250$ K (curves 3 and 4). This behaviour is also observed for τ_r which is affected more by light exposure at higher temperatures. Figure 2.9 shows the resulting calculated mobility from the data given in Figure 2.8. Curves 1 to 4 display activated behaviour with an activation energy of about 0.16 eV with no kinks suggesting that there is no change in transport mechanism in the temperature range shown.

C. Effects of doping on photoconductivity

Photoconductivity and its dependence on incident light intensity and temperature have been investigated for a series of doped a-Si films at a photon energy of 2 eV by Anderson and Spear [8]. The films were prepared by glow-discharge decomposition of silane at substrate temperatures

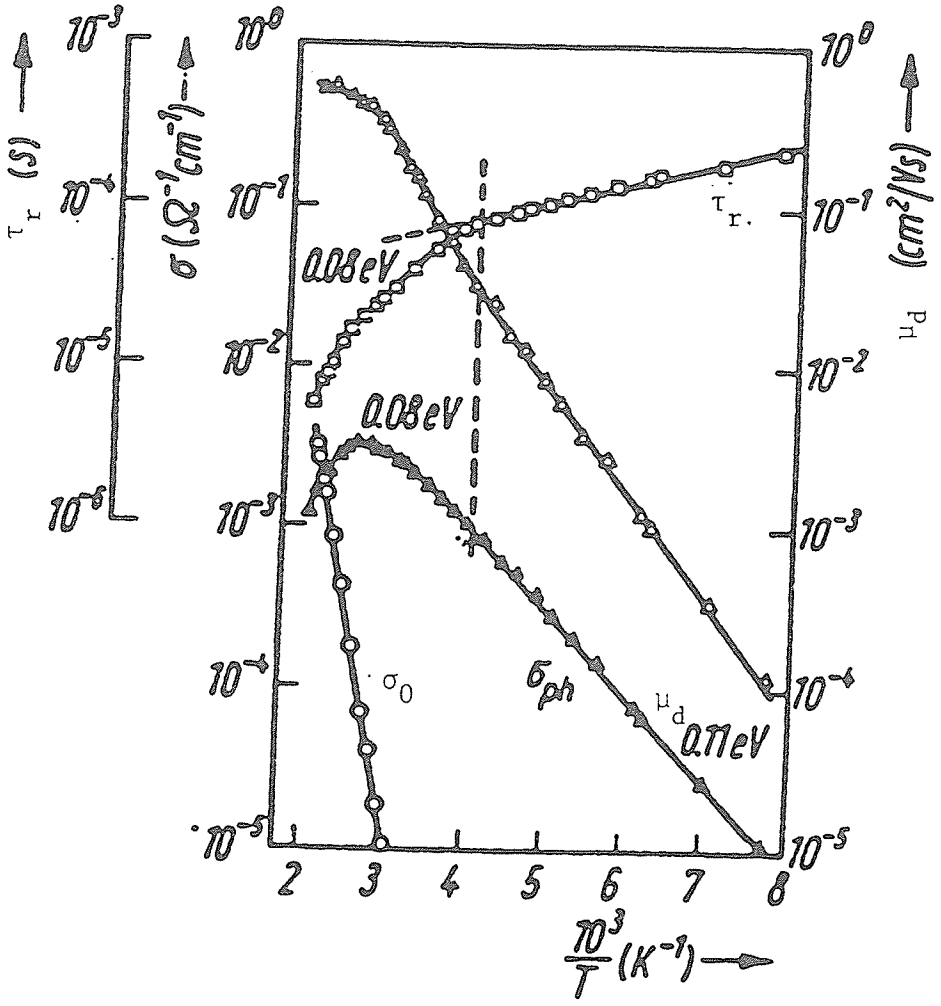

Figure 2.7: Temperature dependence of the steady-state photoconductivity σ_{ph}, response time τ_r, and the calculated mobility μ_d of a-Si (T_s = 530 K) [6].

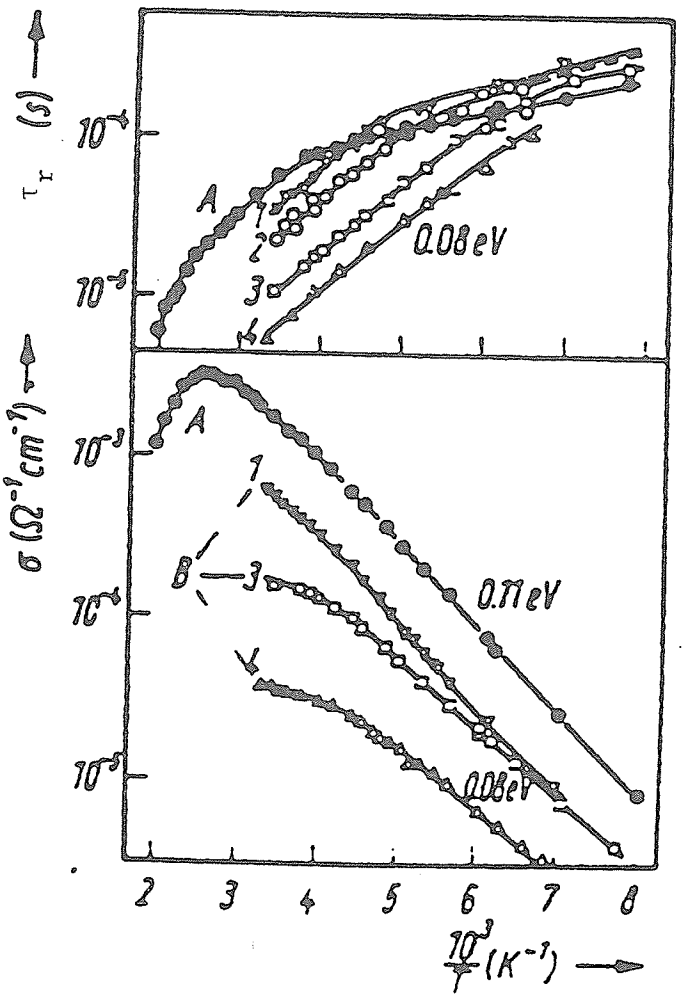

Figure 2.8: Steady-state photoconductivity σ_{ph} and response time τ_r of a-Si (T_s = 530 K) as a function of temperature. A: as deposited; curves 1 to 4; exposed to light of 1.96 eV and 7.5 mW/cm for 5, 15, 60, and 600 min. respectively [6].

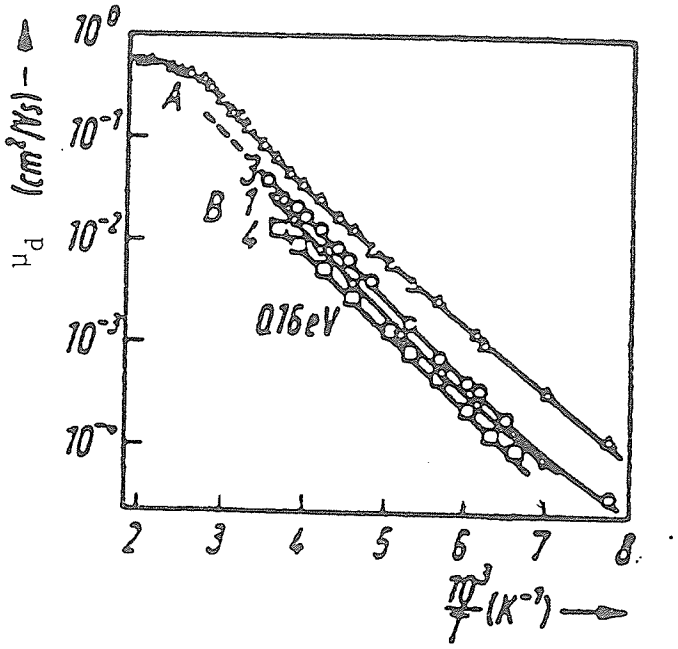

Figure 2.9: Temperature dependence of the mobility calculated from the data in Figure 2.8 [6].

between 500 and 550 K and doped with phosphorus and boron [9]. The dark Fermi level was normally pinned near the mid-gap due to the presence of localized states. Doping however with phosphorus and boron tends to shift the position of the dark Fermi level over a range of 0.8 eV without appreciable alteration of the distribution of localized states as shown in Figure 2.10. The position of the dark Fermi level E_F, depends on the doping. With phosphorus doping, the photo-conductivity increases with the doping level, and reaches a peak at a critical level. With further doping the photocon-ductivity tends to decrease when E_F approaches the conduc-tion band tail states. Slight boron doping moves the dark Fermi level toward the valence band and leads to a consider-ably reduction in photoconductivity.

Figure 2.10 shows the values for ν ($\sigma_{ph} \propto I^{\nu}$) close to 0.9 in undoped or boron doped films. ν never equals unity for these samples so that the carrier lifetime is never en-tirely independent of light intenstity [Equation (2.2)]. The rapid rise in the photoconductivity is accompanied by a sharp drop in ν to values between 0.6 and 0.5 implying two distinct regimes of either monomolecular or bimolecular rec-ombination.

Anderson and Spear [8] have observed that the onset of saturation of the photoconductivity coincides almost exactly with the transition from the predominantly monomolecular to bimolecular recombination as shown in Figure 2.11. E_{Fn} is

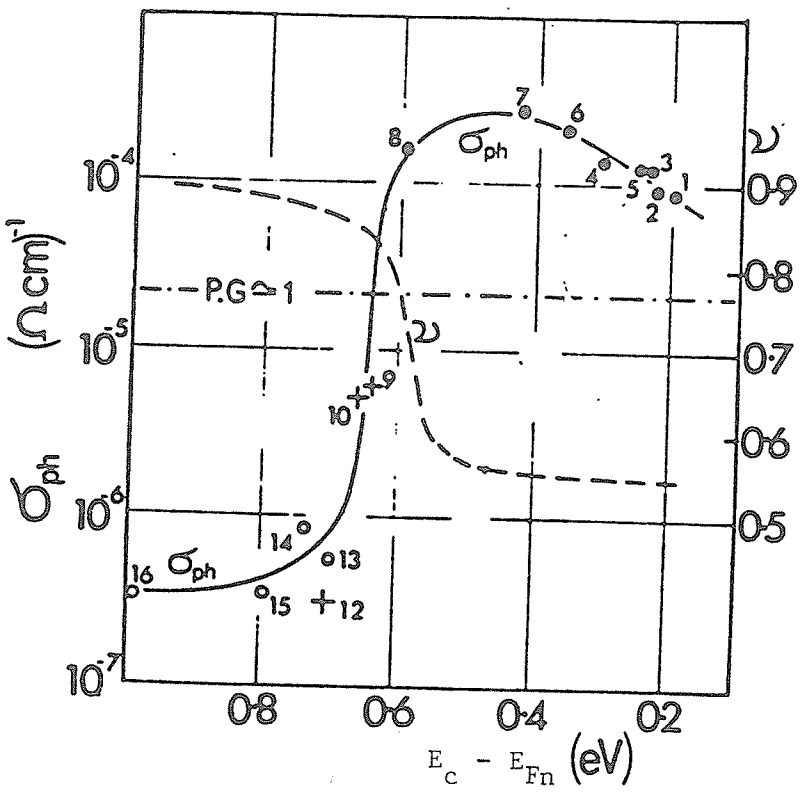

Figure 2.10: Photoconductivity at 295 K plotted against $E_c - E_F$, the position of the dark Fermi level for phosphorus doped (■), undoped (+) and boron doped (●) a-Si specimens. The broken line represents the exponent ν in the intensity dependence $\sigma_{ph} \propto I^{\nu}$. σ_{dark} is a typical dark conductivity curve. P.G. 1 refers to unit photoconductive gain at a field of 3 x 10 V/cm [8].

the steady state Fermi level for the electron distribution in the system and T and I refer to a specific temperature and light intensity, respectively. It seems that the photoconductivity in glow-discharge a-Si films attains its optimum value when the steady state electron Fermi level has moved to a position between 0.30 and 0.35 eV below E_c. That is, the condition in which bimolecular recombination takes over. Apparently, if the position of the electron Fermi level lies between 0.30 and 0.35 eV below E_c, the critical condition for the change in recombination process as suggested earlier, the E_x - peak in N(E) (see Figure 2.12) will be occupied with electrons. The transition in recombination mechanism occurs when the negative charge in the E_x - peak, centered at an energy of 0.4 eV below E_c, has reached its maximum value. The photoconductivity begins to saturate at its maximum value, and from this point the bimolecular recombination takes over from the predominately monomolecular recombination.

Rehm et al. [10], have also investigated photoconductivity of boron and phosphorus doped a-Si films for the temperature range from 100 to 400 K. Their samples were prepared by glow-discharge decomposition of silane as described by Spear and LeComber [9]. They have observed that an increase in doping increases the photoconductivity as shown in Figure 2.13. The photoconductivity is thermally activated and can be expressed as [10]

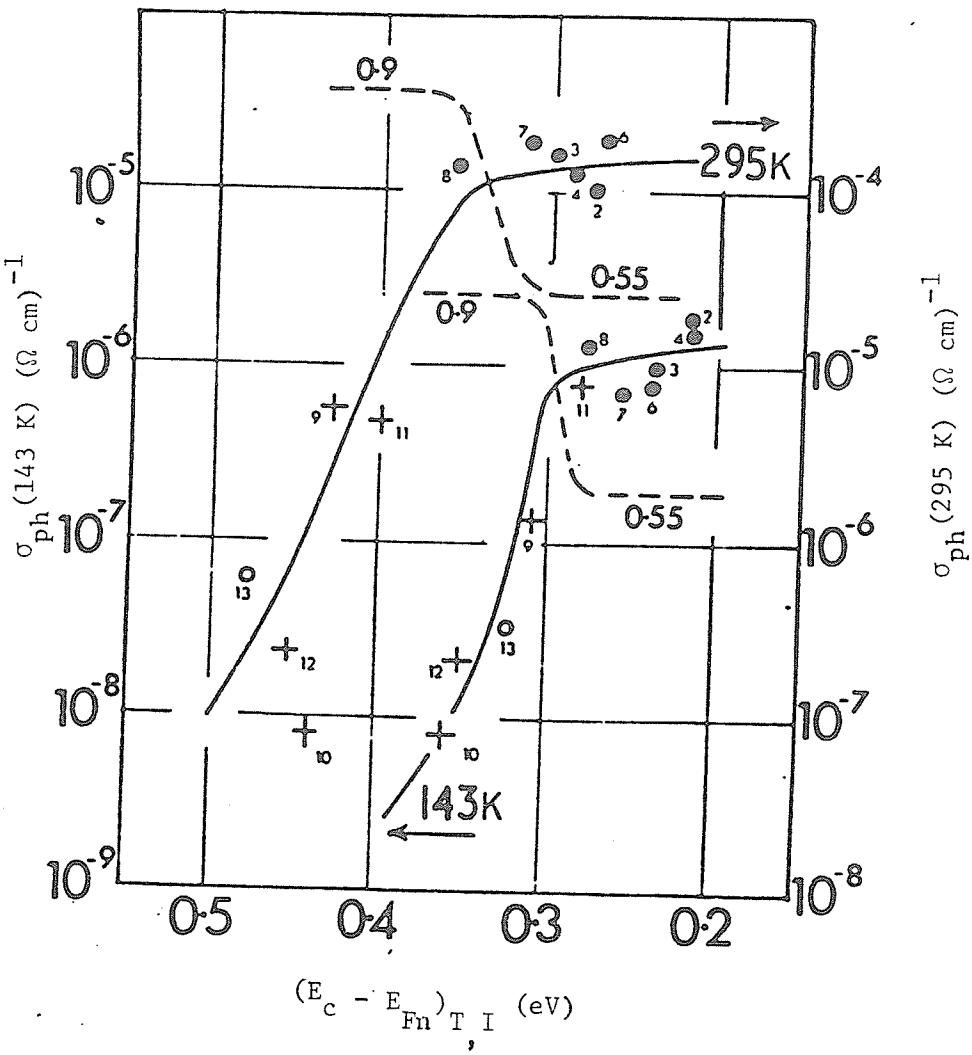

Figure 2.11: Photoconductivity of a-Si at 295 K and at 143 K plotted against the steady-state Fermi level position at a photon flux of 7×10^{14} s^{-1} cm^{-2}. The broken lines illustrate at each temperature the exponent in the intensity dependence $\sigma_{ph} \propto I^{\nu}$ plotted on a linear scale [8].

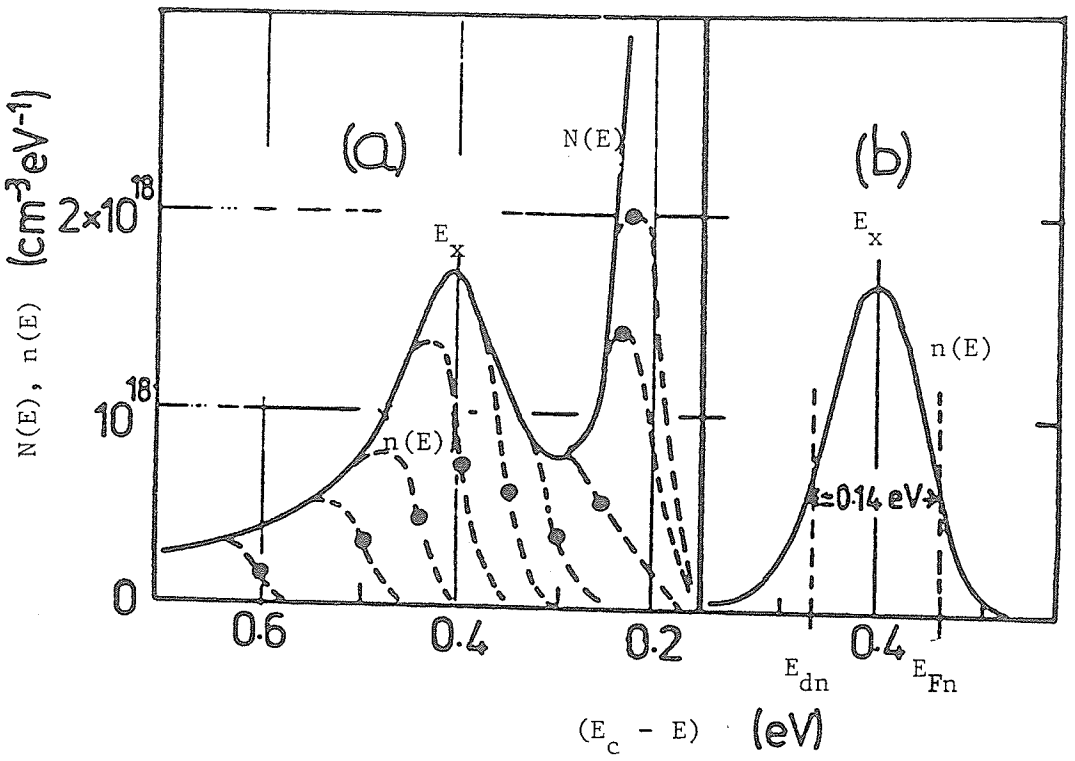

Figure 2.12: (a) Linear plot of the density of states N(E) against the energy measured from E_c. The broken lines represent the thermal equilibrium electron occupation n(E) at 143 K when the Fermi level lies at the energy marked by the dots. (b) A likely electronic charge distribution when E_{Fn} has reached the critical energy at about 0.33 eV below E_c. E_{dn} is the demarcation level for electrons [8].

$$\sigma_{ph} = \sigma_{ph0} \exp(-E_A/kT) \quad , \qquad (2.6)$$

where E_A is the activation energy which, in an intermediate temperature range, is independent of temperature as shown in Figures 2.14 and 2.15. Increasing doping generally decreases the activation energy of the photoconductivity, E_A. The pre-exponent factor, σ_{ph0} , increases with doping in the low doping levels and decreases in the high doping levels.

The effect of boron doping is qualitatively similiar to that of phosphorus doping and is shown in Figure 2.14. The photoconductivity of boron doped Si is much lower than that of phosphorus doped or undoped Si. The photoconductivity shows no clear dependence on boron concentration, and σ_{ph0} reaches in most cases the same order of magnitude as for phosphorus doping. By introducing additional localized states in the gap by implantation of inert-gas ions (bombardment with 100 KeV He^+ ions), the photoconductivity decreases from the original 10^{-5} to 10^{-9} $(\Omega\text{-cm})^{-1}$ as shown in Figure 2.15. However, the photoconductivity can be restored to almost its original value by annealing (curve 6). Figure 2.16 shows the photoconductivity versus annealing temperature for phosphorus doping, which also indicates the behaviour for boron doping.

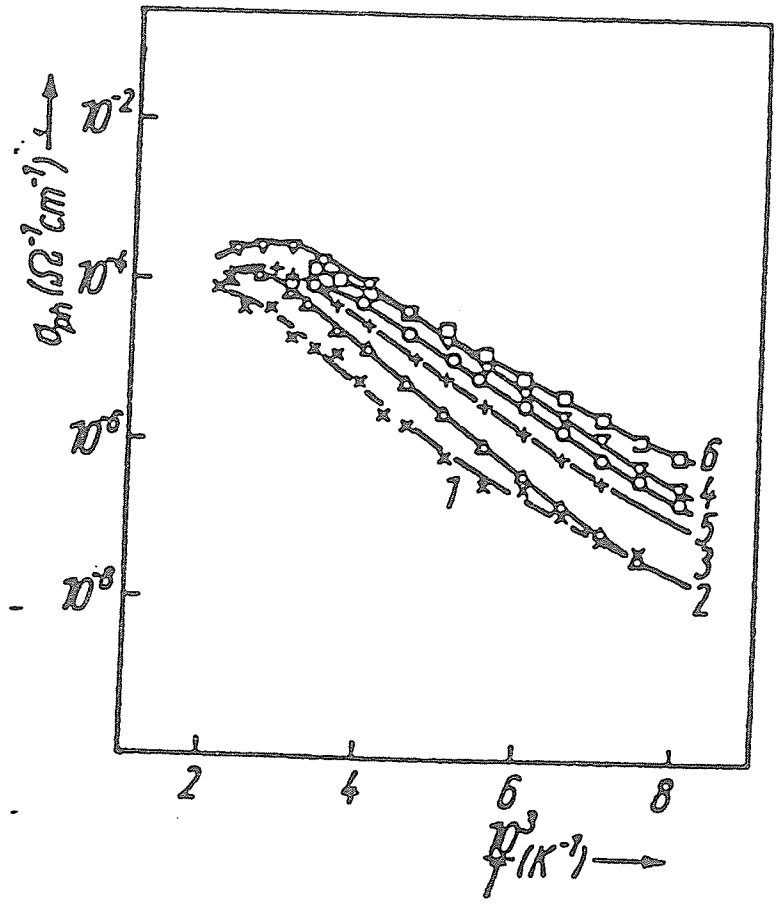

Figure 2.13: Photoconductivity of phosphorus-doped a-Si films. The ratios N_{PH_3}/N_{SiH_4} and the deposition rates for the particular curves are: (1) undoped, 10 Å/s; (2) 2×10^{-6}, 1 Å/s; (3) 2×10^{-6}, 2.5 Å/s: (4) 10^{-5}, 2.5 Å/s; (5) 10^{-3}, 15 Å/s; (6) 2×10^{-3}, 1 Å/s [10].

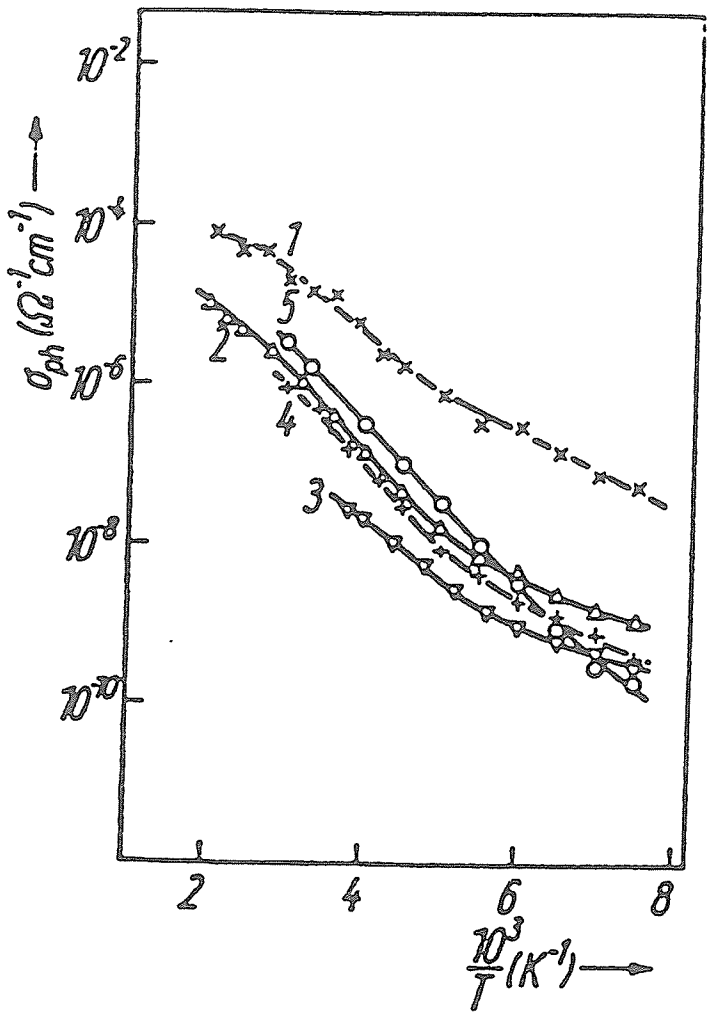

Figure 2.14: Photoconductivity of boron-doped a-Si films. The ratios $N_{B_2H_6}/N_{SiH_4}$ and the deposition rates for the particular curves were: (1) undoped, 10 Å/s; (2) 5×10^{-4}, 0.6 Å/s; (3) 2×10^{-2}, 0.6 Å/s; (4) 5×10^{-2}, 0.6 Å/s; (5) 2×10^{-2}, 10 Å/s [10].

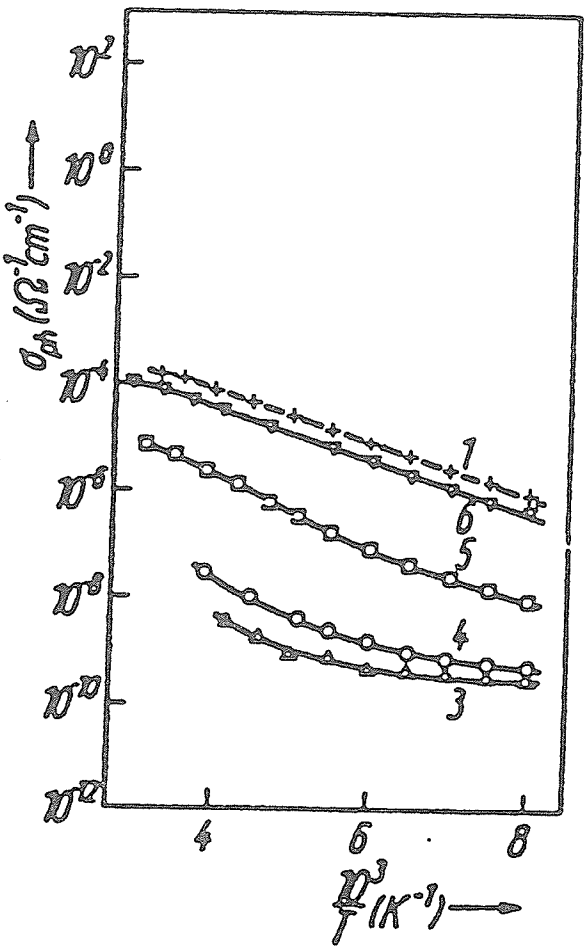

Figure 2.15:
Photoconductivity of phosphorus-doped a-Si films after bombardment with 100 keV He^+ ions (5×10^{-2} cm , $N_{PH_3}/N_{SiH_4} = 2 \times 10^{-3}$). (1) before bombardment, (2) through (6) after bombardment and annealing at temperatures T_A; (2) T_A = 20, (3) 80, (4) 120, (5) 200, (6) 340 C [10].

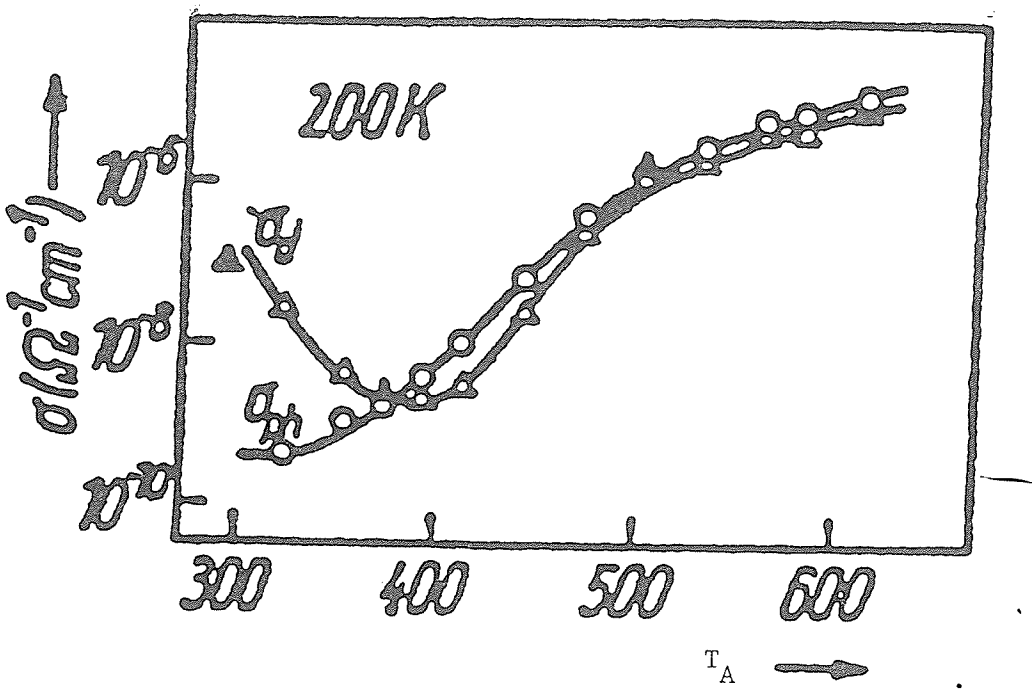

Figure 2.16: Dark and photoconductivity (at T = 200 K) of a phosphorus-doped He^+ bombarded a-Si film ($N_{PH_3}/N_{Si:H_4} = 2 \times 10^{-3}$) versus annealing temperature T_A [10].

D. Photoconduction processes

Suzuki et al. [3] have reported that the onset of photoconductivity at room temperature for evaporated a-Si films is at a photon energy of about 0.6 eV and that this critical photon energy conincides with the photon energy for the optical transitions from the filled states at E_F into the extended states at E_c, the Fermi level being at about 0.6 eV below E_c. For photon energies of approximately 1.4 eV the photoconductivity may be due to electron transistions from a high density of localized states below E_F to the extended states above E_c. That the mobility gap of evaporated a-Si is about 0.1 eV smaller than that of glow-discharge grown a-Si films, indicates the presence of significant conduction through the localized states close to the mobility edge.

The J_{ph} - I relation is very useful in determining the nature of recombination centers present in the gap, particularly when the photocurrent is significantly larger than the dark current. The value of $\nu = 0.9$ in the relation $J_{ph} = C' I^{\nu}$, given in Figure 2.4 for r.f. glow-discharge a-Si films [5] indicates that the recombination centers are virtually uniformly distributed in the energy gap through which the quasi-Fermi level is swept as the illuminating light intensity is increased. For monomolecular recombination the electron lifetime τ_n is less sensitive to illumination intensity. The value of $\nu = 0.5$, however, reflects bimolecular recombination, and in this case τ_n decreases as the il-

lumination intensity is increased. Bimolecular recombination can occur in a photoconductor when there are both trapping centers as well as deep recombination centers present [7]. For films prepared at substrate temperatures below 300 C the presence of a significantly higher density of deep recombination centers is indicated by the conducting region having $\nu = 0.9$.

The results in Figure 2.5 for d.c. glow-discharge grown a-Si films show a value of ν = 0.70 to 0.75 in the relation $J_{ph} = C' I^{\nu}$. These values are too low to reflect a uniform distribution of deep electron traps, but rather indicate a continuous exponential or quasi-exponential distribution. Comparison of the photoconductivity characteristics of r.f. and d.c. glow-discharge grown a-Si films at deposition temperatures above 300 C indicates that there is a difference in the distribution of recombination centers between these two techniques which could be associated with the difference in the kinetics between these two types of discharges.

The temperature dependence of the photoconductivity for evaporated a-Si films as shown in Figure 2.6 shows an activated behaviour [3]. Regarding Figure 2.6, E_{pl} is the activation energy of trap controlled drift mobility. Photoconduction at temperatures above about 450 K arises from photoelectrons excited into the conduction band which are redistributed to localized states below E through trapping and thermal release. The trap controlled drift mobility of electrons is given by [3]

$$\mu_d = \mu_0 \, B \exp[-(E_c - E)/kT] \quad , \qquad (2.7)$$

where μ_0 is the mobility at E_c and B is a constant. For a single trap level at energy E_t, E equals to E_t and B to N_c/N_t, where N_c is the effective density of states at E_c and N_t the density of traps at E_t. For a linear or a uniform distribution of localized states, E equals E_L, the energy of the lowest localized states, the localized states being considered to be extended to about 0.45 eV below E_c.

The photoconductivity of glow-discharge grown a-Si films has a thermally activated behaviour [6]. In addition, the activation energy is temperature dependent as shown in Figure 2.7. Such a temperature dependence indicates that there are two competing recombination processes, one dominates below 250 K with a weak temperature dependence, and the other above 250 K. The change in slope of the mobility near $10^3/T = 4\ K^{-1}$ as shown in Figure 2.7 can be interpreted as a change in the transport mechanism [11]. However, the temperature dependence of the response time τ_r, suggests that near this critical temperature the recombination mechanism changes.

The effect of exposing a photoconductor to light of band gap energy on photoconductivity is shown in Figures 2.8 and 2.9. The effect of the light is to change the temperature

dependence of the photoconductivity and to reduce the magnitude of the photoconductivity. Long exposure to light of energy equal to the band gap results in a reduction of the activation energy.

The reduction in the magnitude of the photoconductivity may be explained in terms of the relationship between the photoconductivity and the position of the Fermi level as well as the effect of exposure to light on the Fermi level. There exists a close relationship between the photosensitivity and the position of the Fermi level for glow-discharge a-Si films [8]. If the Fermi level is shifted by some means, for example by doping, from a location near the middle of the gap to a position approximately 0.2 eV towards the conducting states, the photoconductivity is enhanced by about three orders of magnitude, indicating a change from monomolecular to bimolecular recombination. In a-Si films fabricated at high substrate temperatures, the position of the Fermi level is usually quite high and hence these films have a higher photoconductivity. However, exposure of these films to a light of energy equal to the bandgap can reverse this behaviour since the light causes a shift of the Fermi level away from the conducting states [12].

Anderson and Spear [8] have reported such an effect of doping on photoconductivity. This has been discussed previously for glow-discharge grown a-Si films. The photoconductivity saturates and predominately bimolecular recombination

takes over from predominately monomolecular recombination when the E_x- peak (see Figure 2.12) in the localized state density distribution just begins to become occupied by electrons. The enhancement of photoconductivity by phosphorus doping and the change of recombination behaviour can be seen in Figure 2.17. It is assumed that holes are quickly trapped due to a high density of tail states, and that the dominating carriers are electrons. Positively and negatively charged centers arise in the middle of the gap from the overlap of the tail states. These charged centers have a high capture cross section for carriers of opposite charge and therefore act as effective recombination centers. When E_F is moved from its location in an undoped film (B) towards the conduction band (A) by doping, the number of positive states decreases, thus enhancing the electon lifetime. The recombination process is monomolecular as long as the dominating recombination path is via these charged midgap states. At higher light intensities or larger shifts of E_F, recombination occurs by transitions between maxima in the charge distribution of the trapped electrons and holes as a bimolecular process.

Rehm et al. [10] have reported that for glow-discharge grown a-Si films, phosphorus doping increases the photoconductivity. Also, the temperature activation energy generally decreases with increasing phosphorus doping. An increase in the density of localized states reduces the magnitude of

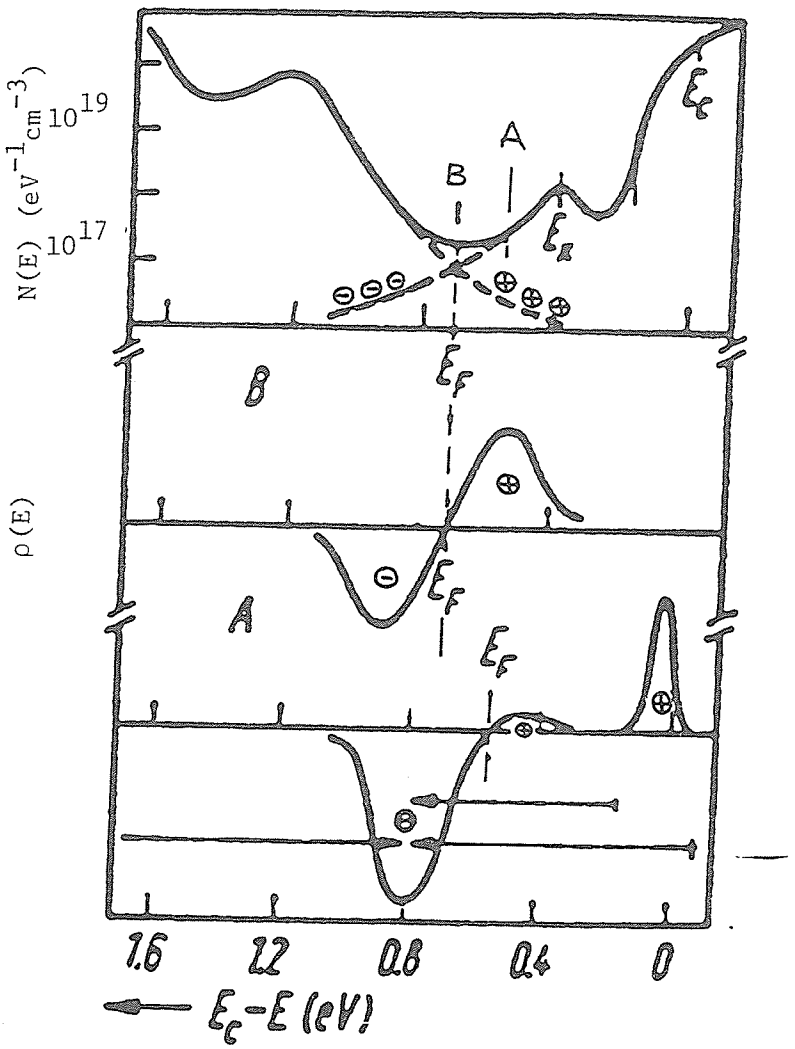

Figure 2.17: Density of states N(E) and charge distribution according to [8]. Arrows indicate the predominating recombination processes [6].

the photoconductivity. If the a-Si is subjected to heat treatment (annealing), the density of localized states can be reduced with a subsequent increase in the photoconductivity.

Changing the structure and the doping level can change the photoconductivity by either affecting the lifetime of the excess carriers and/or by changing their drift mobility μ_d. In principle, it is difficult to separate the two influences, because both the lifetime and the mobility can be temperature activated, and both can have structure-and-doping sensitive prefactors. Assuming that the lifetime is temperature independent, the activated factor in $\sigma_{ph} = \sigma_{ph0}\, e^{-E_A/kT}$ (Equation 2.6) comes from the activation of μ_d [10],

$$\mu_d(T) = \mu_{d0} \exp(-E_p/kT) \quad . \tag{2.8}$$

The flat portions in the curves of Figure 2.15 at low temperatures may be interpreted as being due to hopping photoconductivity [13] since they occur at a high localized state density and can be annealed away [10]. The lowering of the temperature activation energy by annealing after introduction of additional localized states by He^+ ion bombardment has been interpreted as follows [10]. The lowering of the temperature activation energy by annealing after He^+ bom-

bardment is due to a widening of the band tail by bombardment, leading to high activation energies for photoconductivity, and by a reduction in the width of the band tail by subsequent annealing. The decrease in the activation energy with increasing phosphorus doping is explained as due to the opening up of another conduction channel in the band tail with a lower activation energy [10]. This second path may be related to conduction in an impurity band connected with a lower value of μ_{d0} in Equation (2.8). Since σ_{ph0} in $\sigma_{ph} = \sigma_{ph0}\, e^{-E_A/kT}$ rises with doping, the drop in μ_{d0} may be overcompensated by an increase in lifetime. Such lifetime changes are expected because the doping alters the charge of recombination centers in the gap [8].

2.1.2 Luminescence

A. Recombination processes

The understanding of various recombination processes, and of the conditions under which each occurs, is of great importance to the understanding of optoelectronic properties.

It is generally accepted that a-Si prepared by glow-discharge has a lower density of localized states compared to evaporated or sputter deposited films. Field-effect measurements [14], indicate that the density of states of glow-discharge grown films has a maximum at about 0.4 eV from the band edges and decrease to about 10^{17} cm^{-3} eV^{-1} at the middle of the gap. The recombination processes can be categor-

ized as excitonic, band-to-trap and trap-to-trap transitions.

Since silicon demonstrates weak electron-phonon coupling, the non-radiative mechanism put foward by Dexter et al. [15], are most likely not operating and the multiphonon transistion rate is generally very small [16]. Therefore exciton recombination is radiative. Excitons in silicon, because of weak self-trapping and the absence of the non-radiative channel, have a relatively longer lifetime of about 10^{-5} s as compared to 10^{-9} to 10^{-11}s for chalcogenides. The weaker phonon coupling in silicon implies that the exciton is more mobile since the hopping energy is smaller. A combination of the weak self-trapping and the longer lifetime suggests that exciton ionization can occur at room temperature, Therefore, in silicon at room temperature, a photogenerated exciton will normally be ionized, to create free carriers, which, in turn give photoconductivity.

Street [17], and Davis et al. [18,19,20] have discussed the processes of photogeneration of charge carriers using the Onsager model [21]. After photoexcitation the electron and hole will diffuse apart a distance R_A determined by the diffusion constant and the thermalization time, which is proportional to the excess kinetic energy. The electron and hole are then bound by Coulombic attraction of energy $e^2/4\pi\varepsilon\varepsilon_0 R_A$. If R_A is larger than a critical distance R_0, which is defined by

$$e^2 / 4\pi\varepsilon\varepsilon_0 R_0 = kT \quad , \tag{2.9}$$

then the electron and hole will diffuse apart. If $R_A < R_0$, they form an exciton and hop together. An applied electric field tends to increase R_A because the carriers tend to diffuse further apart during thermalization, as well as to reduce R_0 because it enhances the escape rate. This model depends only on the existence of a short mean free path of carriers in extended states as in silicon.

At low photon energies there are alternative absorption mechanisms [17], and they are

1. Excitonic absorption without phonon interactions. The configurational coordinate diagram, as shown in Figure 2.18, shows that the exciton can exist without lattice distortion. Excitation to this state (path I) gives excitonic absorption which will be broadened by disorder defects.

2. Excitation of a self-trapped exciton. This is also shown in Figure 2.18 (path II) and is characterized by a zero phonon energy lying below that for the uncoupled exciton, but with a much broader linewidth because of the phonon interaction. This mechanism is apparently significant in silicon.

3. Absorption at a defect. An optical transition of an electron from D^- (charged defect) to the conduction band or from the valence band to D^+. Absorption of this type can

produce free carriers to contribute to photoconduction because the carriers may diffuse away from the neutral center.

4. Excitation of a D^+, D^- pair. The excitation of a close D^+, D^- pair is another possible absorption mechanism. Strong transistions only occur for close pairs when there is a large overlap of the wave functions. The contribution to the total absorption from transistions of this type will be proportional to the density of pairs.

Figure 2.19 is a schematic diagram of the competing mechanisms appropriate to glow-discharge grown silicon [17]. There are only two recombination channels; the radiative recombination of band tail, or defect bound excitons, and the non-radiative recombination between deep traps. The fast non-radiative recombination of excitons is absent. This explains why silicon exhibits neither the photostructural change nor the strongly energy dependent luminescence excitation spectrum that are found in chalcogenides [22]. Because the exciton is not strongly self-trapped, ionization can readily occur at a high enough temperature. Thus the photoconductivity quantum efficiency does not show strong dependence on excitation photon energy and applied field. Furthermore, the high mobility of excitons enhances its capture by deep traps.

Whilst excitons can readily dissociate into free carriers, free carriers do not interact to form excitons. This is shown by the photoconductivity lifetime being much larger

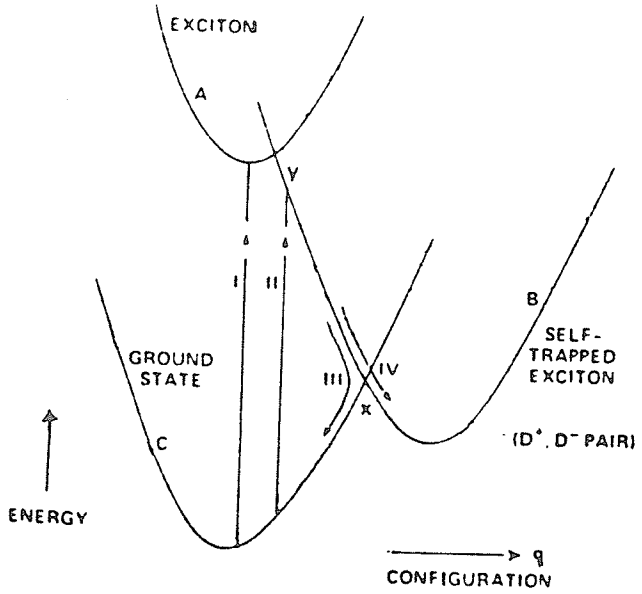

Figure 2.18: Configurational coordinate diagram for a self-trapped exciton appropriate for a-Si films. The excitation paths are I and II, and the recombination paths are III and IV. The self-trapped exciton is a D^+, D^- pair [17].

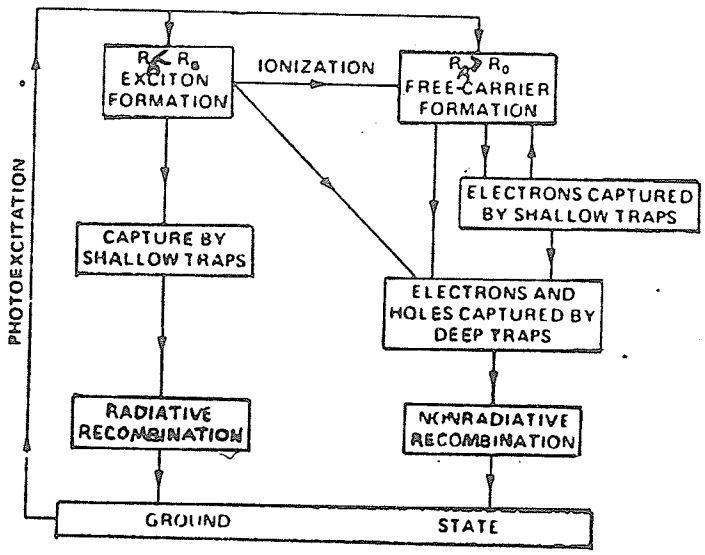

Figure 2.19: Flow diagram representing the interrelation of the excitation and recombination processes appropriate to amorphous glow-discharge deposited silicon [17].

than the radiative lifetime. Presumably the reason is that holes are rapidly trapped by deep traps in a time of the order of the radiative lifetime and thermalized to their recombination edge. Electrons, which are the more mobile carriers, diffuse in band tail states for a much longer time than holes because the density of electron traps is lower than that of hole traps in undoped material. The photoconductivity lifetime is determined by one of two possible transitions for the electrons. The first is capture by electron traps denoted by E_x [23]. This mechanism gives monomolecular behaviour for the photoconductivity with the final recombination of electrons and holes occurring at a longer time. The second possibility is the direct recombination of the electron with a trapped hole at its recombination edge. Experimental data show that the dominant process depends on doping [24]. In p-type samples the photoconductivity is monomolecular, indicating that the electrons are captured at E_x. In n-type material the response is bimolecular presumably because states at E_x are filled and thus can not capture electrons. Instead, the recombination must be directly to trapped holes.

B. Photo- and electro-luminescence

Pankove and Carlson [25], have observed luminescence from p-i-n junctions and from Schottky barriers made of a-Si which was produced by the d.c. glow-discharge decompostion

of silane. Their results for the photo-luminescence and electro-luminescence of a p-i-n diode are shown in Figure 2.20. The peak in both photo-luminescence and electro-luminescence spectra occur at 1.27 eV with a width at half-maximum of 0.2 eV. The high energy edge of the spectra cuts off at about 1.6 eV. In monocrystalline Si, the peak of the photo-luminescence spectra is at 1.09 eV as expected from the fundamental transition across the gap of Si.

The Schottky barrier to the a-Si exhibits, generally, the same photo-luminescence and electro-luminescence spectra as the p-i-n junction [25]. The application of a reverse bias to the Schottky barrier causes a quenching of the photo-luminescence when the average internal field exceeds about 10^5 V/cm. This effect is shown in Figure 2.21. Pankove and Carlson [25] have also reported that the emission peak shifts to lower energies with increasing temperature at a rate $dE/dT = -2.55 \times 10^{-4}$ eV/ K compared to $dE_g/K = -2.3 \times 10^{-4}$ eV/ K for the energy gap of crystalline Si. The internal quantum efficiency is estimated to be about 10 % as derived from photo-luminescence efficiency.

The photo-luminescence of a-Si prepared by r.f. glow-discharge has been reported by Engemann and Fischer [26]. They have observed the maximum of the luminescence band lying at about 1.2 eV which is close to the electrical and optical band gaps. Consquently, luminescence transitions occur mainly between localized states in the tails of the conduction and valence bands.

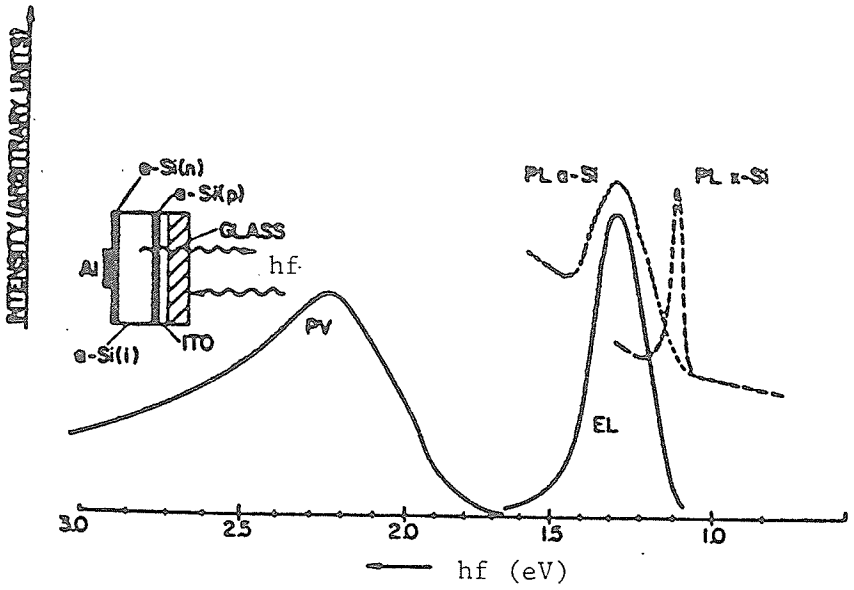

Figure 2.20: Spectra of electroluminescence, photoluminescence, and photovoltaic collection efficiency obtained in a-Si at 78 K. The photoluminescence spectrum of crystalline Si is shown for comparison. The inset shows the structure of the p-i-n diode [25].

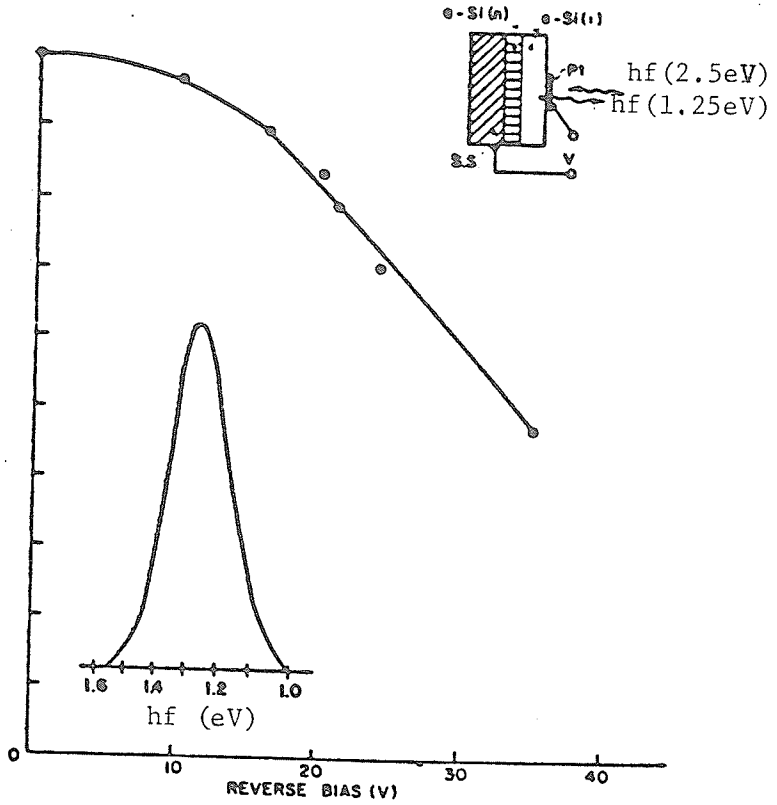

Figure 2.21: Quenching of photoluminescence as a function of reverse bias across the Schottky barrier in a-Si. One inset shows the structure of the diode; the other inset shows the photoluminescence emission spectrum [25].

Figure 2.22 shows that the photoluminescence intensity increases about two orders of magnitude when the substrate temperature T_s is increased from 50 to 170 C, and then saturates at a constant value. At T_s > 170 C the quantum efficiency is of the order of unity for r.f. glow-discharge grown a-Si [26]. At T_s = 100 C the photoconductivity efficiency increases twice as rapid as compared to the luminescence efficiency and saturates at T_s > 300 C. It is argued that photoconductivity is proportional to N_r^{-2}, whereas photoluminescence is proportional to N_r^{-1} where N_r is the density of recombination centers. Note that T_s, the substrate temperature, is correlated with N_r.

The photo-luminescence intensity as shown in Figure 2.23 decreases with temperature at temperatures above 80 K with an activation energy of 0.12 to 0.13 eV, indicating an activated non-radiative recombination process. The excess carrier concentration determinded from photoconductivity and drift mobility is constant in this temperature range. This implies that the process governing the decay of luminescence and photoconductivity must be different. The activation energy of the radiative recombination can be interpreted as the binding energy of the most tightly bound pairs with strong correlation between the excited electron and hole by Coulombic interaction (bound electron-hole pair) [26]. It is also worth noting that the activation energy (0.12 eV) depends very little on the frequency of the radiation.

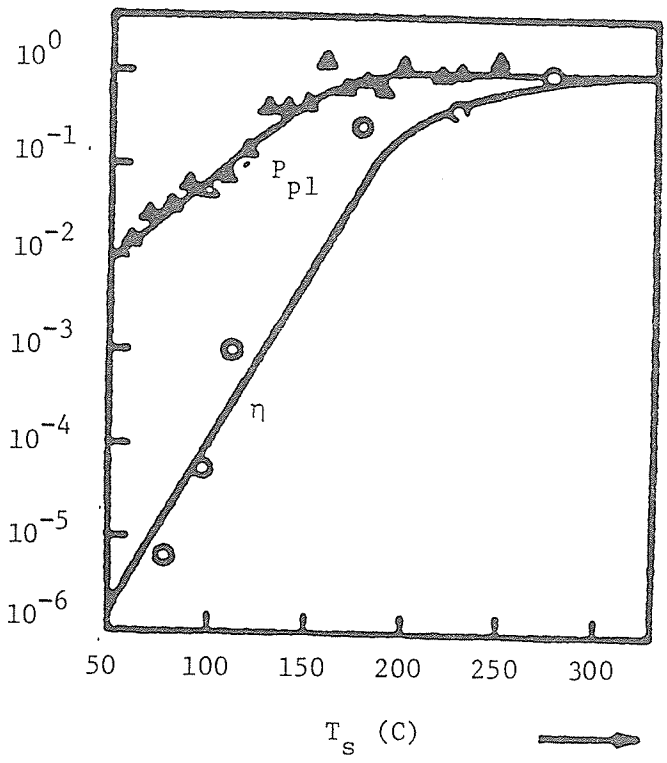

Figure 2.22: Efficiency of luminescence (Δ) and photoconductivity (O) versus substrate temperature for a-Si films [26].

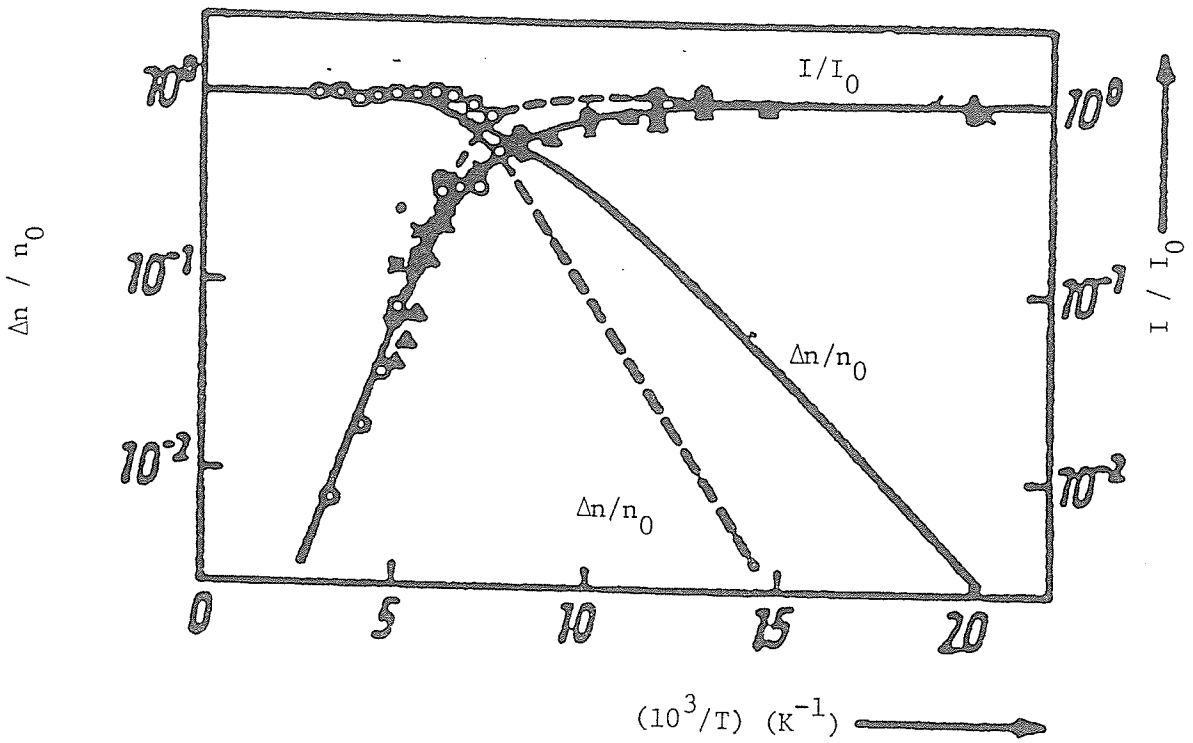

Figure 2.23: Temperature dependence of photoconductivity (□) and photoluminescence for a-Si films. T_s = 520 K (○); 440 K (△); 400 K (●); 320 K (x) [26].

C. Effects of doping on luminescence

Nashashibi et al. [22] have reported that the spectra for photo-luminescence for pure a-Si agrees closely with that of Engemann and Fischer [29], and that doping with phosphorus or boron causes some broadening and a shift of the maximum to a lower photon energy in the photo-luminescence spectra. The most striking effect of doping is the large reduction in the photoluminescence quantum efficiency P_{pl}, especially at low temperatures. At low temperatures ($T < 50$ K) P_{pl} tends to reach a constant value (P_{pl0}) for both phosphorus and boron doping. For temperatures greater than 200 K, P_{pl} in the phosphorus doped samples is somewhat larger than that in the undoped sample. For boron doping, P_{pl} is smaller than that in undoped samples, at all temperatures. Some of the results (note that the phosphorus doped samples are n-type and boron doped samples are p-type) are summarized in Figure 2.24.

For undoped a-Si, the temperature dependence of P_{pl} can be described by a standard expression [22]

$$P_{pl} \propto [1 + \tau_R/\tau_a] \quad , \tag{2.10}$$

where τ_r is the radiative lifetime, and τ_a is a lifetime associated with an activated non-radiative process of the form $\tau_a = \tau_1 \exp(\Delta E/kT)$, with ΔE = 150 meV. Doping is shown to

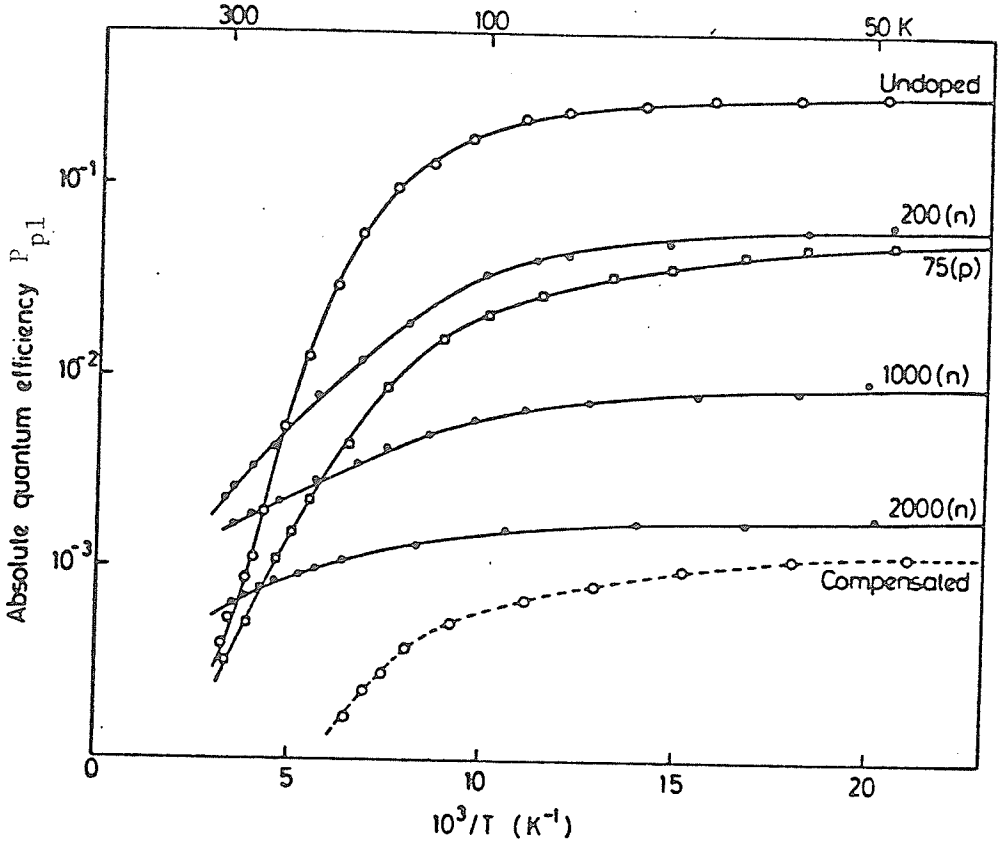

Figure 2.24: Log P_{pl} versus T^{-1} for undoped a-Si, and various n and p type samples (full lines). The doping levels (M) are indicated for each sample. The dashed curve shows data for a compensated sample with M = 1700 p.p.m. of phosphine and 1840 p.p.m. of diborane. All these data were obtained using a photon excitation energy of 2.30 eV [22].

reduce η_0 (Figure 2.24) and this implies the existence of an additional non-radiative process, which is temperature independent for temperatures less than about 50 K. The quantum efficiency P_{pl} can be written as [22]

$$P_{pl} = P_{plc}^{-1} \left[1 + \frac{\tau_R}{\tau_t} + \frac{\tau_R}{\tau_a}\right] \quad , \qquad (2.11)$$

Here it is assumed that a fraction $(1 - P_{plc})$ of the carriers are captured by the non-radiative centers, and also that carriers are removed from an energy state of depth ΔE by a temperature independent, non-radiative process, with a lifetime τ_t.

D. Effects of fabrication conditions on luminescence

The structure and electronic properties of amorphous tetrahedral semiconductors are sensitive to sample preparation and fabrication conditions. In evaporated or sputtered films, the most important variable is the temperature of deposition and annealing. Glow-discharge (plasma) deposited a-Si films can have properties greatly different from those produced by sputtering or evaporation. The most important factor for glow-discharge deposited films in the incorporation of hydrogen which seems to be responsible for an increase in the band gap of the material [27]. Raising the temperature of deposition or annealing in plasma deposited

films appears to have an effect similiar to that in evaporated Si, that is, decreasing the density of localized states.

Street et al. [28], have studied the photo-luminescence of plasma deposited a-Si films as a function of r.f. power, gas concentration, substrate temperature, gas pressure, applied electric field, etc.. In addition to the substrate temperature T_s, r.f. power and the concentration of silane in argon are equally important. These three factors are found to be the most important factors.

Figure 2.25 shows the effects of r.f. power and gas concentration on the luminescence intensity. The peak occurs at 1.4 ± 0.1 eV. As the power increases, the spectrum broadens and the peak shifts to a lower photon energy. The relation between luminescence intensity and r.f. power and silane concentration is given in Figures 2.26 and 2.27. Generally, the intensity decreases according to the same logarithmic dependence on power, for all samples grown at an r.f. power in the range, 1 to 40 W. The intensity increases proportionally to the square root of silane concentration as shown in Figure 2.26.

The luminescence intensity increases with substrate temperature T_s as shown in Figure 2.28. At $T_s > 300$ C the luminescence intensity begins to decrease. Figure 2.29 shows the luminescence spectra versus T_s. At low temperatures, the peak becomes broad and shifts to a low energy. A sim-

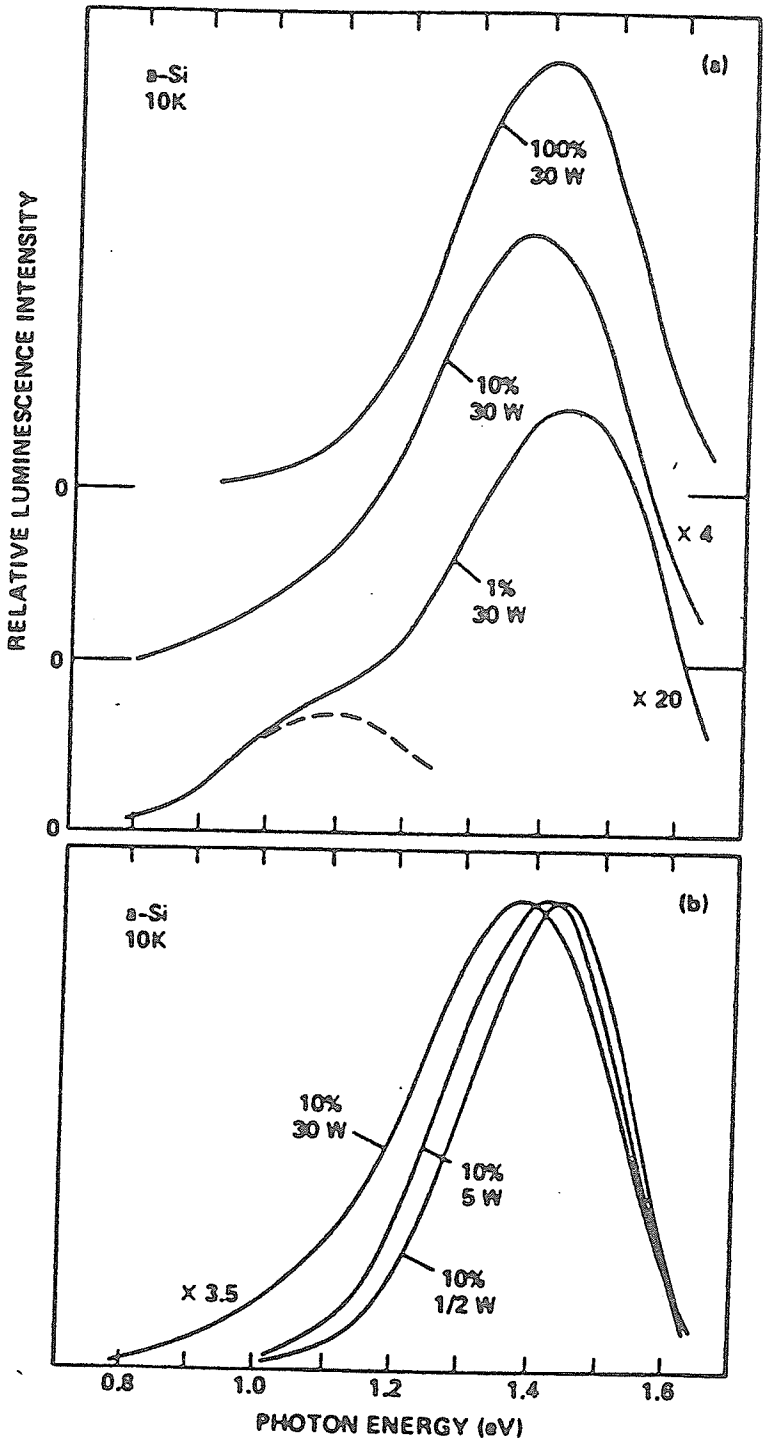

Figure 2.25: (a) Luminescence spectra of a-Si films deposited at 30-W r.f. power and different gas concentrations. The dashed line represents the shape of the luminescence peak responsible for the low-energy shoulder in the spectrum. (b) Luminescence spectra for films with the same gas concentration (10%) but different power. Substrate temp. = 230 C, gas press. = 0.15 torr, flow rate = 140 cm /s [28].

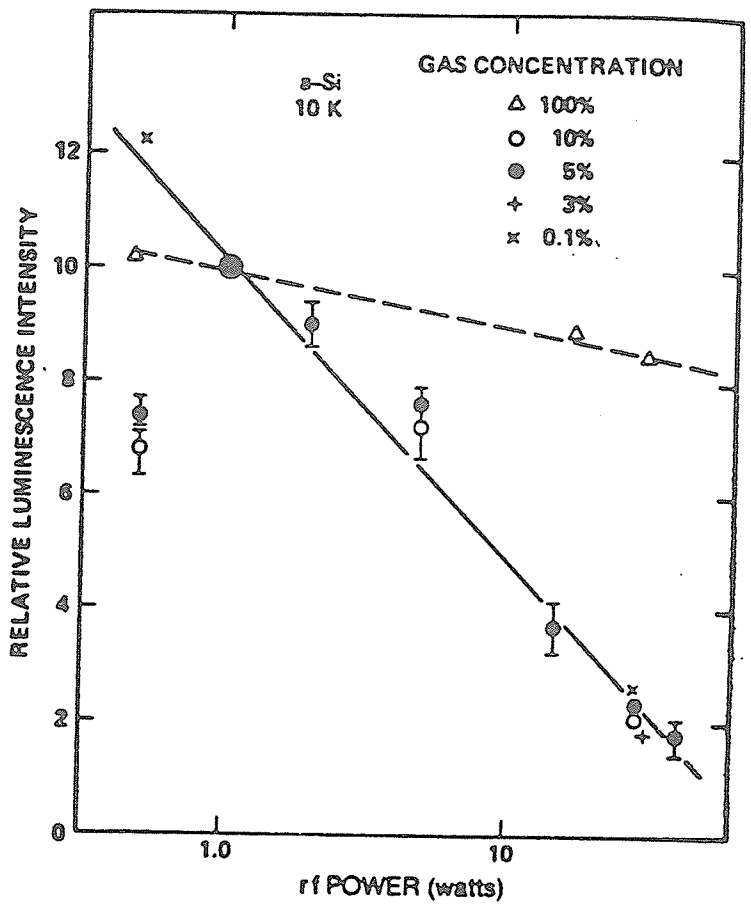

Figure 2.26: Relative change in luminescence intensity with deposition power for a-Si films. For each gas concentration the intensities are normalized to the value at 1 W. The variation with gas concentration is shown in Figure 2.27 Substrate temp. = 230 C, gas press. = 0.15 torr, flow rate = 140 cm /s. [28].

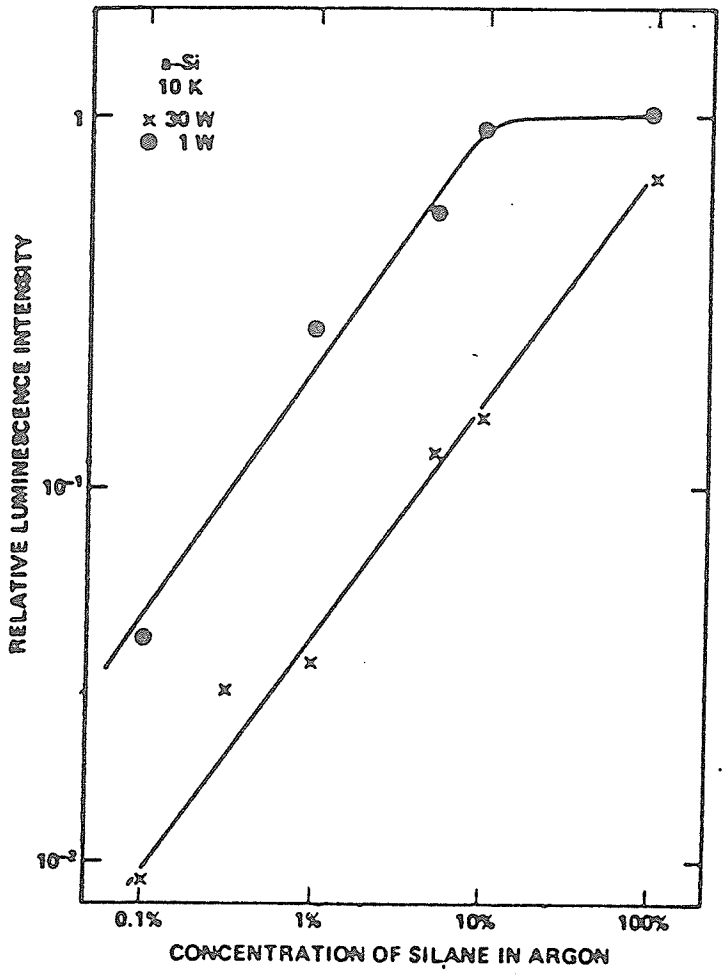

Figure 2.27: Variation of luminescence intensity with gas concentration for two values of r.f. power (1 w and 30 W) for a-Si films. Substrate temp. = 230 C, gas press. = 0.15 torr, flow rate = 140 cm /s. [28].

iliar effect has also been reported by Engemann and Fischer [29] who found also additional luminescence peaks near 1.1 and 0.9 eV.

The dominant luminescence is associated with recombination of electron-hole pairs that are presumed to be in band tail states at the respective band edges [30]. The evidence for not associating the peak with recombination at defects is due partly to the fairly high luminescence energy as compared with the band gap, and partly, to the strong decrease in luminescence intensity because of the introduction of defects [31]. Any defect states are primarily non-radiative. Furthermore, in the majority of luminescent materials, non-radiative transitions proceed through deep localized states. However, the measurement of the luminescence intensity is a useful technique for the study of the density of localized states in the forbidden gap [28]. Since a change in luminescence intensity is the result of variation in the localized state density, any properties which involve states in the gap will show a dependence on these parameters. Possibly luminescence measurements can be used to characterize various samples fabricated by different techniques.

The effects of fabrication conditions can be clearly seen by comparing luminescence measurements of different groups. Engemann and Fischer [29] observed the dominant peak at 1.25 eV, with other lines at 1.1 and 0.92 eV, while Spear et al. [23] observed only a main peak at 1.3 eV but lower peaks

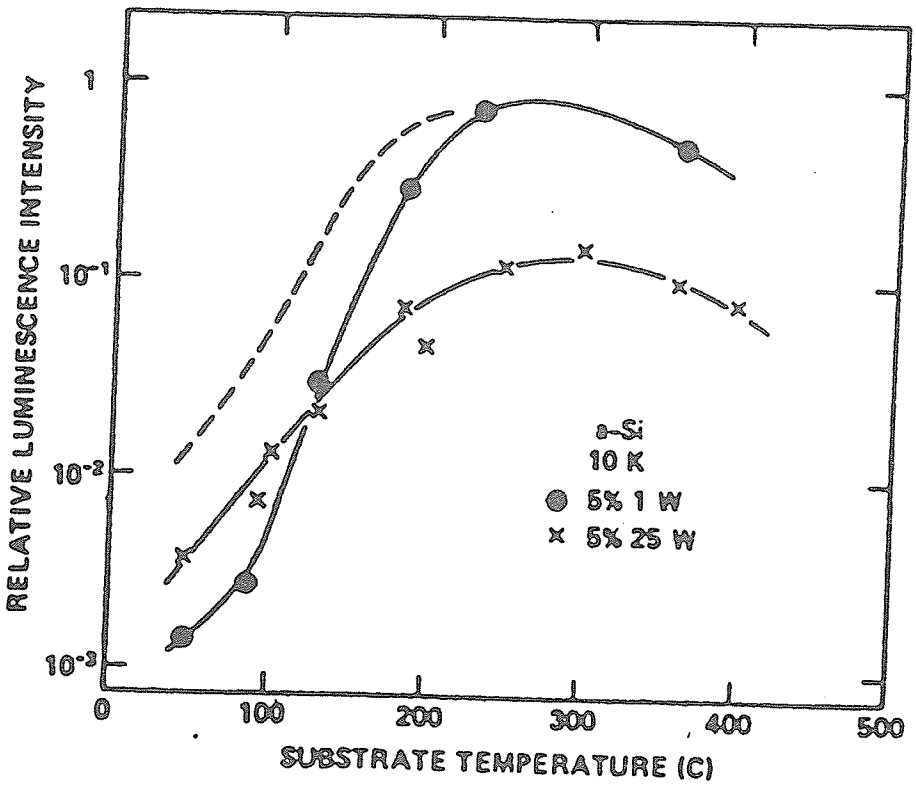

Figure 2.28: Dependence of the luminescence intensity on substrate temperature for 1-W and 25-W a-Si samples of 5% gas concentration. The dashed line illustrates the dependence observed by Ref. 29. Gas press. = 0.15 torr, flow rate = 140 cm /s [28].

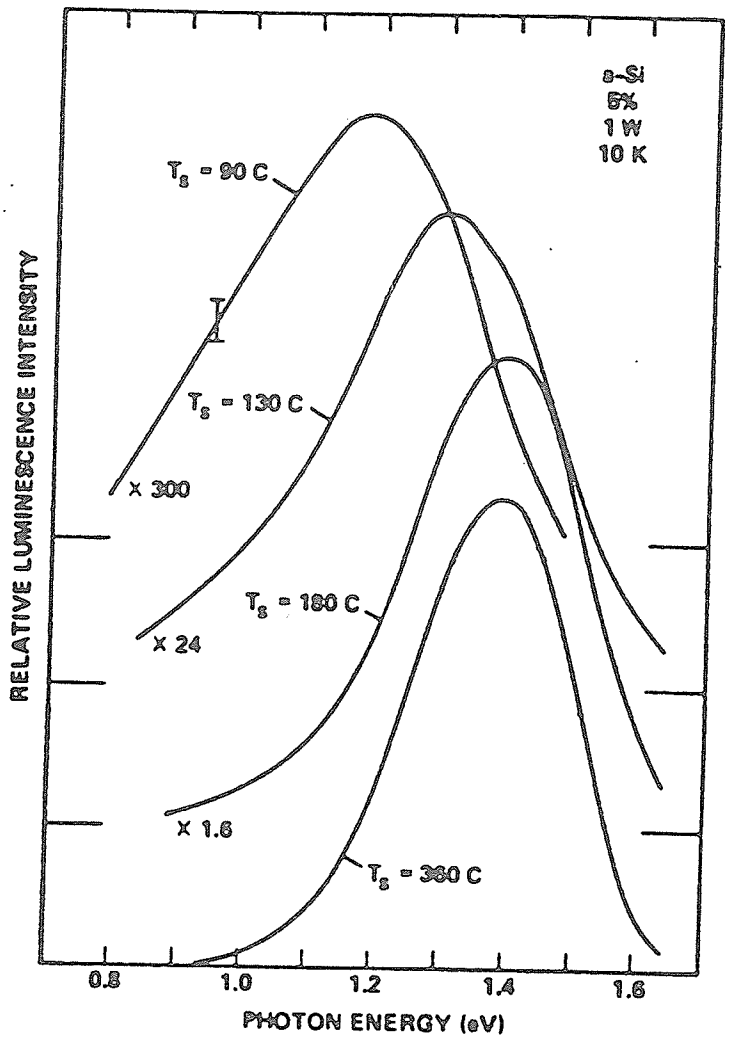

Figure 2.29: Luminescence spectra of a-Si samples for the various indicated substrate temperatures, T_s. Gas press. = 0.15 torr, flow rate = 140 cm /s [28].

were not observed. On the other hand, Pankove and Carlson [25], observed a luminescence peak at 1.44 eV for a-Si films fabricated in SiH_4-H_2 gas mixtures. Also, silicon samples reactively sputtered in hydrogen give luminescence spectra different from that obtained from glow-discharge samples [32].

Possible mechanisms have been put foward [28] for the systematic shifts of the luminescence peak and they are:

(a) The band gap may vary with deposition conditions, the most obvious way being the change in the hydrogen content as mentioned earlier [27].

(b) The distribution of zero-phonon energies for the luminescence transition could change, for example, because of a change in shape of the band tails.

(c) An increase in the electron-phonon coupling strength would broaden the spectrum and shift the peak with respect to the zero-phonon energy. Optical absorption measurements indicate that the shift in luminescence is due to an increase in the strength of the electron-phonon coupling while the zero-phonon energy remains unchanged [28].

E. Theory of luminescence

Excited carriers that form pairs bound together by Coulombic forces are responsible for luminescence whereas dissociation of such pairs leads to photoconductivity and non-radiative recombination. The fact that the luminescence

properties of a-Si could only be explained by monomolecular recombination, suggests a strong correlation between electrons and holes after excitation. A decay rate proportional to the bound pair concentration is in keeping with monomolecular recombination kinetics [26]. It is also speculated that the incorporation of a high concentration of hydrogen in a-Si (about 0.1 molar % for deposition at 400 C) provides a high density of neutral centers which can capture electron-hole pairs to form bound excitons [25].

It has been found that the photo-luminescence in glow-discharge grown a-Si shows an activated behaviour as shown in Figure 2.30. The activation energy depends very little on the frequency of radiation [18]. In a bound electron-hole pair model for photoluminescence, Mott [18] has derived an expression for the number of photons emitted per quantum absorbed as

$$P_{pl} = 1 \; / \; [1 + (\omega'/A') \exp(-W/kT)] \quad , \qquad (2.12)$$

where ω' is the chance per unit time that the bound pair will recombine, A' is the chance per unit time of radiation for each pair of carriers and W is the bonding energy of the electron-hole pair. In Figure 2.30 the dotted curve is calculated from Equation (2.12) with $A' = 10^{8}\ s^{-1}$ and $\omega' = 10^{12}\ s^{-1}$. The solid curve is the data of Engemann and Fischer [26] as shown in Figure 2.23.

Mott [18] has also analyzed the electroluminescence based on the bound pair model. The chance that an electron radiates is [18]

$$P_{el} = (n / N_{rc}) (A' / [A' + \omega' \exp(-W/kT)]) \quad , \quad (2.13)$$

where n is the number of carriers per cm^3 contributing to electron and hole current. N_{rc} is the number of charged recombination centers per cm , with cross section for trapping holes, S_h.

Pankove and Carlson [25] have suggested that the electron-hole pair is an exciton bound to a neutral defect, because the most probable transition energy is 1.28 eV, which is lower than the mobility gap (1.55 eV). Mott [18], however, has suggested that the lowest localized band edge state in the conduction band is about 0.2 eV below the mobility edge, and if it is assumed that the same range of localized states exists for the valence band, then the emitted intensity for a pair of carriers in band-edge states with Coulombic energy 0.12 eV should be 1.55 - 0.4 - 0.12 = 1.03 eV, somewhat lower than the most probable energy of radiation so far observed, but corresponding to the lower limit of the electroluminescence band. The emission may not be associated with any specific defects as previously suggested.

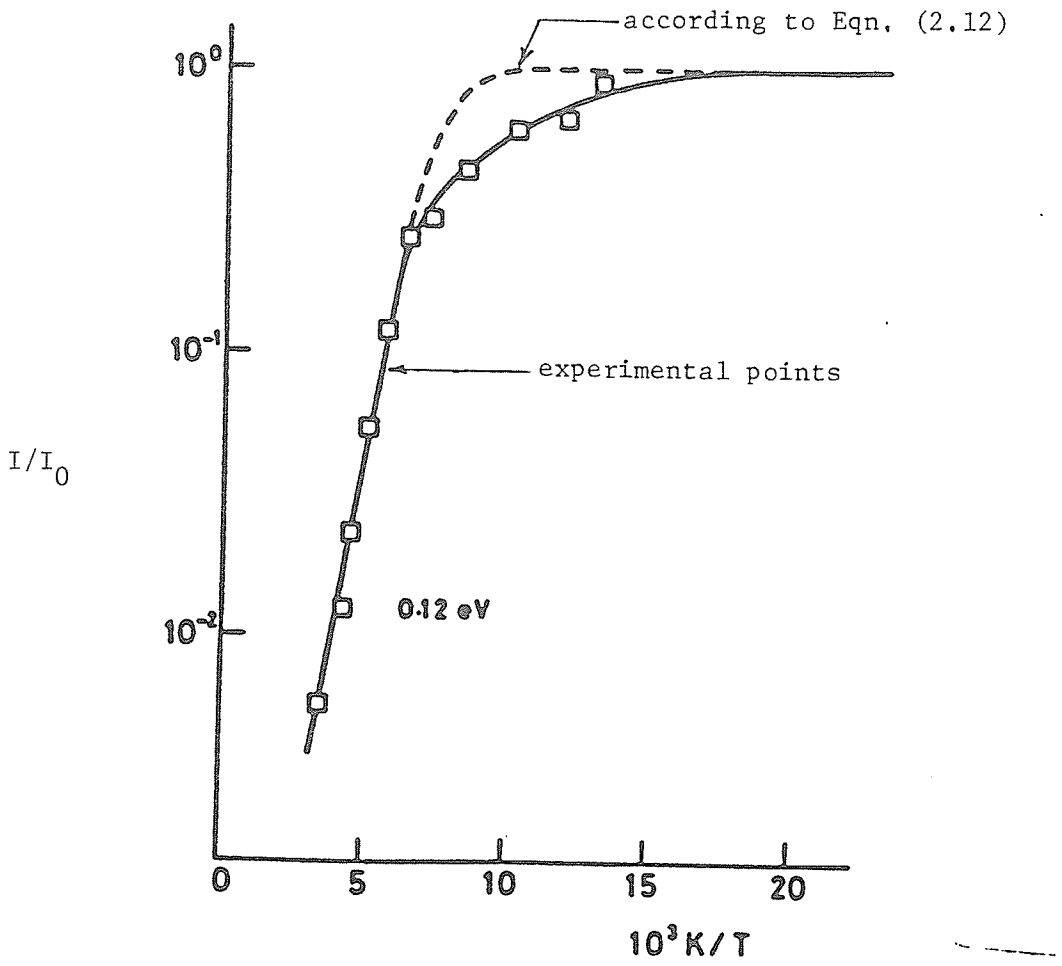

Figure 2.30: Intensity of photoluminescence as a function of 1/T for glow-discharge deposited a-Si [18].

We have mentioned previously that for either boron or phosphorus doped glow-discharge a-Si samples the quantum efficiency of the photo-luminescence is reduced by doping [22]. This is explained as due to the field-quenching mechanism based on ionized donors and defects [22]. The quantum efficiency of the photo-luminescence, P_{p10}, at absolute zero temperature, falls with phosphorus doping (n-type) because of the electric fields set up by ionized donors, N_D^+, and occupied (charged) lower lying defect states and tail states. Engemann and Fischer [33] have shown that P_{p10} in undoped a-Si is greatly reduced by external electric fields of order 10^6 V/cm.

2.1.3 Photoemission

There is relatively little work done on photoemission in a-Si [34-38]. Peterson et al. [34], have studied photoemission in a-Si films prepared by a sublimation technique. Figure 2.31 shows that the yield of all a-Si films is higher than that for crystals. This is to be expected since the work function of a-Si is about 4.4 eV, which is lower than that of crystalline Si, which is 4.73 eV. The yield decreases exponentially towards lower photon energies. It is impossible to fit the amorphous yield data to a power law near threshold as is done for crystals. Figure 2.32 shows the energy distribution of a-Si films are compatible with the existence of an exponential tail in the density of states between the valence band and the Fermi level.

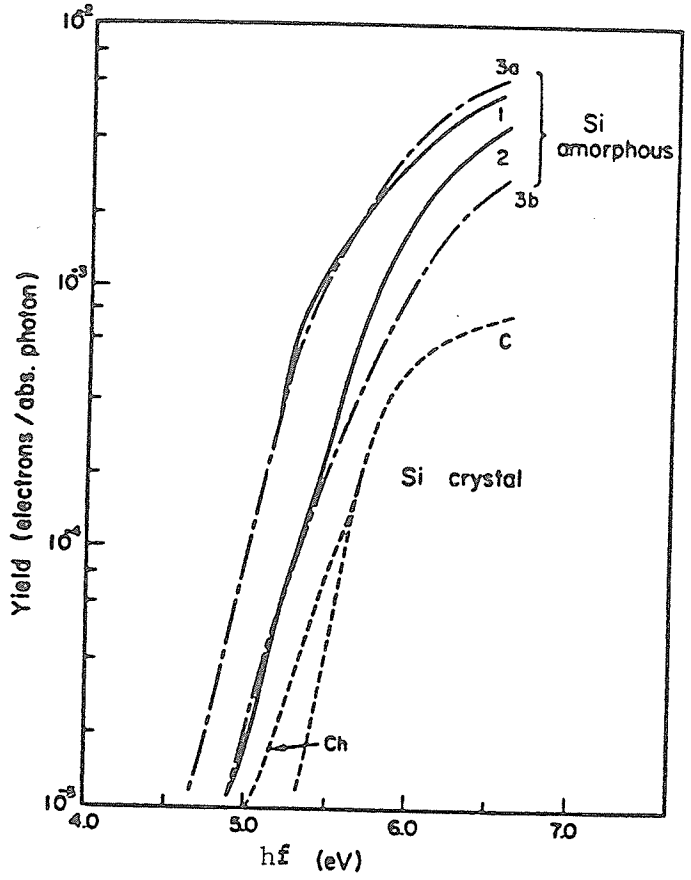

Figure 2.31: Photoelectric yield spectra of amorphous and crystalline silicon. C: cleaved Si; Ch: cleaved and heated; 1,2,3: amorphous films; 3a, as deposited; 3b, after mild heating [34].

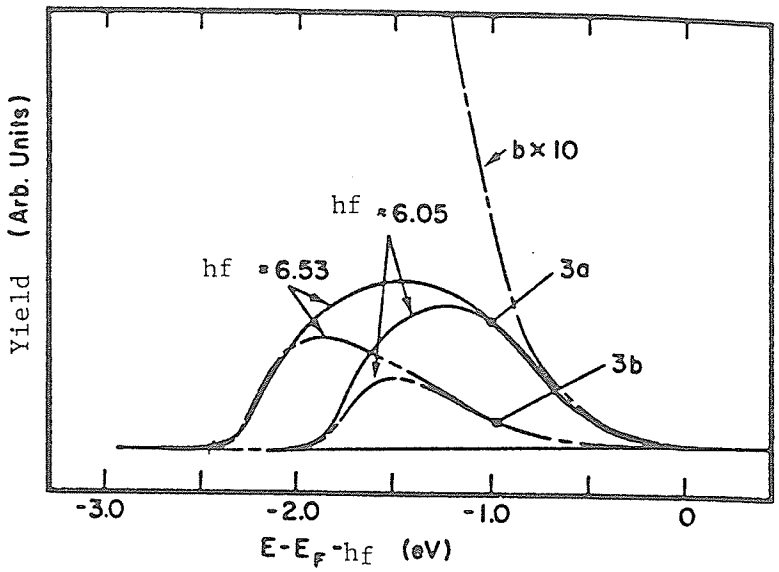

Figure 2.32: Energy distributions of a-Si film before and after heat treatment at two different photon energies hf. Curves 3a: freshly deposited films; curves 3b, after mild heat treatment. These curves were obtained from the film giving the yield spectra 3a and 3b in Figure 2.31 [34].

Fischer and Erbudak [35] have also obtained similiar photoemission results for a-Si, which supports the tailing in the density of states. Their results do not agree with the arguements of Pierce and Spicer [36,37]. Pierce and Spicer [36] compared photoelectron energy distribution curves for a-Si with those of an Au film and crystallized Si and found no evidence for tailing of the density of states for slowly evaporated films.

2.1.4 Effects of Film Fabrication Conditions on Optoelectronic Properties

As stated earlier, the electical and optical properties of a-Si films are strongly influenced by both the method of preparation and the film fabrication conditions. Thermal evaporation [37,39-42,43-45], sputtering [46-48], or the glow-discharge decomposition of silane [4,11,14,45,49,50] are possible techniques for the production of a-Si films.

Discharge-grown a-Si films may contain up to an estimated concentration of 50 atomic percent of hydrogen [51]. Many, but not all, of the properties of a-Si are directly related to the prescence of bonded hydrogen. Apart from its ability to reduce the density of localized states by saturation of dangling bonds, the influence of hydrogen on the transport and recombination mechanisms is not yet clearly understood. The more important factors in discharge grown samples appear to be, the type of discharge and the substrate temperature during deposition (T_s) [5], in determining the optical and

optoelectronic properties. The localized states and recombination centers are affected by the type of discharge and T_s. For T_s greater than 300 C, the a-Si films grown in an r.f. glow-discharge exhibits bimolecular recombination, while those grown in a d.c. glow-discharge exhibit recombination dominated by gap states with an exponential or quasi-exponential distribution. This indicates that the kinetics of the discharge used is an important parameter in determining its electronic properties. Glow-discharge grown a-Si films are characterized by high resistivity, up to 10^{10} Ω-cm [52-54], good photoconduction properties [52-54], low junction space-charge densities ($<10^{16}$ cm^{-3}) [52], and a high optical bandgap which is nominally 1.7 eV, but can be in the range 1.5 to 1.9 eV depending on controllable experimental conditions. For discharge-grown a-Si films [5], the optical band gap decreases and the absorption coefficient increases as the deposition temperature is raised or after proper annealing of the films.

Amorphous Si films produced by evaporation or sputtering methods in the abscence of hydrogen [46,55] are characterized by low resistivity (about 10^3 Ω-cm) for as-prepared films, a band gap of 1.2 to 1.44 eV [46], and poor photoconductivity. For those films, the resistivity and band gap increase and the optical absorption coefficient decreases after thermal treatment.

The poor properties of sputtered a-Si films, such as low resistivity, poor photoconductivity and poorly defined optical band gap of about 1 eV, have been attributed to a high density of dangling bonds resulting in a high density of localized states. However, the electrical and optical properties of sputtered a-Si films can in fact be varied over a wide range, and properties similiar to those of glow-discharge grown films can be realized [56]. Amorphous silicon films prepared by sputtering in Ar/H_2 gas mixtures fall in this category of films. Thus it appears that glow-discharge grown films are not unusual or distinct in their properties from sputter-deposited films. Reduction of the number of localized states by appropriate selection of depositions can shift the Fermi level away from the mobility edge for electrons and toward the center of the band gap, resulting in higher conductivity activation energies and corresponding lower conductivities. The photoconductive response of the films is intimately related to the density of localized states. Films prepared in the presence of H_2 exhibit good photoresponse, indicating the saturation of dangling bonds by hydrogen is responsible for the low density of localized gap states in decomposed silane a-Si, rather than other mechanisms unique to that particular deposition technique.

2.2 AMORPHOUS GERMANIUM

Transport in amorphous Ge films proceeds by two qualitatively different mechanisms [57]:

(1) Motion of conduction band electrons and valence band holes among the states intrinsic to the network. This mechanism is dominant at relatively high temperatures.

(2) Transport, by tunneling and/or hopping, of carriers between extrinsic states with energies in the bandgap. Sputtered films contain a distribution of voids of the order of 5 to 10 Å diameter as determined from structural measurements [58]. Optical, transport, and electron-spin-resonance measurements have indentified that the majority of bandgap electrons are those associated with these internal void intersurfaces [59,60].

Deposition or annealing at high temperatures [60], decreases the low-temperature conductivity, which is consistent with a reduction in the localized state density and a decrease in the void volume. Hydrogenated a-Ge films can have properties quite different from those of unhydrogenated a-Ge [61,62]. This is interpreted as being due to a reduction of localized states as a result of the strong bond formed between hydrogen and Ge on void surfaces. Paul[63] has discussesd the influences of hydrogen on recombination and the Ge-H bonding- and antibonding-state energies. For highly hydrogenated samples, the possibility of changes in the valence and conduction band density of states needs to be examined.

The photoresponse of a-Ge is generally much smaller than that of a-Si. As a result, photoconductivity studies are rather limited [64-68] and less well understood. Absorption measurements for evaporated a-Ge films have been reported [64,69-71]. Figure 2.33 shows the spectral dependence of the photoconductivity for 800 Å films [64]. The threshold region at low photon energies is not sharp. The results were similiar no matter whether the films were deposited in ultra-high vacuum or in standard vacuum (about 10^{-6} torr). The effect of annealing was to shift the threshold to higher photon energies but no sharpening of the edge is observed [64,72]. The same effect can also be obtained by raising the substrate temperature [72]. The photoconductive response ($\beta\mu\tau \simeq 10^{-10}$ cm^2/V) is reported to be less than the dark conductivity in evaporated a-Ge [73]. Ellipsometric measurements of the optical constants on evaporated a-Ge films in the range of interband transitions have been reported [74]. The results indicate transitions between the initial and final states with an energy gap of about 1.5 eV. Energy dependent densities of states and/or matrix elements are used to explain the measured optical constants for photon energies greater than 3.0 eV.

Figure 2.34 shows the effective number of electrons involved in transistions up to energy hf for sputtered a-Ge films [75]. The value for the effective number of electrons reach about 1.85 electrons per atom at 4.5 eV for both

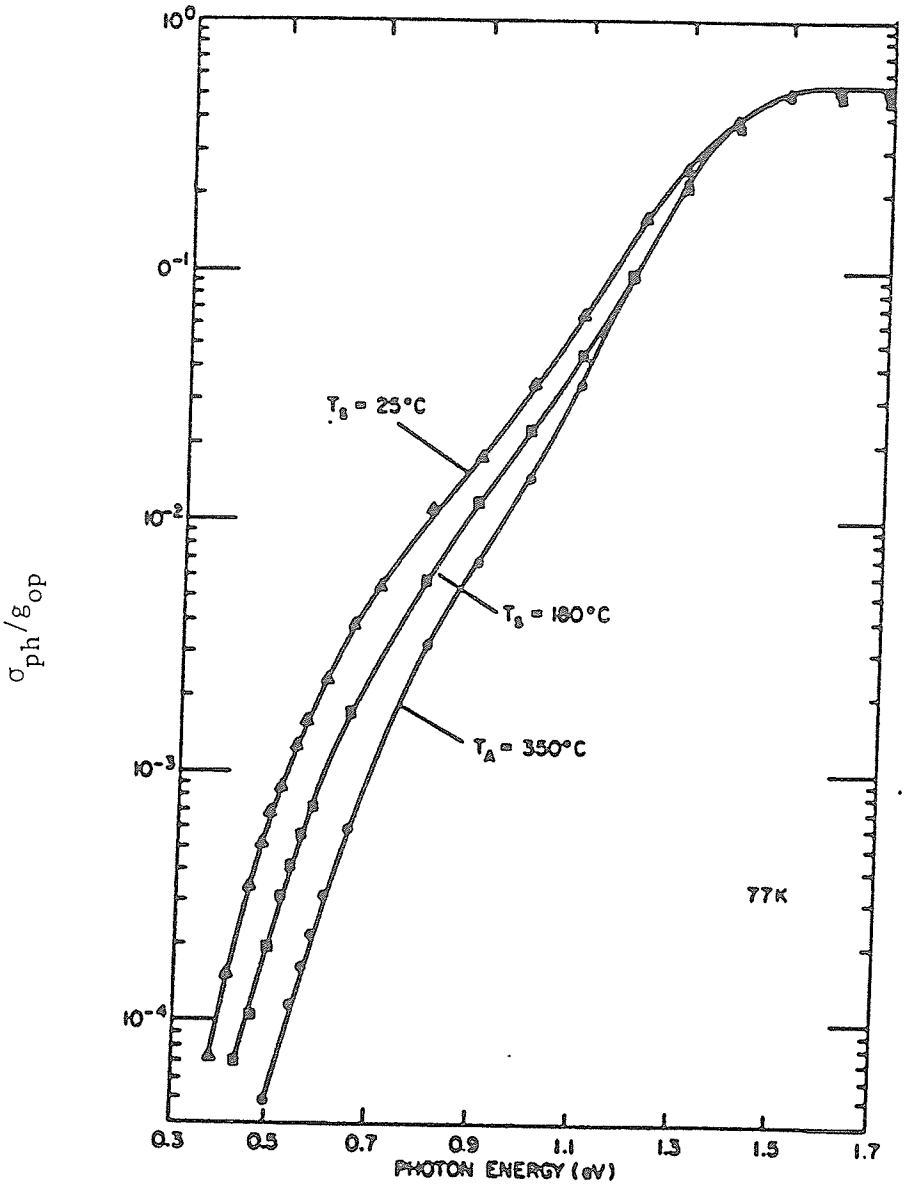

Figure 2.33: Spectral dependence of the photoconductivity per incident photon for evaporated a-Ge films. Curves were normalized to a value of $\sigma_{ph}/g_{op} = 0.5$ at a photon energy of 1.5 eV. The triangles and squares are data for ultra high vacuum films deposited at substrate temperatures T_s of 25 C and 180 C, respectively, and measured in situ. The circles are for a film deposited in standard vacuum and annealed after air exposure to 350 C [64].

amorphous and crystalline Ge. The absorption edge of hydrogenated a-Ge produced by sputtering is shown in Figure 2.35 [62]. The incorporated hydrogen forms bonds with individual dangling bonds on void surfaces in the films. The absorption edge position and, to a lesser extent, its shape are dominated by the effects of voids [76]. The effect of annealing on hydrogenated-sputter-produced a-Ge suggests that annealing produces absorption edge shifts by dangling bond removal and by network reorganization.

Moustakas et al. [63], have reported the steady state and transient photoconductivities as functions of photon energy, light intensity and temperature on a series of a-Ge(H) films, deposited by r.f. sputtering. The dependence of the photoconductance on light intensity is shown in Figure 2.36. For the hydrogenated films the photoconductance varies linearily with light intensity at room temperature and becomes slightly sublinear at lower temperatures. A similiar light intensity dependence has been reported for evaporated a-Ge [65]. At 298 K, the photoresponse increases with the degree of hydrogenation, while at 77 K, it decreases. Temperature dependence of the photoconductance shows that at high temperatures the photoconductance is thermally activated and at lower temperature, the photoconductance is only weakly temperature dependent. A weak dependence of the photocarrier lifetime on temperature and on hydrogenation is also observed [63].

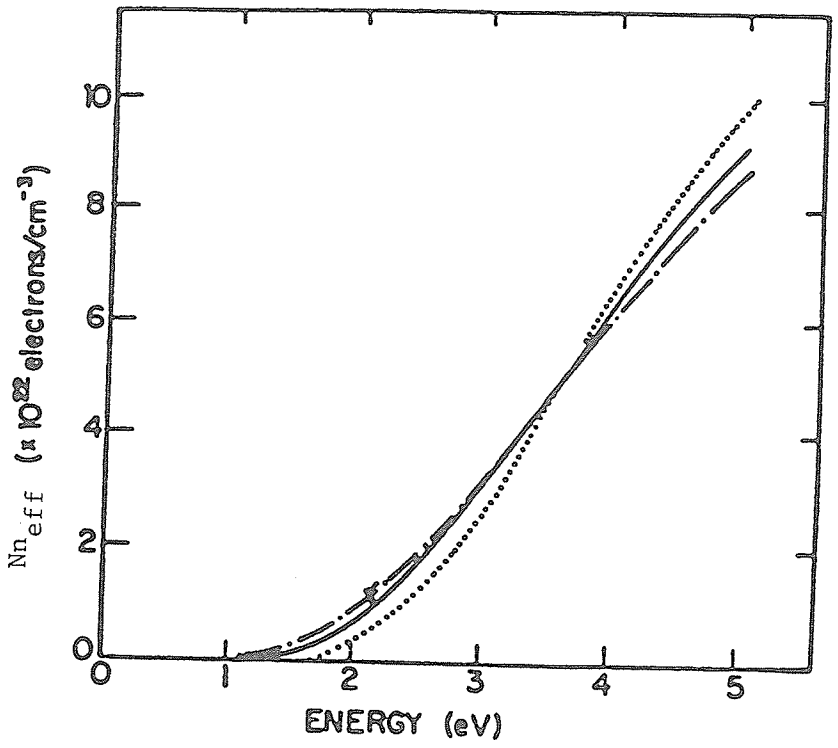

Figure 2.34: The effective number of electrons involved in transistions up to energy hf in a-Ge: sputtered onto substrates at 25 C (—•—) and at 350 C (——); crystalline material (• • •) [75].

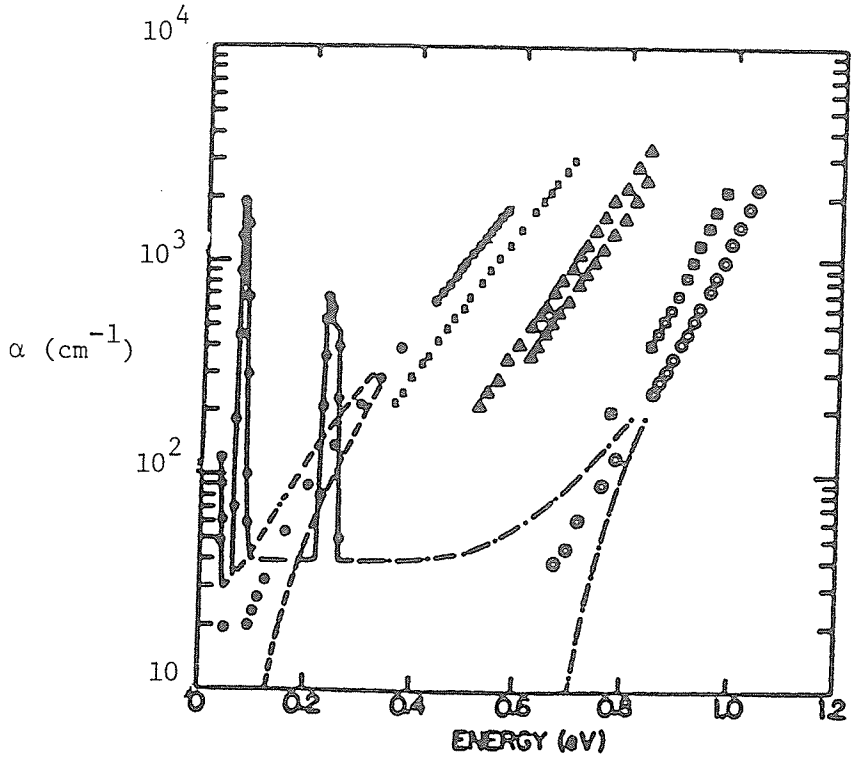

Figure 2.35: Absorption coefficient versus photon energy for $Ge_{1-x}H_x$ films; • • • 0, xxx 0.1, △ 0.028, ▲ 0.03, □ 0.051, and ⬭ 0.08 [62].

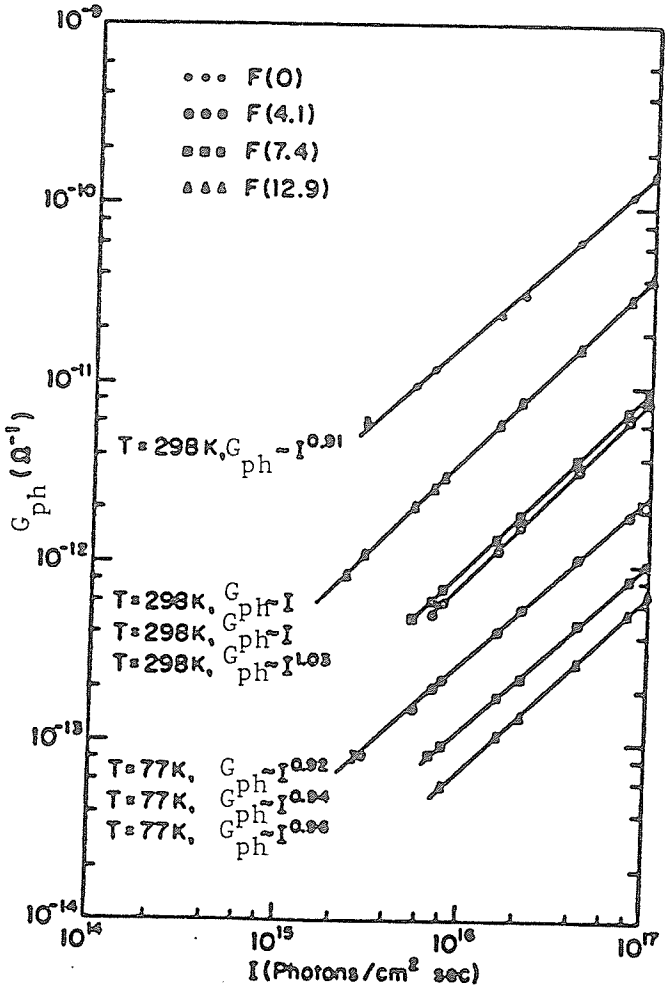

Figure 2.36: Photoconductance of a-Ge films at indicated temperatures, measured at hf = 1.96 eV, versus light intensity [63].

Kramer [77], has reported a theoretical calculation of the complex band structure, the imaginary part of the dielectric constant, and the density of states of electrons for a-Ge using a generalized pseudopotential formalism based on the Green's function techniques. x-ray photoelectron spectra of the total valence band for evaporated a-Ge has been reported by Ley et al. [38]. The results indicate a definite band structure. The results support the theoretical model of Joannopoulos and Cohen [78]. Joannopoulos and Cohen [78], have shown that a short-range disorder model can account well for the density of states and the optical properties of a-Ge. Tsay et al. [79], have also discussed the optical properties and electronic structure of a-Ge in terms of an assembly of atoms with short-range disorder. Theoretical calculations for the absorption edge have also been reported [80].

2.3 AMORPHOUS SILICON - GERMANIUM ALLOY FILMS

The number of studies on $Si_{1-x}Ge_x$ films is extremely limited. Van Dong et al. [2], however, have reported the photoconductivity of hydrogenated amorphous $Si_{1-x}Ge_x$ alloy films grown by sputtering. Figure 2.37 shows the temperature dependence of photoconductivity for various compositions of Ge. The addition of a moderate amount of a-Ge ($x = 0.18$) does not significantly change the photoconductivity except at high temperature. Two activation energies,

one at low (0.06 eV) and the other at high (0.13 eV) temperature, have been observed. In the $J_{ph} \propto I^{\nu}$ dependence (Figure 2.38), the higher value of ν can be attributed to predominantly monomolecular recombination controlled by deep centers and the lower value of ν is interpreted as due to bimolecular recombination controlled by shallow traps. This transistion occurs at x = 0.25 to 0.30.

$Si_{1-x}Ge_x$ films with $x < 0.25$, have properties similiar to those of a-Si(H) [2]. In hydrogenated a-$Si_{1-x}Ge_x$ films containing a moderate amount of Ge (x = 0.18), the energy gap is close to the optimum value for solar photovoltaic cell, and these films may prove to be of interest for photovoltaic conversion of solar energy. Onton et al. [1], have reported the results of optical absorption measurements on hydrogenated a-$Si_{1-x}Ge_x$ films grown by glow-discharge, and they found a linear dependence of the optical gap on alloy composition.

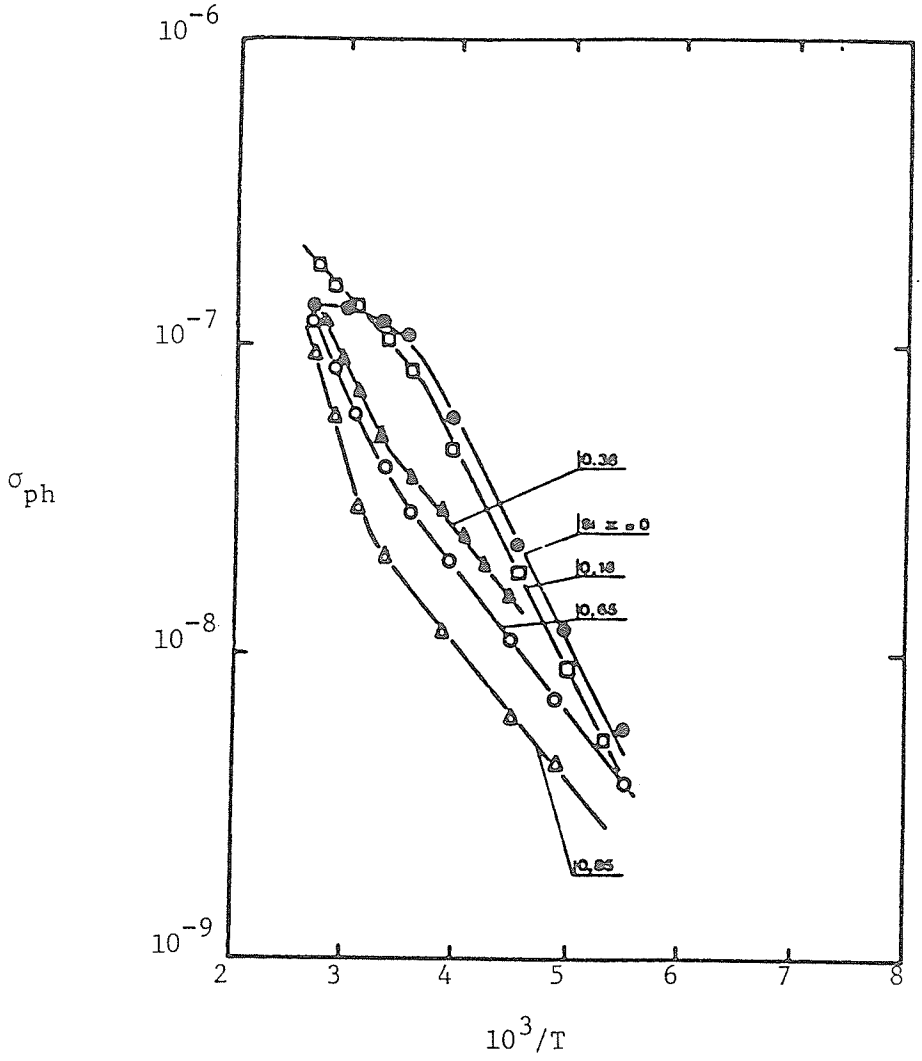

Figure 2.37: Temperature dependence of photoconductivity for hydrogenated $Si_{1-x}Ge_x$ alloys [2].

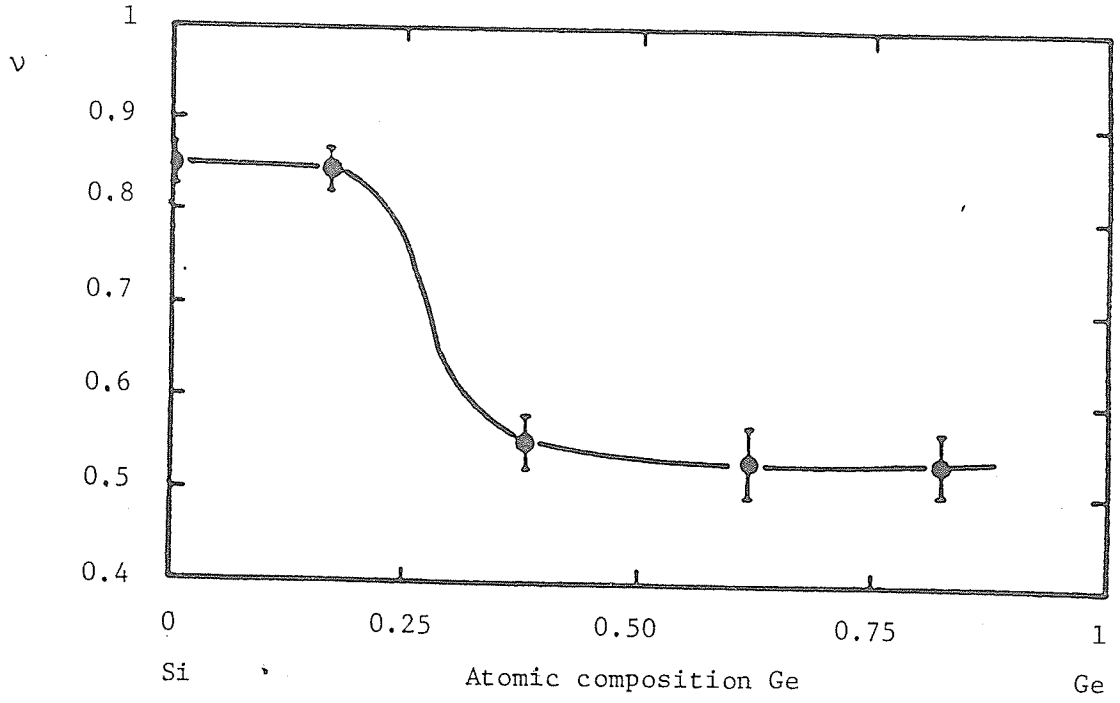

Figure 2.38: The exponent ν in the intensity dependence $\sigma_{ph} \propto I^{\nu}$ as a function of composition x for a-$Si_{1-x}Ge_x$ films [2].

Chapter III

EXPERIMENTAL TECHNIQUE

The samples of amorphous $Si_{1-x}Ge_x$ were prepared by radio-frequency (r.f.) sputtering from a target consisting of Si segments placed on a Ge wafer. Both Si and Ge were of 99.999% purity. The Ge content (x) was varied by varying the total area of the Si segments placed on the Ge wafer. The substrate was a glass plate coated by a sputter-deposited Mo film which served as a bottom electrode. The substrate temperature was 225 C and the sputtering atmosphere was Ar (75%) + H_2 (25%) at a pressure of 6×10^{-3} torr at an r.f. power of 210 W. An aluminum electrode was finally deposited on the top surface of the film to form a sandwich configuration. The electrodes provided nearly ohmic contact up to a field of about 10^4 V/cm. Aluminum and molybdenum electrodes on glow-discharge a-Si films can provide, respectively, ohmic contacts for hole and electron injection up to a field of 8×10^3 V/cm [81].

During photoconductivity measurements both positive and negative polarities of applied voltage were used. Reference to a positive applied field, (+)F, means that the illuminating top Al electrode is at a positive potential with respect to the bottom electrode. Likewise, negative applied field,

(-)F, would mean the illuminated Al electrode is at a negative potential with respect to the non-illuminated bottom electrode.

The photocurrent was measured using the arrangement as shown in Figure 3.1. The current amplifier used was capable of measuring a time constant as low as 10 μs which was much lower than the decay time of the photocurrent. Two different light sources were used to excite the samples. A He-Ne laser supplied red light of wavelength λ = 632.8 nm (hf = 1.96 eV) and a light emitting diode supplied infrared light of wavelength λ = 940 nm (hf = 1.32 eV). By measuring the output of each light source and calculating the power incident on the sample, the incident photon flux was determined.

The photon flux density of each light source was determined by measuring the total radiant power. The distance of the light source to the top electrode of the sample was such that, effectively, all the radiant power was incident on the top electrode. Knowing the total power, the number of photons incident on the top electrode can then be determined. For red light (λ = 632.8 nm) the measured radiant power was 0.44 mW or 0.44×10^{-3} J/s or 2.75×10^{15} eV/s. Since the energy of a single photon is 1.24/0.6328 = 1.96 eV/photon, 0.44 mW is equivalent to $2.75 \times 10^{15}/1.96 = 1.4 \times 10^{15}$ photons/s. The top electrode area is 3.14×10^{-2} cm^2, thus the photon flux density is $1.40 \times 10^{15}/3.14 \times 10^{-2} = 4.47 \times 10^{16}$ photons/s-cm^2.

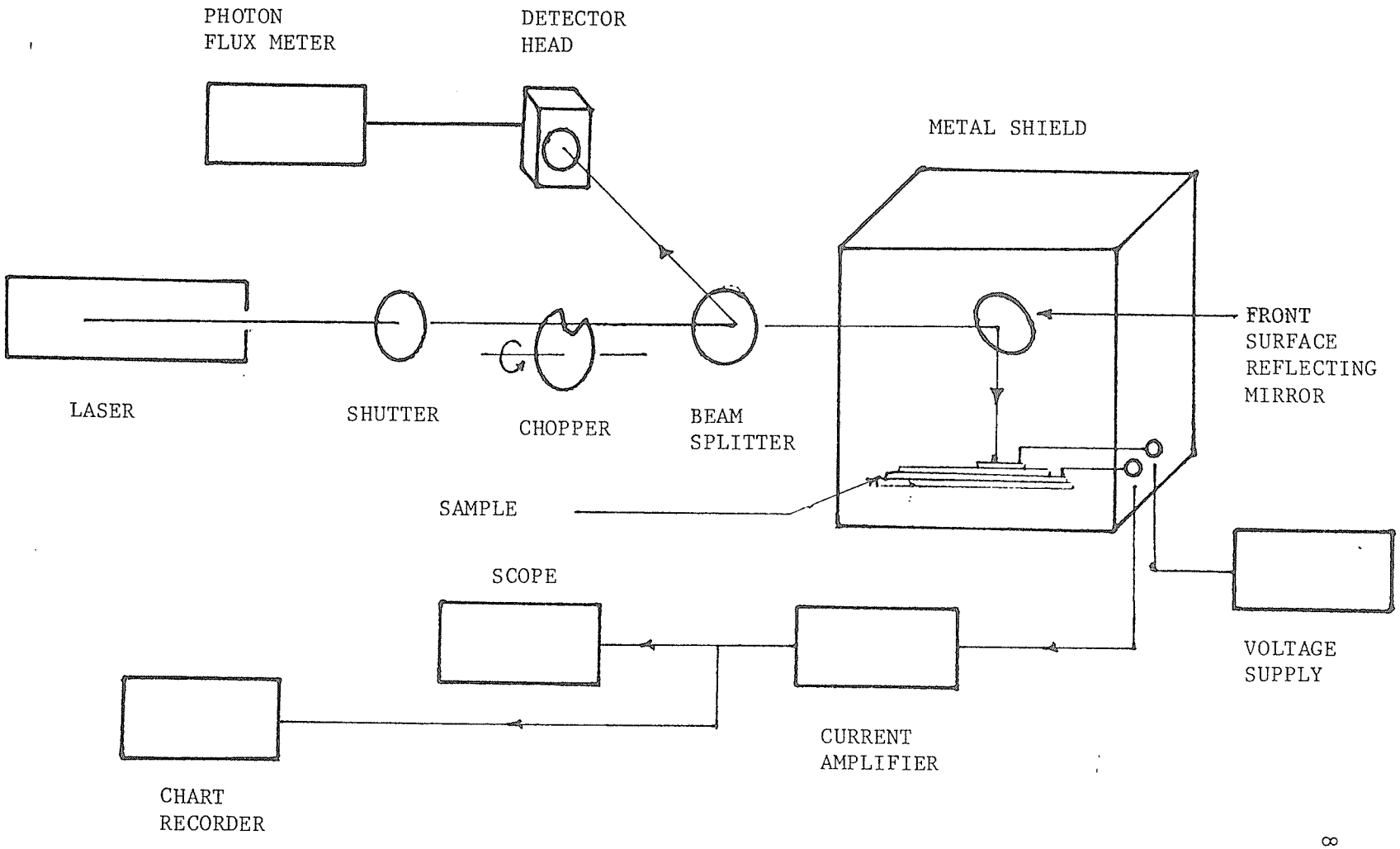

Figure 3.1 Experimental setup.

The photocurrent was measured as a function of applied electric field and light intensity using rectangular light pulses of sufficient duration and separation so as to allow ample time for the transient photocurrent to rise and decay to their steady state dc levels. All measurements were made at room temperature (20 C).

The sandwich cell structure of $Si_{1-x}Ge_x$ film samples is shown in Figure 3.2. For light excitation of wavelength 632.8 nm, most of the light is absorbed in a narrow layer underneath the top electode, since the absorption coefficient α of a-Si is approximately 2×10^4 to 5×10^4 cm^{-1} at 632.8 nm [5,82] for glow-discharge a-Si. Hence we have nonuniform illumination of the sample. The nonuniform distribution of carriers in space under an applied field will give rise to diffusion and drift of nonequilibrium carriers. For light excitation of wavelength 940 nm we would expect the light to be absorbed by the electodes rather than the $Si_{1-x}Ge_x$ film itself. This results in carrier injection into the film from the electrodes rather than photogeneration of carriers from within the film itself.

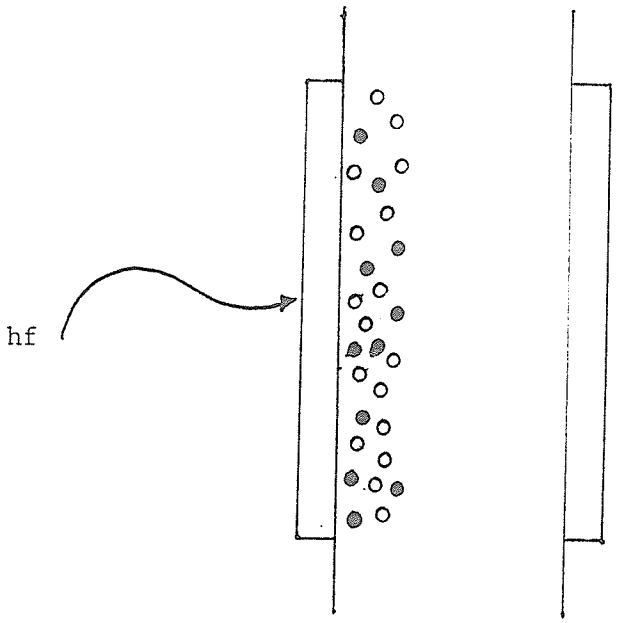

Figure 3.2: Sandwich configuration used for photoconductivity measurements.

Chapter IV

EXPERIMENTAL RESULTS

Transient photoconduction characteristics for hydrogenated amorphous $Si_{1-x}Ge_x(H)$ thin films for x = 0, 0.10, and 0.25 have been measured using a He-Ne laser light of wavelength 632.8 nm (red) and a LED of wavelength 940 nm (infrared). The former is in the high absorption region and the latter in the low absorption region for these films. In this chapter we shall present the results about the waveshapes of the photoresponse, the photoresponse times and the steady state photocurrents as functions of applied electric field and incident light intensity.

In all cases data are presented for (+)F only since data for (-)F is almost identical. The typical waveshape of the transient photocurrent is shown in Figure 4.1. The transient part of the photocurrent consists of two main features which we can call the fast and slow sections. These sections occur on both the rise and fall of the photoresponse. The rising fast section is associated with the initial transit of injected carriers before trapping and space charge become significantly effective . The slow section of the rise is due to the time required for the free carriers and traps to reach a dynamic thermal equilibrium. The fast

potion of the decay is due to free carrier recombination. The slow section of the decay is associated with the time required for trapped carriers to thermalize to the conduction band and fall into the recombination centers. Similiar characteristics have been observed in crystalline solids containing both deep and shallow traps [83].

The response times, τ_r and τ_d, are, respectively, the times required for the photocurrent to rise and to fall to some appropriate level during the slow section of the transient photocurrent. This appropriate level is defined to be 1/e of the difference between the magnitude of the photocurrent at the beginning of the slow section and that at the end of the slow section. The definitions of τ_r and τ_d are illustrated in Figure 4.2. Also defined in Figure 4.2 is the ratio of the fast section to the steady state photocurrent on the rising edge, R_r, and that on the decaying edge, R_d.

In all samples both the response times, τ_r and τ_d, decrease with increasing exciting light intensity for both wavelengths, 632.8 nm and 940 nm, as shown in Figures 4.3 and 4.4. It can also be seen that τ_r is always less than τ_d irrespective of the light intensities used. However, as the light intensity is increased the difference between τ_r and τ_d tends to decrease.

The dependence of the photoresponse time on the applied field is given in Figures 4.5 and 4.6. The photoresponse

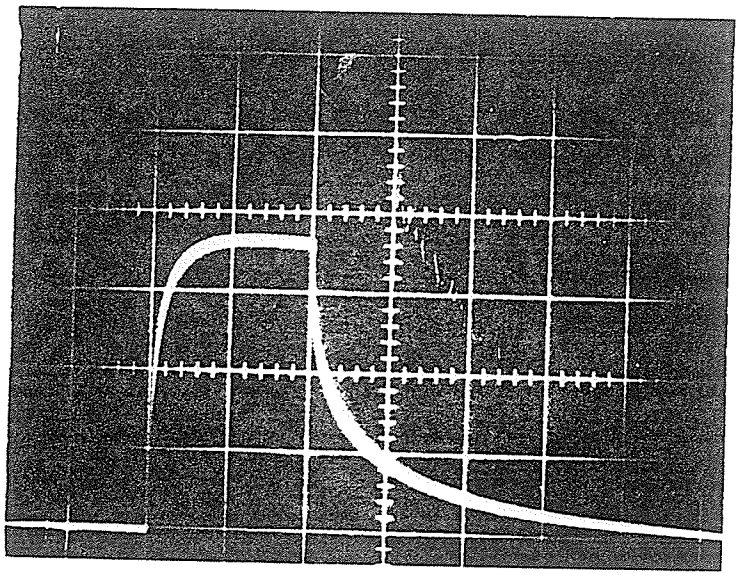

Figure 4.1: Oscilligram of a typical photoresponse for an $a\text{-}Si_{1-x}Ge_x(H)$ film.

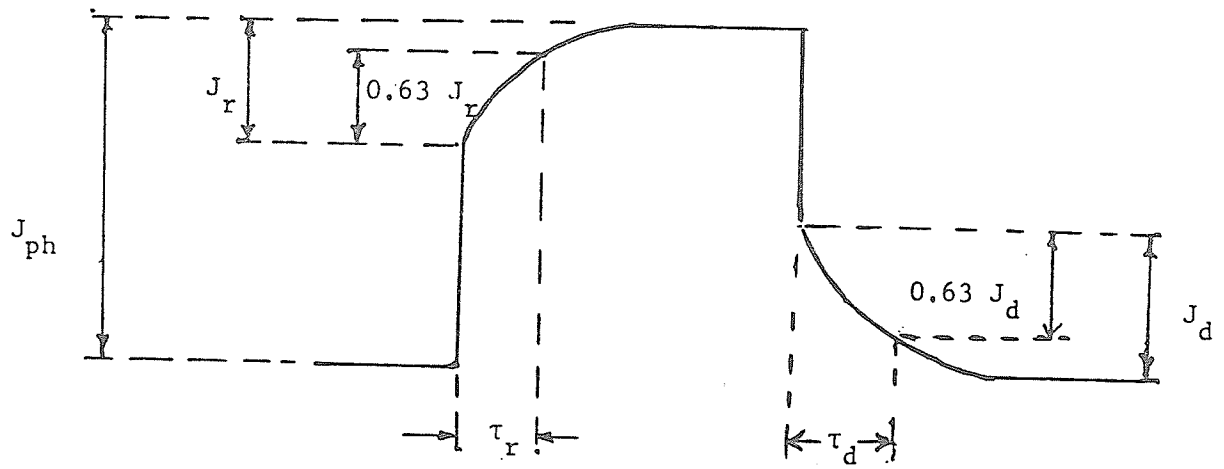

$$R_r = \frac{J_{ph} - J_r}{J_{ph}} \qquad R_d = \frac{J_{ph} - J_d}{J_{ph}}$$

Figure 4.2: Typical photoresponse and definition of response times, τ_r and τ_d, and the ratio of fast section to steady state photocurrent, R_r and R_d.

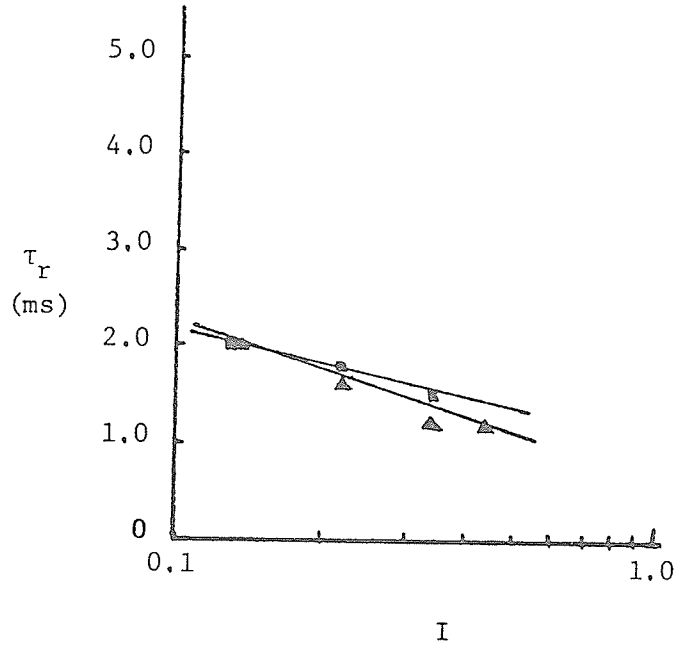

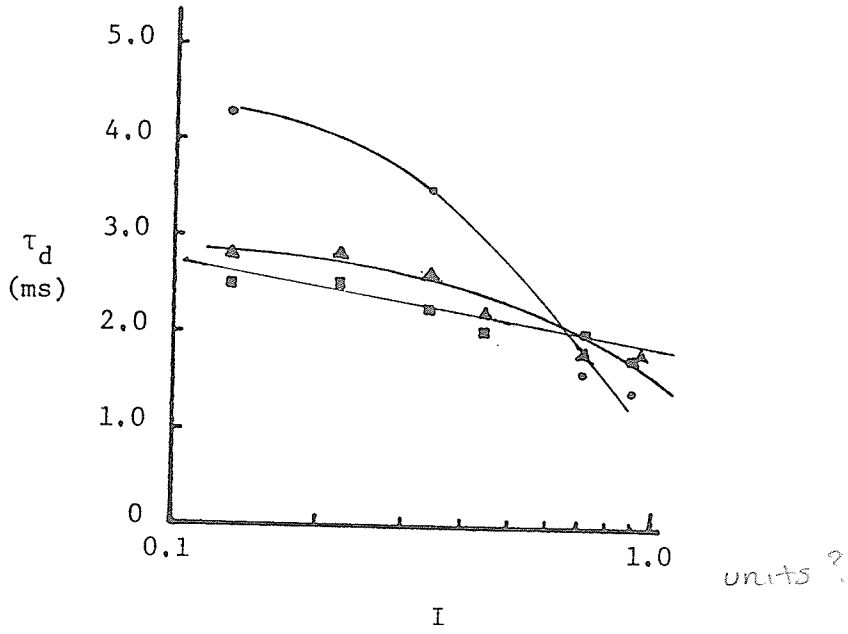

Figure 4.3: Response times, τ_r and τ_d, as a function of relative illuminating light intensity for a-$Si_{1-x}Ge_x$ (H) films. λ = 632.8 nm; F = + 10^4 V/cm; ● x = 0; ■ x = 0.10; ▲ x = 0.25.

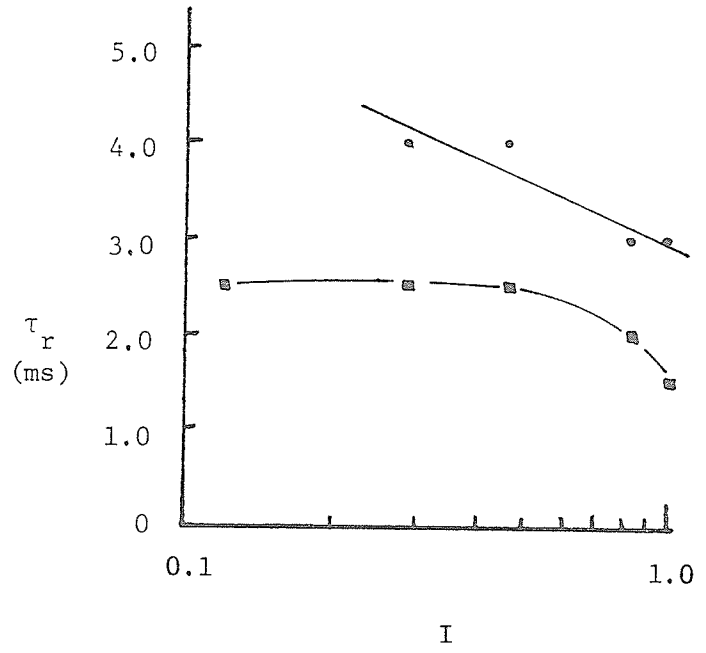

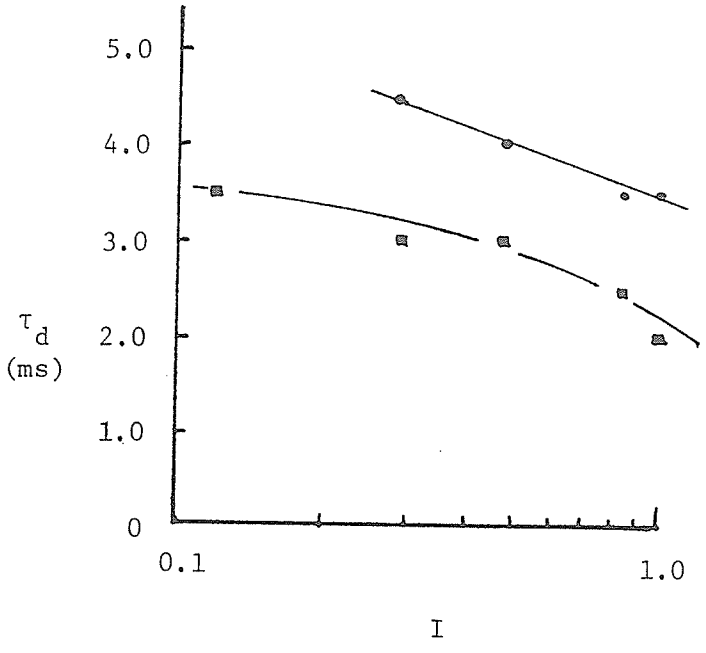

Figure 4.4: Response times, τ_r and τ_d, as a function of relative illuminating light intensity for a-$Si_{1-x}Ge_x$(H) films. λ = 940 nm; F = + 10^4V/cm; ● x = 0; ■ x = 0.10.

time τ_d for both red and infrared light decreases with increasing applied electric field. Only τ_d is shown since it was found that the dependence of τ_r on F was very similiar to that of the corresponding τ_d, though the magnitude of τ_r was slightly less than that of τ_d. A change in polarity of the applied field did not significantly alter the shape of the curves in Figures 4.5 and 4.6 but changed the magnitude of the time constants. Generally it was found that for both λ = 632.8 nm and 940 nm, a (-)F applied field inceases both τ_r and τ_d by a nominal value of 50%. Also for x = 0.25 and λ = 632.8 nm the decrease with field of the time constants was much larger for lower light intensities.

Figures 4.7 and 4.8 show the magnitude of the fast section normalized to the steady state photocurrent for both the rise and fall at various intensities. For excitation of λ = 940 nm only the fast section for the rise is plotted because the ratio of the fast section to the steady state photocurrent is approximately equal for both the rising and falling edges. For λ = 632.8 nm, R_r is higher than R_d for all samples throughout the same intensity range. In contrast, for λ = 940 nm, R_r and R_d are approximately equal. Also for λ = 632.8 nm, R_r and R_d increase with increasing intensity while for λ = 940 nm, R_r and R_d are relatively independent of light intensity. The variation of R_r and R_d with intensity is approximately the same for all values of x for both λ = 632.8 nm and λ = 940 nm. However, the magnitude of R_r and R_d decreases as x increases.

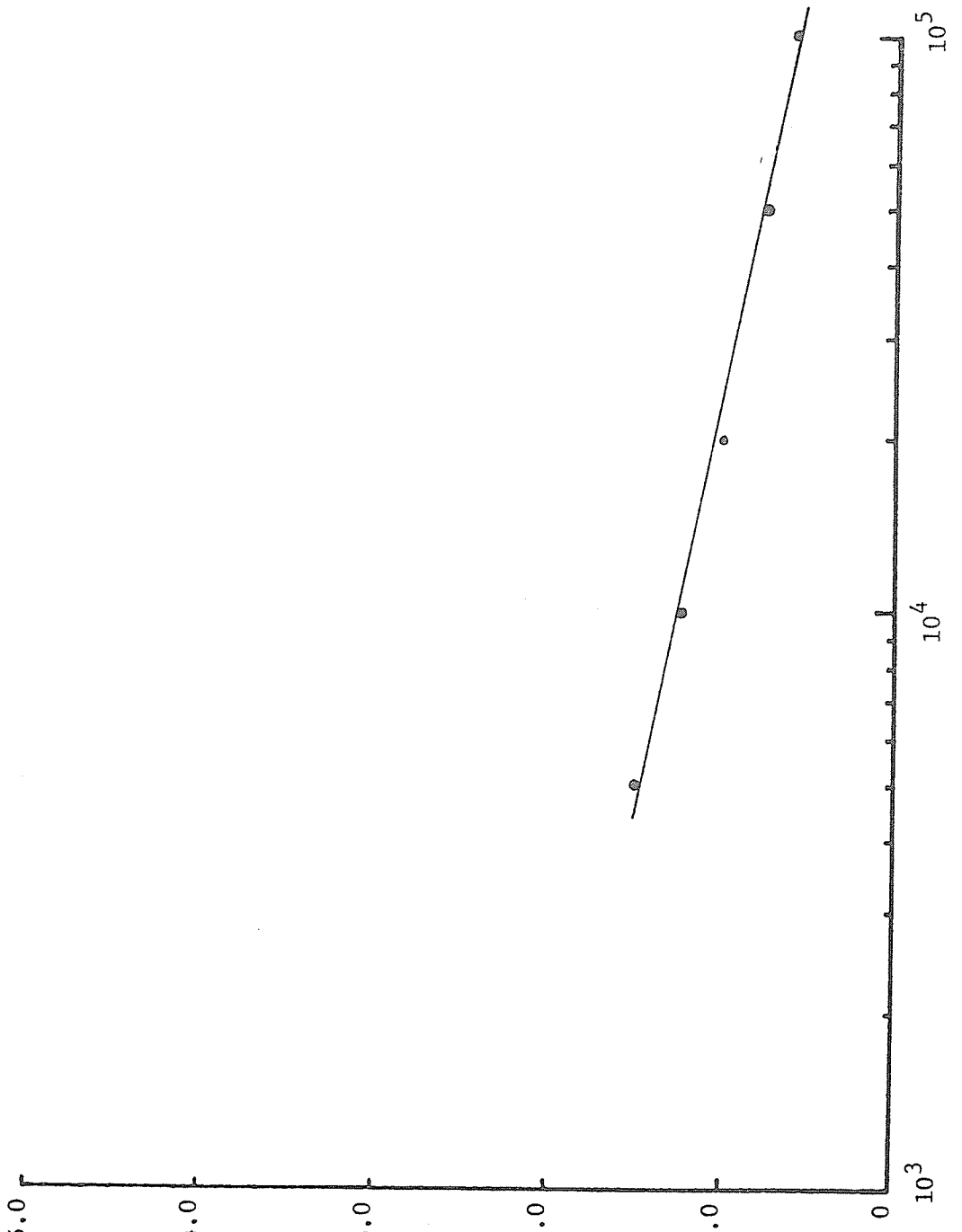

Figure 4.5 Response time τ_d as a function of the applied field for a-$Si_{1-x}Ge_x$(H) films. λ = 632.8 nm, x = 0.

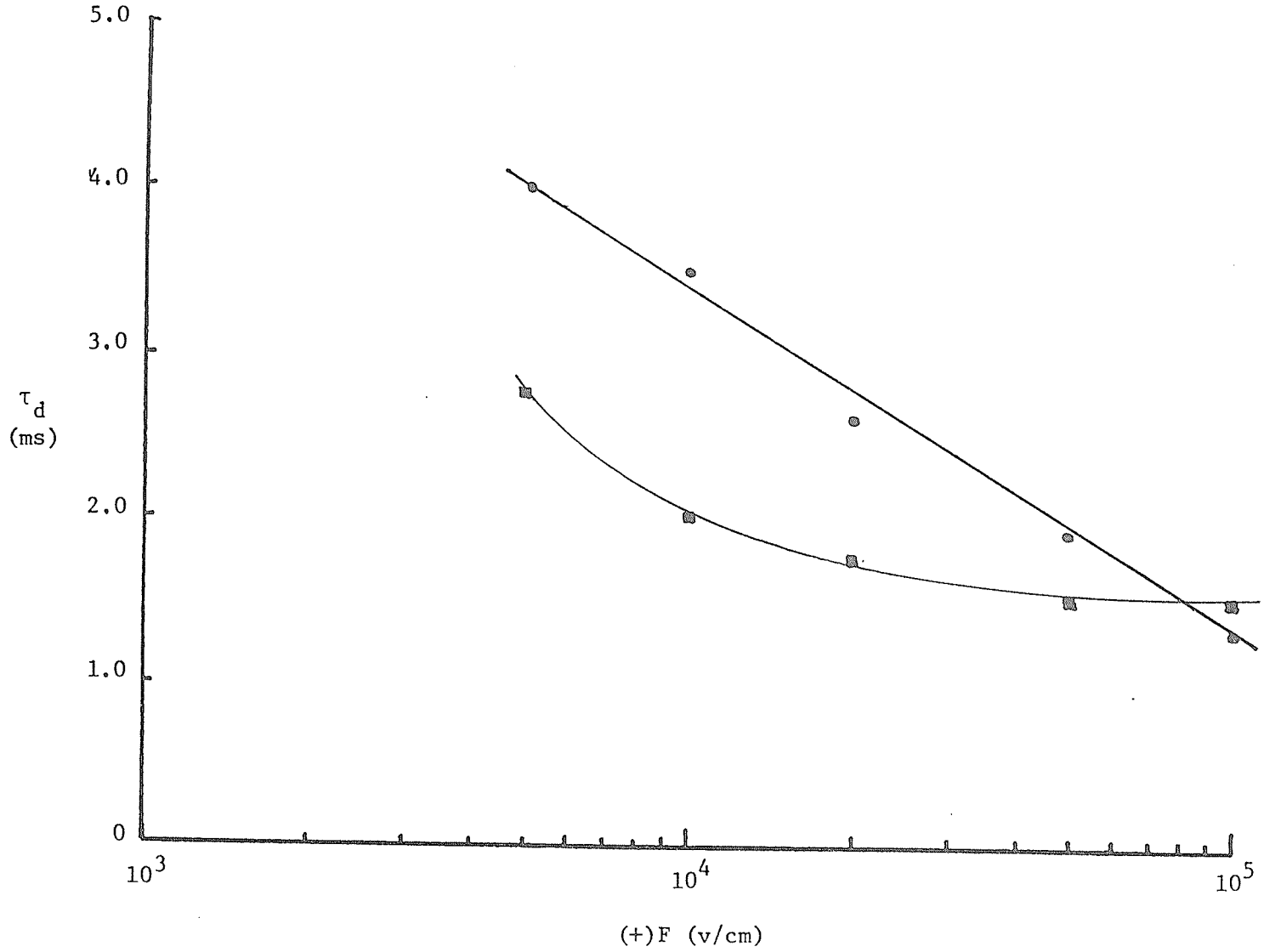

Figure 4.6 Response time τ_d as a function of the applied field for a-$Si_{1-x}Ge_x$ (H) films. λ = 940 nm, x = 0, x = 0.10.

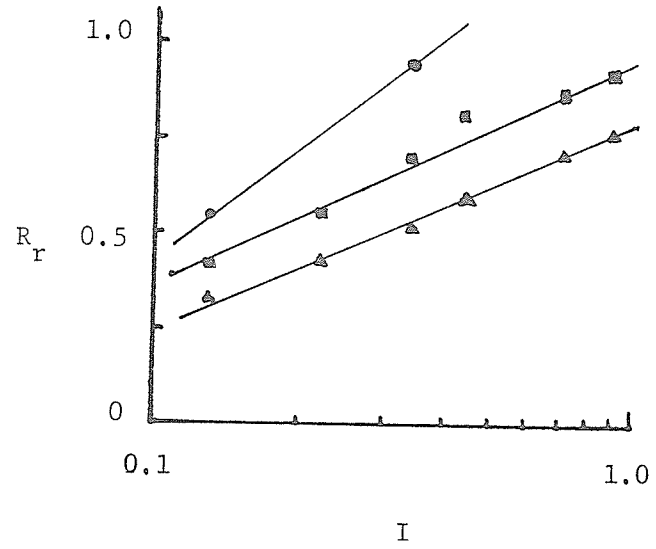

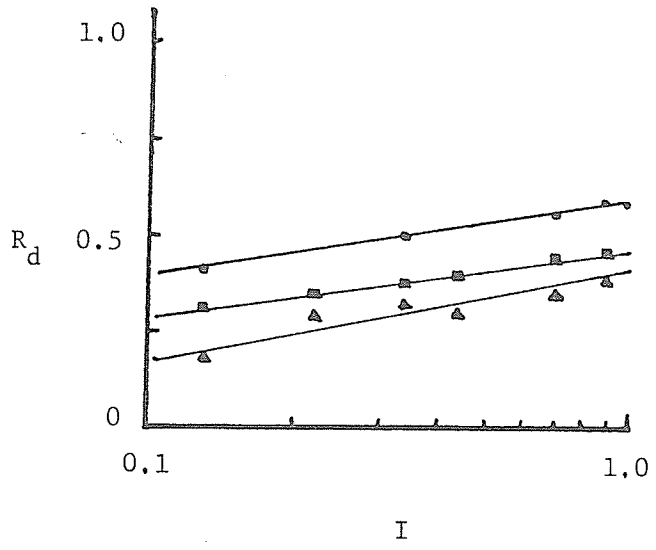

Figure 4.7: Fast sections, R_r and R_d, as a function of relative illuminating light intensity for a-$Si_{1-x}Ge_x$ (H) films. λ = 632.8 nm; F = + 10^4 V/cm; ● x = 0; ■ x = 0.10; ▲ x = 0.25.

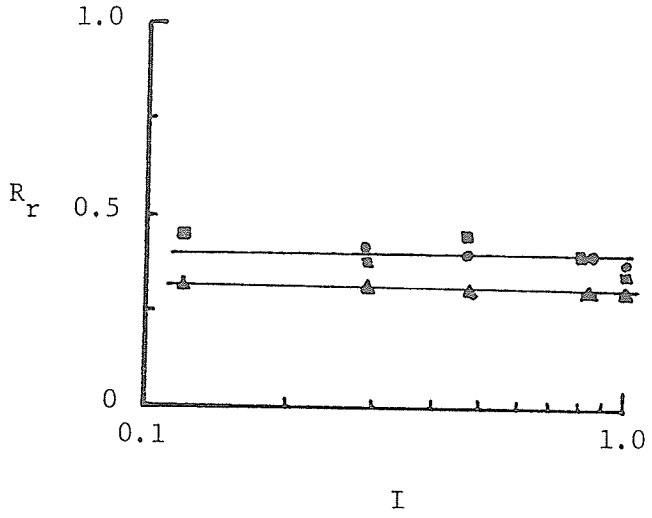

Figure 4.8: Fast section, R_r, as a function of relative illuminating light intensity for a-$Si_{1-x}Ge_x$ (H) films. λ = 940 nm; F = + 10^4 V/cm; ● x = 0; ■ x = 0.10; ▲ x = 0.25.

The photogenerated carrier density and carrier lifetime as functions of light intensity are shown in Figures 4.9 and 4.10. Figure 4.9 shows the photogenerated electron concentration, n, and the electron lifetime, τ_n, as functions of light intensity, which are calculated from (discussed in sec. 5.2) the measured photocurrent. The data are shown for $F = (+)10^4$ V/cm, but for $F = (-)10^4$ V/cm the results are very similar. Figure 4.9 shows that for $\lambda = 632.8$ nm there exists a region of supralinear photoconductivity at low intensity. Δn increases according to a power greater than unity ($\Delta n \propto I^{\nu}$). This implies an increase in the lifetime, τ_n. However, at higher intensities, ν tends to decrease to values of less than unity and τ_n begins to level off. As the Ge content, x, increases, ν increases for a fixed light intensity at 632.8 nm. Figure 4.9 also shows that for $x = 0$ and $x = 0.10$, the values of τ_n are approximately equal. For $x = 0.25$,however, the lifetime seems to be enhanced.

For infrared (940 nm) light excitation, the measured photocurrent exhibits a linear dependence on light intensity for all x as shown in Figure 4.10. The magnitude of the photocurrent is approximately the same for $x = 0.10$ and $x = 0.25$. However for $x = 0$ the response is slightly below that of $x = 0.10$ and 0.25.

The effect of the applied field on the photocurrent is illustrated in Figure 4.11 for red illumination and in Fig-

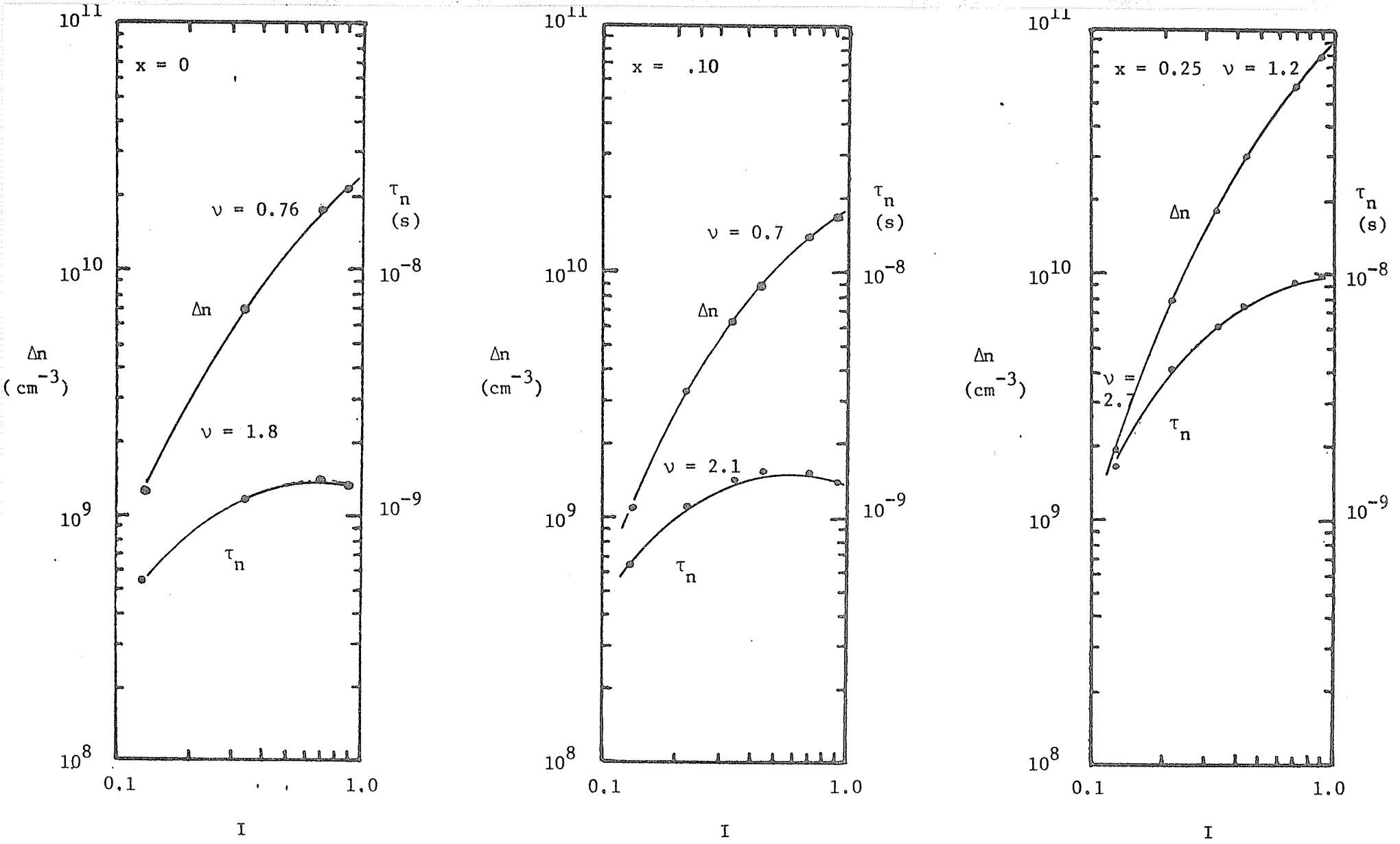

Figure 4.9 Excess electron concentration, Δn, and electron lifetime, τ_n, as a function of the relative illuminating light intensity, I, for a-$Si_{1-x}Ge_x$(H) films. λ = 632.8 nm, F = (+) 10^4 V/cm, $J_{ph} \propto I^{\nu}$.

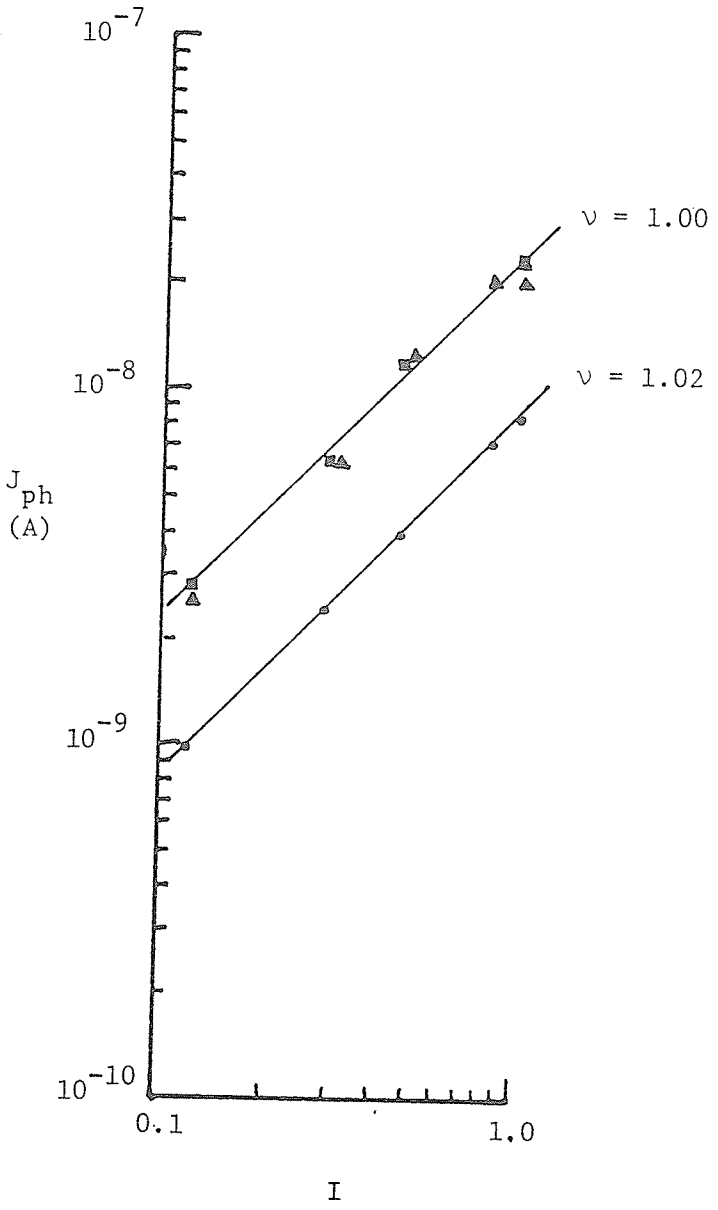

Figure 4.10: Photocurrent, J_{ph}, as a function of relative illuminating light intensity for a-$Si_{1-x}Ge_x$(H) films. λ = 940 nm; F = + 10^4 V/cm; ● x = 0; ■ x = 0.10; ▲ x = 0.25. $J_{ph} \propto I^{\nu}$.

ure 4.12 for infrared illumination. Figure 4.12 shows a linear increase of photocurrent with applied field as expected. However, for illumination at λ = 632.8 nm, only the x =0.10 sample exhibits an approximate linear dependence on electric field. At a field of about 5×10^4 V/cm a sharp rise in the photocurrent begins to appear. For x = 0 and 0.25 the photocurrent increases with field at a power n' slightly greater than unity according to the relation $J_{ph} \propto F^{n'}$.

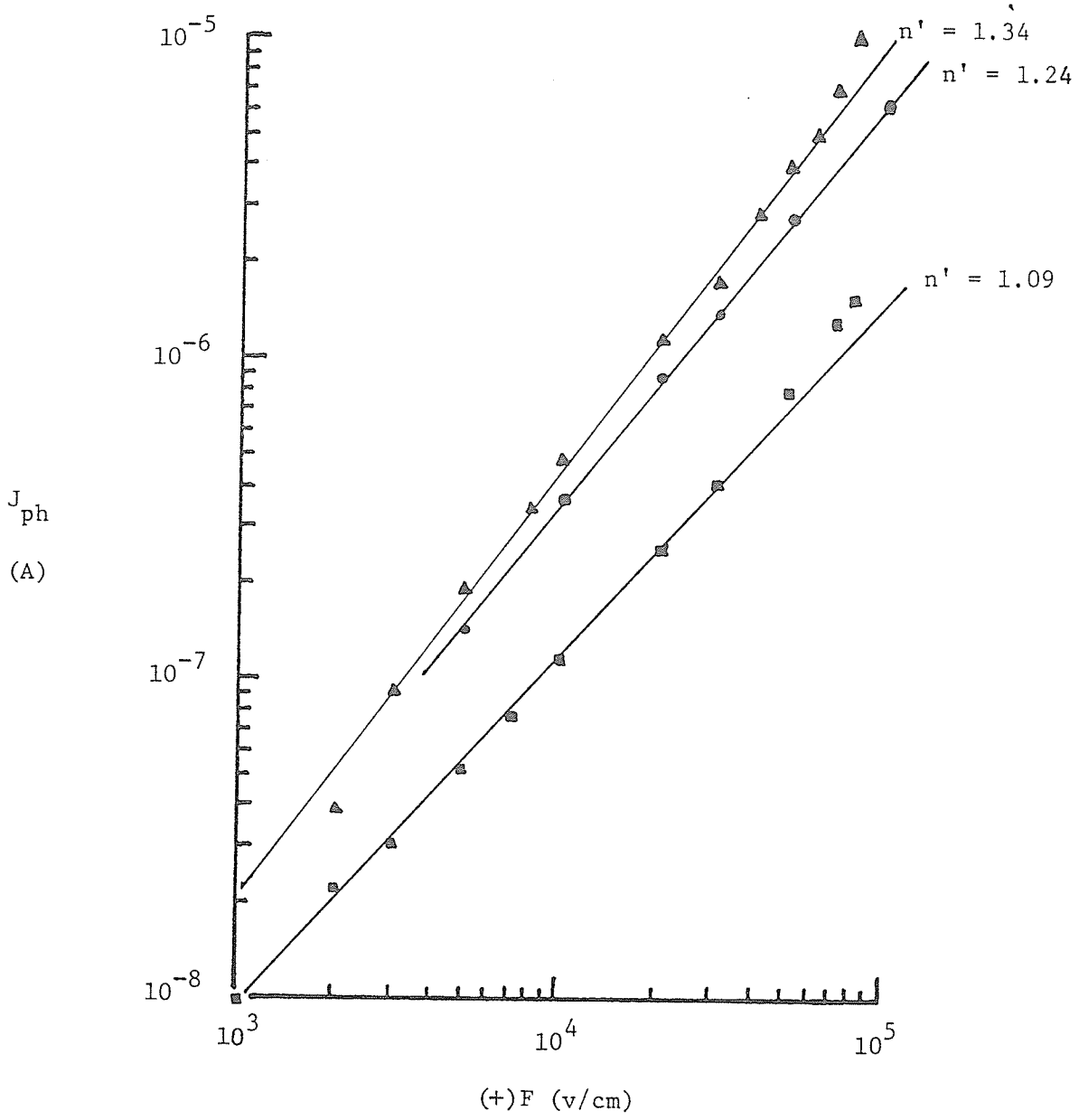

Figure 4.11: Photocurrent, J_{ph}, as a function of applied field for a-$Si_{1-x}Ge_x$(H) films. λ = 632.8 nm; ● x = 0; ■ x = 0.10; ▲ x = 0.25. $J_{ph} \propto F^n$.

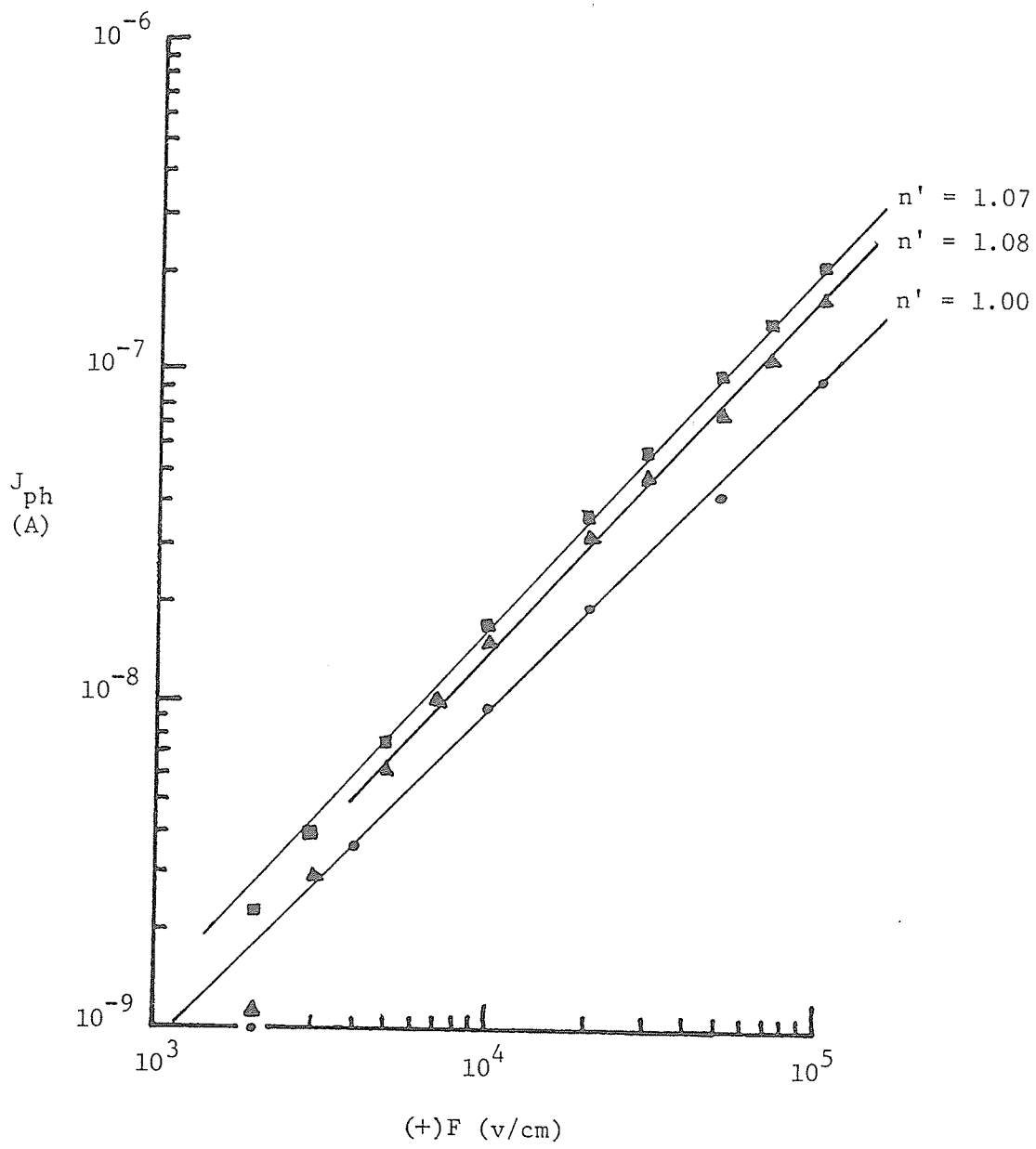

Figure 4.12: Photocurrent, J_{ph}, as a function of applied field for a-$Si_{1-x}Ge_x$(H) films. λ = 940 nm; ● x = 0; ■ x = 0.10; ▲ x = 0.25. $J_{ph} \propto F^{n'}$.

Chapter V

THEORY OF PHOTOGENERATED CARRIER TRANSPORT

5.1 DIFFUSION AND DRIFT OF PHOTOGENERATED CARRIERS

In a semiconductor containing free charges, any disturbance of the charge neutrality, that is the appearance of uncompensated space charge will create an electic field thus producing a current flow directed in such a way so as to re.store the neutrality. For nonuniform illumination with unipolar conduction, the diffusion current disturbs the neutrality and gives rise to a space charge and a field. This field is directed so that it opposes diffusion and further departure from neutrality. Consquently the neutrality is disturbed only in a small region defined by the screening length. The diffusion also extends in this small region. Thus the carriers can not be displaced far during diffusion in the unipolar case because of the electrostatic forces of attraction of the fixed charges of opposite sign.

The region in which excess electrons are accumulated by diffusion will have a negative space charge while in the other region, in which electrons are depleted, the space charge will be positive. These space charges establish a field which prevents further motion of the electrons, that is, prevents further diffusion. A density gradient

(grad n) produces a diffusion current $j = e D \text{ grad } n$ which gives rise to an electric field, F, and consequently a conduction current $j_F = \sigma F = e\mu nF$. The total current j at any point in a semiconductor at any time is given by

$$j = j_D + j_F = e\ (D \text{ grad } n + \mu\ n\ F) \quad . \qquad (5.1)$$

In an isolated semiconductor under thermal equilibrium conditions the total current should be zero; that is, at each point the drift current should compensate the diffusion current. This thermal equilibrium condition corresponds to definite spatial distributions of carriers, space charge and electric field.

To calculate the distribution of these parameters we use Poisson's equation

$$\text{div } F = \rho / \varepsilon \quad , \qquad (5.2)$$

and the continuity equation

$$\partial n / \partial t = g + \beta\alpha I - n/\tau_n + (\text{div } j)/e \quad . \qquad (5.3)$$

Consider a simple one dimensional case where we have a semiconductor sample, Figure 5.1. We assume that at $x < 0$ excess electrons are generated uniformly by the light of intensity I, and at $x > 0$, there is no illumination. At the point $x = 0$ there exists a sharp boundary between darkness and illumination.

The analysis for this relatively simple case [84] leads to the determination of an important parameter which is characteristic of the diffusion in the unipolar case. This parameter is generally refered to as the screening length or Debye length ℓ_e. The screening length, ℓ_e, can in fact, be interpreted as the distance at which the carrier density is 1/e of its initial value. The screening length is governed by the equilibrium electron distribution n_0 for the case of weak excitation ($n_0 >> \Delta n$)

$$\ell_e = [\varepsilon kT/2e^2 n_0]^{1/2} \quad . \tag{5.4}$$

In the case of arbitrary excitation level we must replace n_0 in the expression for ℓ_e with the total density $n = n_0 + \Delta n$. If the density varies with the distance (for illumination in the sandwich cell geometry this is the case), the quantity ℓ_e has different values at different points, increasing with decreasing carrier density.

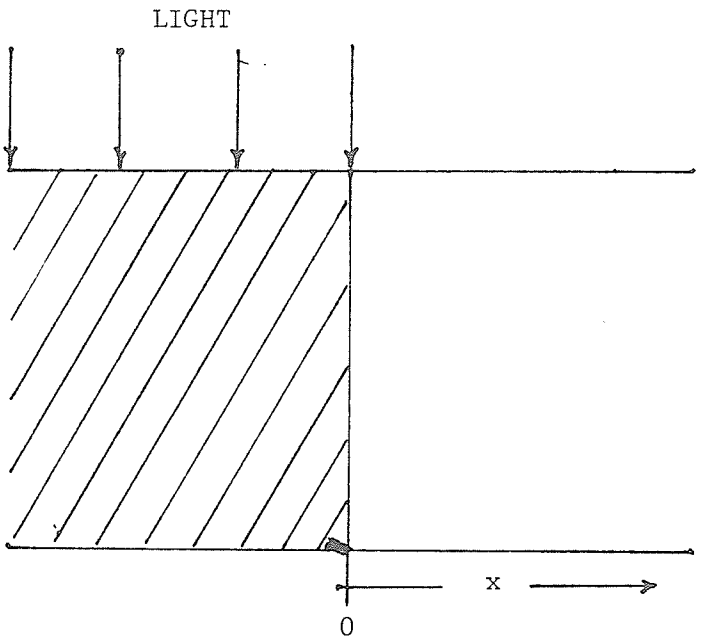

Figure 5.1: Nonuniform illumination of a semiconductor.

Consquently, the dependence of Δn in the case $\Delta n >> n_0$ should be as follows. First the value of n decreases very sharply across the boundary between the illuminated and the dark region due to the high concentration of carriers (n is high means ℓ_e is small). The value for n decreases with increasing x from x = 0 and ℓ_e becomes progressively larger. Thus when $\Delta n >> n_0$, it becomes difficult to determine the effective region over which diffusion is active. We can say however that the main part of the carrier density decrease occurs in a distance ℓ_e whose order of magnitude is determined by the carrier density in the interior of the illuminated region. But there is a density tail, which is due to the considerable lower density in the dark region.

The screening length can be expressed as

$$\ell_e = [D\varepsilon/2\sigma_0]^{1/2} = [D\theta]^{1/2} \quad , \qquad (5.5)$$

where the quantity θ has the dimensions of time and is given by

$$\theta = \varepsilon \; / \; 2\sigma_0 \quad . \qquad (5.6)$$

It is the time required for the carriers to diffuse to a distance ℓ_e, which is equal to $\theta_m/2$, where θ_m is given by

$$\theta_m = \varepsilon / \sigma_0 \quad , \tag{5.7}$$

and is known as the Maxwell time constant and its meaning is as follows. Supposing that a homogeneous semiconductor with a conductivity of σ_0 and a thickness of d is placed between two parallel electrodes of area S. The resistance r is then

$$r = d / s\sigma_0 \quad , \tag{5.8}$$

and the capacitance is

$$C = \varepsilon s / d \quad . \tag{5.9}$$

From Equations (5.8) and (5.9), we have $rC = \varepsilon/\sigma_0$, which is identical to θ_m in Equation (5.7). Thus, θ_m, represents just a rC time constant of the semiconductor. It is also the dielectric relaxation time, that is, it is the effective time for the establishment of the diffusion-drift equilibrium.

5.2 STEADY STATE PHOTOCONDUCTION

The measured total change of the conductivity of a sample in general can not be written in a closed form expression as a function of the quantities e, μ, β, τ, α, and I. The major problem is that the value of I, due to absorption, is not constant for the whole sample. This problem is not serious for the following cases.

1. We can use sufficiently thin samples and weakly absorbed light. Then we can assume approximately the same illumination intensity at all points of the sample. This method, however, restricts the range of wavelengths available for study.

2. If we know the dependence of the photoconductivity on the illumination intensity, and the absorption law, we can express the measured total photoconductivity in terms of the principal phenomenological parameters. This method may be used in a relatively simple fashion only for normal orientation of the light beam with respect to the electric field applied to the sample (the transverse photoconductivity such as that measured using a gap cell geometry).

Consider a sample in the form of a rectangular parallelepiped of dimensions $\ell \times h_t \times d$, which is illuminated with monochromatic light as shown in Figure 5.2. The intensity of light decreases with depth according to the law $I = I \exp(-\alpha x)$ in which is assumed to be constant: any non-linear effects caused by high injection such as free

carrier absorption making α dependent on n, and t, are neglected. The steady state density of electrons is $n_0 + \Delta n_x$ and Δn_x which decreases with depth can be expressed as

$$\Delta n_x = \Delta n_0 \exp(-\alpha x) = \beta \alpha I_0 \tau_n \exp(-\alpha x) \quad . \qquad (5.10)$$

by ignoring the effects of diffusion or drift on the carrier distribution. If we divide the sample into layers of thickness dx, the photoconductivity of one of such layers can be written as

$$e \mu_n \Delta n_x (h_t \, dx / \ell) \quad . \qquad (5.11)$$

Since all layers are in parallel, the photoconductance of the whole sample, G_{ph}, may be found by a summation over the whole thickness d

$$G_{ph} = (h_t/\ell) \, e \mu_n \int_0^d \Delta n_x \, dx \quad . \qquad (5.12)$$

Substituting Equation (5.10) into Equation (5.12) we obtain

$$G_{ph} = (h_t/\ell) \, e \mu_n \beta \tau_n I_0 (1 - e^{-\alpha d}) \quad . \qquad (5.13)$$

For sufficiently thick samples, that is $\alpha d \gg 1$, we have

$$G_{ph} = (h_t/\ell)\, e\, \mu_n\, \beta\, \tau_n\, I_0 \quad . \tag{5.14}$$

Thus the photoconductivity of "thick" samples for the transverse case is independent of the absorption ceoefficient and is governed only by the total amount of light power I_0 penetrating into the sample.

From Equation (5.13), the photoconductivity can be expressed as

$$\sigma_{ph} = G_{ph}(\ell/h_t d) = e\, \mu_n\, \beta\, \tau_n\, I_0\, (1 - e^{-\alpha d})/d \quad . \tag{5.15}$$

Comparing this to the standard equation for uniform carrier generation used in experiments;

$$\sigma_{ph} = e\, \mu_n\, n \quad , \tag{5.16}$$

we obtain

$$\begin{aligned} n &= \beta\, I_0\, [(1 - e^{-\alpha d})/d]\, \tau_n \\ &= g_{op}\, \tau_n \quad , \end{aligned} \tag{5.17}$$

where g_{op} is the volume-generated rate which is given by

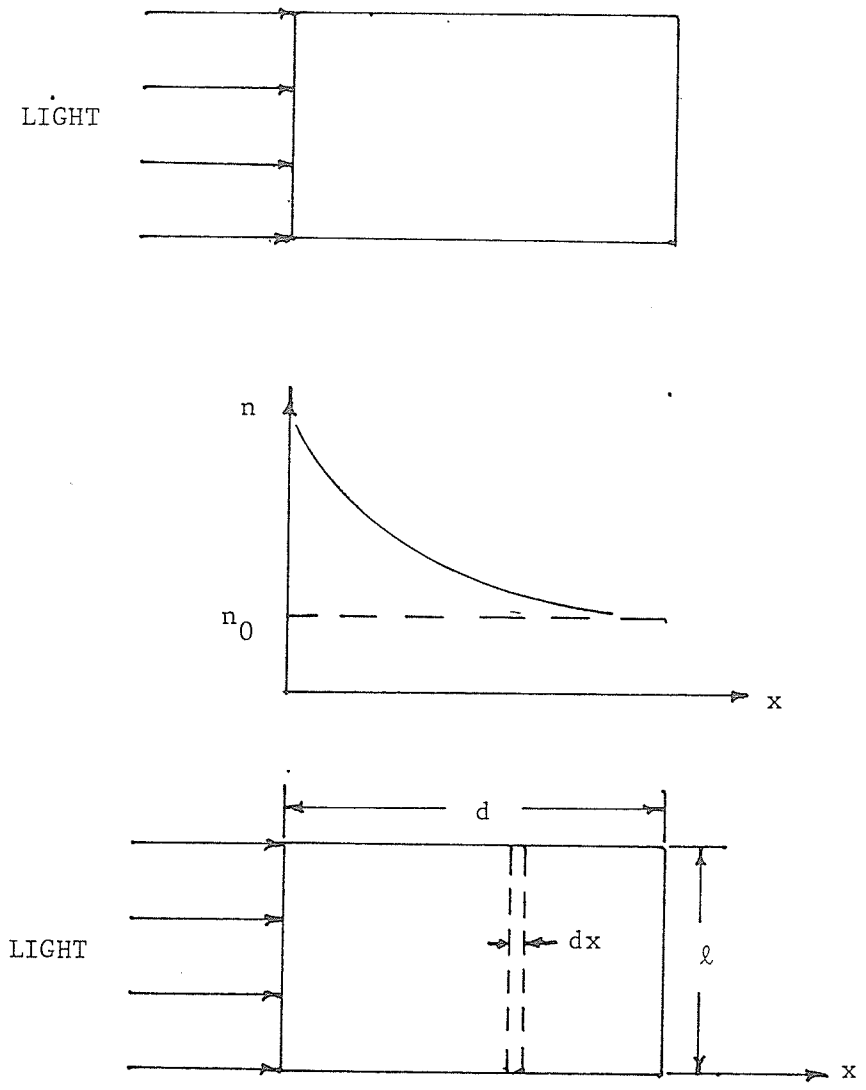

Figure 5.2: Uniform illumination of a semiconductor and resulting excess carrier concentration distribution, $\Delta n(x)$.

$$g_{op} = \beta I_0 (1 - e^{-\alpha d})/d \quad . \tag{5.18}$$

where I_0 is the incident photon flux in $cm^{-2} s^{-1}$. Surface reflection effect has been ignored in deriving Equation (5.17).

For the case of longitudinal photoconductivity (such as photoconductivity measured in a sandwich cell geometry), the light beam is parallel to the applied field as shown in Figure 3.2. Then the measured photoconductance of the whole sample G_{ph}, depends in a complex fashion on the distribution function of the Δn (or σ_{ph}). Assuming that in a sample the nonequilibrium carrier (for example, electrons) density varies along the sample: $\Delta n = \Delta n(x)$ (Figure 5.3) and consquently $\sigma_{ph} = \sigma_{ph}(x)$. The photoconductance of the whole sample is the change in conductance due to light and is given by

$$G_{ph} = G_I - G_0 \quad , \tag{5.19}$$

where G_I and G_0 is the photoconductance of the whole sample with and without illumination. By writing Equation (5.19) in terms of the conductivities, we obtain

$$G_{ph} = \frac{s}{\int_0^{\ell} \frac{dx}{\sigma_0 + \sigma_{ph}}} - \frac{s}{\ell}\sigma_0 \qquad (5.20)$$

$$= \frac{s\sigma_0}{\ell}\left\{ \frac{\ell}{\int_0^{\ell} \frac{dx}{1 + \sigma_{ph}(x)/\sigma_0}} - 1 \right\} ,$$

where s is the transverse cross sectional area and ℓ is the length of the sample.

By assuming the distribution of the carrier density to be of exponential form as given by Equation (5.10) and applying the integral

$$\int_0^{\ell} \frac{dx}{1 + A\, e^{-\alpha x}} = [x + (1/\alpha)\, \ln|1 + A\, e^{-\alpha x}|]\Big|_0^{\ell} \quad . \qquad (5.21)$$

Equation (5.20) can be transfomed to

$$\sigma_{ph} = (\ell/\, s)\, G_{ph} = \sigma_0 \left\{ \frac{\ell}{\ell + \frac{1}{\alpha} \ln \frac{1 + A\, e^{-\alpha x}}{1 + A}} - 1 \right\} \quad . \qquad (5.22)$$

We have used a parameter A which is defined in the following equation

$$\frac{\sigma_{ph}(x)}{\sigma_0} = \frac{e\, \mu_n\, \Delta n_0\, e^{-\alpha x}}{e\, \mu_n\, n_0} = \frac{\beta\, \alpha\, I_0\, \tau_n\, e^{-\alpha x}}{n_0} = A\, e^{-\alpha x} \quad . \qquad (5.23)$$

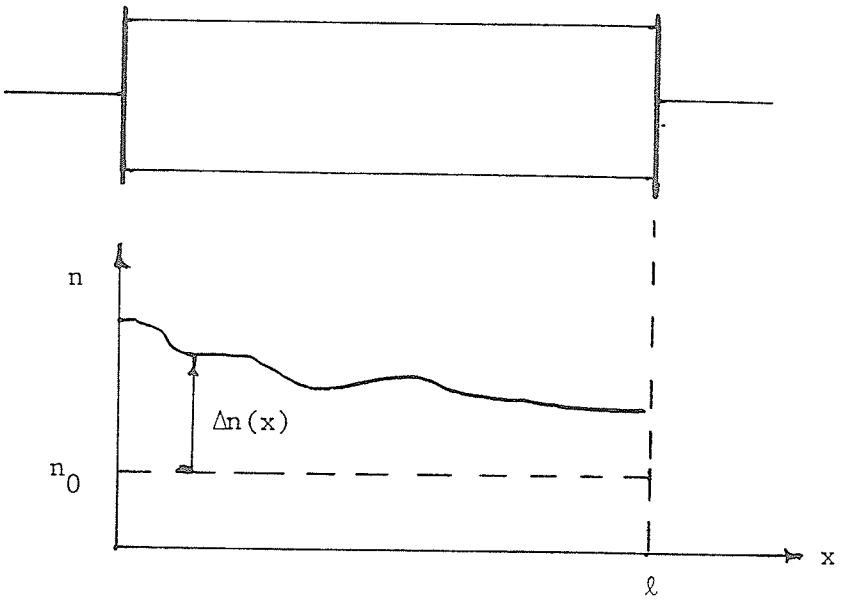

Figure 5.3: Arbitrary distribution of excess electron concentration, $\Delta n(x)$, in a semiconductor.

The data given in Figure (4.9) was calculated with the use of Equation (5.22). To calculate Δn and τ_n we measure the photocurrent density and find the change in conductivity due to illumination by using

$$\sigma_{ph} = J_{ph} / F \quad , \tag{5.24}$$

where the applied field is assumed to be constant and is derived from the known applied voltage and sample thickness. Using Equation (5.22) and the calculated σ_{ph}, we can determine A. τ_n can then be determined if n_0 is estimated by dark conductivity measurements using

$$\sigma_0 = e\, n_0\, \mu_n \quad . \tag{5.25}$$

For a-Si(H), μ_n and the quantum efficiency, β, can be taken as 1 cm^2/V-s and unity for λ = 632.8 nm, respectively, [6,82]. I_0 must be corrected for reflection and attenuation by the top electrode if a sandwich cell geometry is used. I_0 becomes I_0 (1 - R) $\exp(-\alpha_e\ d_e)$ where R is the reflectivity of the top electrode, α_e is the absorption coefficient of the electrode and d_e is the electrode thickness. The reflectivity is taken as 0.85 and the absorption coefficient is taken as 8×10^5 cm^{-1} for an Aluminum electrode. For

each electrode the thickness was determined by the transmission data. When we deposited the top electrode on the a-Si film, we also deposited a similiar electrode on a glass substrate located next to the film at the same time. The latter was used for transmission measurements. The average excess carrier concentration density can be calculated from the relation

$$\Delta n = g_{op}\,\tau_n = I_0\,(1-R)\,e^{-\alpha_e d_e}\,(1 - e^{-\alpha d})\,\tau_n/d \quad , \tag{5.26}$$

where α and d are the absoption coefficient and the thickness of the a-Si film. α for a-Si(H), can be taken as 2×10^4 cm^{-1} [82]. g_{op} is the average volume-generation rate of carriers.

5.3 TRANSIENT PHOTOCONDUCTION

5.3.1 Intensity Dependence of R_r and R_d

We now analyze the results for the general waveshape of the photoresponse, more specifically R_r and R_d, and the response times τ_r and τ_d as functions of the light intensity. We have established that the relaxation of the photocurrent is due to optical transistions of carriers in energy and the photocurrent is a result of an increase in concentration of the excess carriers drifting in an applied field. In addition the excitation produces both holes and electrons, but

holes are quickly trapped and the photocurrent is mainly due to excess electrons in the extended states.

We shall use the model for the distribution of states as shown in Figure 5.4. The reasons for the specific features that are shown will become apparent later. The density of localized states in the bandgap is assumed to decrease exponentially from E_c and E_v toward the middle of the bandgap. It is also assumed that a concentration of localized states, qualitatively of the shape shown in Figure 5.4, is centered about the midgap. The dark Fermi level, E_F, is located slightly above the midgap as estimated from dark conductivity measurements for glow-discharge a-Si prepared at high substrate temperatures [85].

Assuming that the excess carrier concentration, Δn, is much larger than the thermal equilibrium concentration, n_0, we can write

$$n = \Delta n + n_0 \simeq \Delta n \quad . \tag{5.27}$$

The equation governing the electron concentration in the conduction band is

$$dn/dt = g_{op} - n(N_r-n_r)\upsilon S_n - n(N_t-n_t)\upsilon S_n + n_t \upsilon S_n N_c \exp[-(E_c-E_{te})/kT] \quad , \tag{5.28}$$

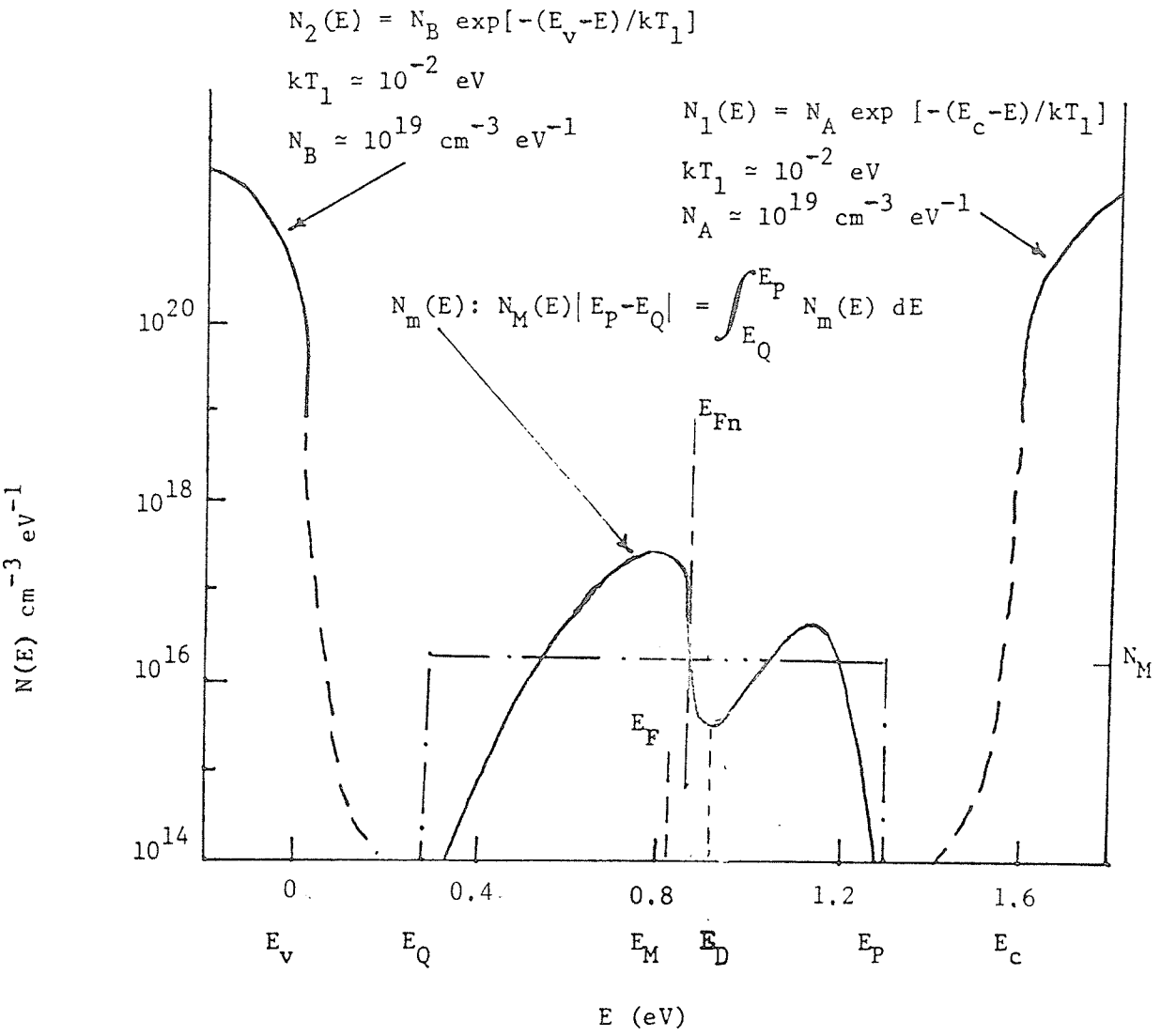

Figure 5.4: Density of states distribution, N(E), as a function of energy, E. Tailing of states from E_c and E_v is assumed to be approximately exponential and E_M denotes the midgap.

where υ is the thermal velocity of the free electrons, S_n is the capture cross section of an unoccupied level for a free electron, N_r and N_t are the densities of recombination centers and trapping levels, respectively; n_r and n_t are the densities of recombination and trap levels occupied by an electron, respectively; E_{te} is an effective trap depth, N_c is the effective density of states in the conduction band, and g_{op} is the volume-generated rate of carriers due to light excitation.

The total density of localized states N_t are assumed to act as traps for a quasi-continuous distribution of localized states through the bandgap (Figure 5.4). E_{te} is an effective trap depth for a quasi-continuous distribution of traps through the bandgap. The demarcation level for the electrons is assumed to be close to the quasi-Fermi level for electrons, E_{Fn}, so that levels above E_{Fn} act as traps. Since most of the trapped electrons will be trapped in the vicinity of E_{Fn} we may use E_{Fn} to characterize the effective trap depth, E_{te}.

Figure 5.5 shows that for a rectangular pulse illumination of a sample, the fast section of the rise is the section from $t = 0$ to $t = t_A$; and the fast section of the decay is that from $t = t_{ss}$ to $t = t_B$. The ratio of the fast section to the steady state photocurrent is defined as R with subscript r or d denoting rising or decaying transient.

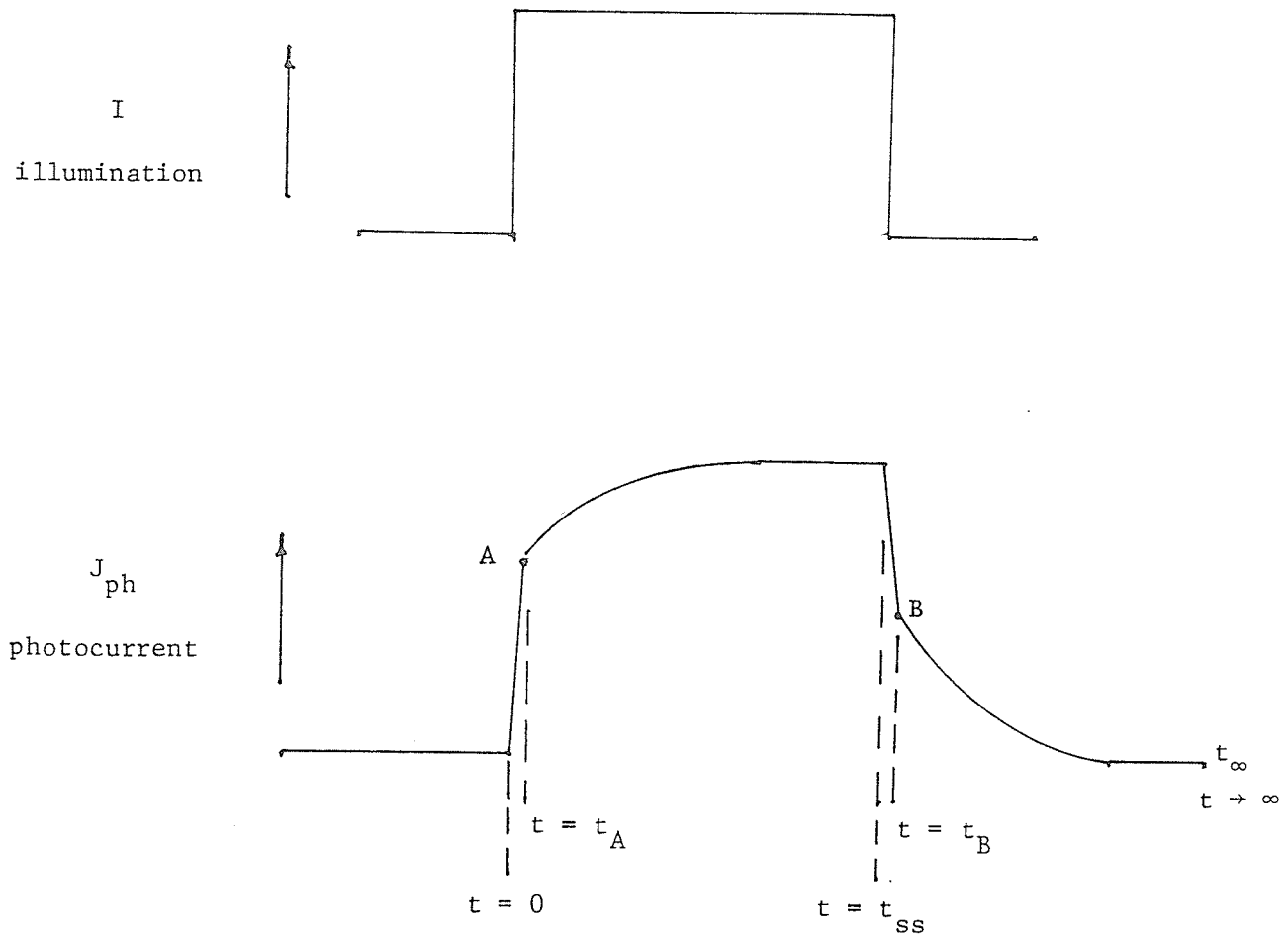

Figure 5.5: The waveshape of the photocurrent caused by the application of a rectangular pulse illumination.

After the cessation of light illumination, if the rate of generation from traps (detrapping) is a tenth the rate of recombination of free carriers into recombination centers, the free carrier density will drop to a tenth its initial value before replenishment from traps begin to keep pace with it. The first 90 percent drop in free carrier density is as rapid as in a trap-free material ($\tau = \tau_n$). The remainder of the drop will be trap-controlled ($\tau = \tau_{r,d}$ which is termed the slow section of the decay). This means that in Figure 5.5, point B corresponds to the state where the carrier generation from the traps is approximately equal to the rate of their recombination, or

$$n_t(t_B) \cup S_n\, n_1(t_B) = n(t_B) / \tau_n \quad , \tag{5.29}$$

where

$$\tau_n = [(N_r - n_r) \cup S_n]^{-1}$$

$$n_1(t_B) = N_c \exp[-(E_c - E_{te}(t_b))/kT]$$

Solving Equation (5.29),we obtain

$$n(t_B) = n_t(t_B) \cup S_n\, n_1(t_B)\, \tau_n = g(t_B)\, \tau_n \quad . \tag{5.30}$$

In the steady state, $dn/dt = 0$. Thus the carrier density $n(t_{ss})$ can be found from Equation (5.28) where g_{op} is expressed as

$$g_{op} = n\,[(1/\tau_n) + N_t \cup S_n] - n_t \cup S_n\, n_1 \quad , \tag{5.31}$$

on the assumption that $N_t - n_t \simeq N_t$. Solving Equation (5.31) for $n_t(t_{ss})$, we have

$$\begin{aligned} n_t(t_{ss}) &= \left[g_{op} + n_t(t_{ss}) \cup S_n\, n_1(t_{ss})\right] \Big/ \left[(1/\tau_n) + N_t(t_{ss}) \cup S_n\right] \\ &= \left[g_{op} + g(t_{ss})\right] \Big/ \left[(1/\tau_n) + N_t(t_{ss}) \cup S_n\right] \quad . \end{aligned} \tag{5.32}$$

The ratio of the fast decay to the steady state photocurrent, R_d, is given by (see Figure 5.5)

$$R_d = 1 - [n(t_B)/n(t_{ss})] = 1 - \frac{g(t_B)\,\tau_n}{\dfrac{g_{op} + g(t_{ss})}{(1/\tau_n) + N_t(t_{ss}) \cup S_n}} \quad . \tag{5.33}$$

Now during the fast section of the decay, the trapping and detrapping are so slow that $n_t(t_{ss}) \simeq n_t(t_B)$. With $n_1(t_B) = n_1(t_{ss})$ this gives $g(t_{ss}) \simeq g(t_B)$ [note: $g(t_1) = n_t(t_1) \cup S_n\, n_1(t_1)$]. Regarding $n_1(t_B) = n_1(t_{ss})$, we assume that the value for n_1 during a transient is constant throughout the transient and is determined by the value of

n_1 in the previous steady state condition. That is, in Figure 5.5 the appropriate n_1 for any time, $0 < t < t_{ss}$, is $n_1(t=0)$; and the appropriate n_1 for any time, $t_{ss} < t < \infty$, is $n_1(t=t_{ss})$. The condition prior to the transient (E_{te} or E_{Fn}) determines which levels are acting as traps. From Equation (5.33) and $g(t_{ss}) \simeq g(t_B)$ we can write

$$R_d = 1 - \frac{g(t_{ss})\ \tau_n\ [(1/\tau_n) + N_t(t_{ss}) \cup S_n}{g_{op} + g(t_{ss})} \qquad (5.34)$$

$$= 1 - K'\ [1\ /\ 1 + (g_{op}/g(t_{ss})] \quad ,$$

where $K' = \tau_n\ (\ 1/\tau_n + N_t(t_{ss}) \cup S_n\ )$. Note that if we use $N_t(t_{ss}) - n_t(t_{ss})$ for $N_t(t_{ss})$ and if $N_t(t_{ss}) = n_t(t_{ss})$, then $K' = 1$.

Along the same lines as for the decay, we can argue that the fast section of the rise is associated with the fast process of generation by light and the subsequent recombination of carriers ($g_{op} - n/\tau_n$; $\tau = \tau_n$). Once the rate of capture of free electrons into traps keeps pace with the net generation rate we have the slow section of the rise. That is point A in Figure 5.5 corresponds to

$$g_{op} - n(t_A)/\tau_n = n(t_A)\ N_t(t=0) \cup S_n \quad . \qquad (5.35)$$

Here, again, by assuming $N_t - n_t \simeq N_t$ and $N_t(t_A) = N_t(t=0)$. We have

$$n(t_A) = g_{op} \; / \; [(1/\tau_n) + N_t(t=0) \cup S_n] \quad . \qquad (5.36)$$

The ratio of the fast rise to the steady state photocurrent, R_r, is given by

$$R_r = n(t_A) \; / \; n(t_{ss}) \quad . \qquad (5.37)$$

And from Equations (5.32) and (5.36), Equation (5.37) becomes

$$R_r = \frac{g_{op}}{g_{op} + g(t_{ss})} \quad \frac{(1/\tau_n) + N_t(t_{ss}) \cup S_n}{(1/\tau_n + N_t(t=0) \cup S_n} \quad . \qquad (5.38)$$

By assuming that $N_t(t=0) \simeq N_t(t_A) \simeq N_t(t_{ss})$, that is the excitation does not raise E_{Fn} so much so as to significantly alter N_t, then we have

$$R_r = 1 \; / [1 + (g(t_{ss})/g_{op})] \quad , \qquad (5.39)$$

where N_t is the total trap density from E_{Fn} to E_c. In fact, for our experimental excitation levels, E_{Fn} moves only about 0.10 eV.

Since we have a distribution in energy of the traps, n_t is a function of energy, $n_t(E)$. The generation of electrons from traps, g, at an energy level $E = E_t$ is given by

$$g(E_t) = n_t(E_t) \cup S_n N_c \exp[-(E_c-E_t)/kT] \quad , \qquad (5.40)$$

where $n_t(E_t)$ is the trapped electron density at an energy level E_t in $cm^{-3} eV^{-1}$. An energy level E, at which the localized states act as traps is denoted as E_t; while an energy level E, at which there are localized states, is denoted as E. Suppose that we have a distribution of localized states, N(E), measured from the conduction band edge, E_c, toward the bandgap (see Figure 5.4) given by

$$\begin{aligned} N(E) &= N_m(E) + N_1(E) + N_2(E) \\ &= N_m(E) + N_A \exp[-(E_c-E)/kT_1] + N_B \exp[-(E_v-E)/kT_1] \qquad (5.41) \\ &\qquad \text{for } E_v < E < E_c \quad , \end{aligned}$$

where T_1 is a characteristic temperature and describes the variation of the localized state density with energy. To describe the density of localized states centered about the

midgap we have included the term $N_m(E)$. For simplicity, $N_m(E)$ is assumed to be constant, N_M, for $E_Q < E < E_P$ and of sufficient magnitude such that $N_M \left| E_P - E_Q \right| = \int_{E_Q}^{E_P} N_m(E)\ dE$ and $N_m(E) = 0$ for $E_v < E < E_Q$ and $E_P < E < E_c$. The total generation of electrons at the steady state for a certain E_{Fn} will be approximately given by the summation from $E_t = E_{Fn}$ to $E_t = E_c$ of all contributions at each energy level given by Equation (5.40). That is

$$
\begin{aligned}
g(t_{ss}) &\simeq \int_{E_{Fn}}^{E_c} g(E_t)\ dE_t \\
&\simeq \int_{E_{Fn}}^{E_c} f_e(E_t)\ N(E_t) \cup S_n\ N_c \exp[-(E_c-E_t)/kT]\ dE_t \\
&\simeq \int_{E_{Fn}}^{E_c} \exp[-(E_t-E_{Fn})/kT]\ [N_m(E_t) + N_A \exp[-(E_c-E_t)/kT_1]] \\
&\qquad x \cup S_n\ N_c \exp[-(E_c-E_t)/kT]\ dE_t \quad .
\end{aligned}
\tag{5.42}
$$

Since $N_2(E)$ drops rapidly from E_v (kT_1 is small), it can be neglected in Equation (5.42), thus we can write

$$
\begin{aligned}
g(t_{ss}) &\simeq \cup S_n\ N_c \exp[-(E_c-E_{Fn})/kT] \\
&\qquad x \int_{E_{Fn}}^{E_c} [N_m(E_t) + N_A \exp[-(E_c-E_t)/kT_1]\ dE_t \\
&\simeq \cup S_n\ N_c \exp[-(E_c-E_{Fn})/kT] \\
&\qquad x \left[\int_{E_{Fn}}^{E_c} N_m(E_t)\ dE_t + \int_{E_{Fn}}^{E_c} N_A \exp[-(E_c-E_t)/kT_1]\ dE_t \right] \quad .
\end{aligned}
\tag{5.43}
$$

Since E_{Fn} is between E_Q and E_P and taking N_M is a constant, Equation (5.45) becomes

$$g(t_{ss}) \simeq \upsilon\, S_n\, N_c \exp[-(E_c-E_{Fn})/kT] \times \{ N_M\, |E_P-E_{Fn}| + N_A\, kT_1\, [1 - \exp[\ -(E_c-E_{Fn})]/kT_1] \ \} \quad . \tag{5.44}$$

From our experimental data $(E_c - E_{Fn})$ is estimated to be about 0.7 -0.6 eV so that $[1 - \exp((E_c - E_{Fn})/kT_1)]$ is about unity, then

$$g(t_{ss}) = \upsilon\, S_n\, N_c \exp[-(E_c-E_{Fn})/kT]\ [N_M\, |E_P-E_{Fn}| + N_A kT_1] \quad . \tag{5.45}$$

The generation of electrons due to light excitation, g_{op}, can be expressed in terms of E_{Fn} as

$$g_{op} = n\ /\ \tau_n = (N_c/\tau_n) \exp[-(E_c-E_{Fn})/kT] \quad . \tag{5.46}$$

Hence, we have

$$g(t_{ss})/g_{op} \simeq \upsilon\, S_n\, \tau_n\, [N_M\, |E_P-E_{Fn}| + N_A\, kT_1] \quad . \tag{5.47}$$

It can be seen that as g_{op} increases, E_{Fn} tends to move toward E_P and hence $g(t_{ss})/g_{op}$ decreases.

5.3.2 Intensity Dependence of the Response Times τ_r and τ_d

A decrease in the response time, τ_r or τ_d, with increasing intensity while τ_n remaining approximately constant indicates traps being distibuted in energy rather than being localized at some discrete levels [7]. In fact, N_t states need only be spread over a range of energies through which the quasi-Fermi level, E_{Fn}, moves since it is only the slice of N_t states near the Fermi level, that contribute to the response time. We can write the response time as,

$$\tau_{r,d} = (1 + n_t/n)\ \tau_n \simeq (n_t/n)\ \tau_n \quad . \qquad (5.48)$$

If N_t is uniformly distributed in energy about E_{Fn} so that n_t is approximately constant, an increase in n, due to increasing excitation, g_{op}, predicts that the response time will decrease.

The response time of the rise (τ_r) and decay (τ_d) is the time constant associated with the section of the photocurrent from $t = t_A$ to $t = t_{ss}$ and from $t = t_B$ to $t = t_\infty$, respectively. It is assumed that throughout both these regions the transient is governed by one time constant that remains constant throughout. In light of previous discussion

[Equation (5.48)] the response time is characterized by the ratio n_t/n where for the rise, the n_t/n ratio evaluated at $t = t_A$ establishes τ_r; and for the decay, n_t/n evaluated at $t = t_B$ defines τ_d. From $t = 0$ to $t = t_A$, no significant trapping occurs and we can assume that $n_t(t_A) \simeq n_t(t=0)$. Therefore

$$\tau_r = [n_t(t=0) \; / \; n(t_A)] \; \tau_n \quad . \tag{5.49}$$

Similiarly, from $t = t_{ss}$ to $t = t_B$, no trapping occurs and we can assume that $n_t(t_{ss}) \simeq n_t(t_B)$. Therefore

$$\tau_d = [n_t(t_{ss}) \; / \; n(t_B)] \; \tau_n \quad . \tag{5.50}$$

Now we can write

$$\tau_r/\tau_d = [n_t(t=0)/n_t(t_{ss})] \; [n(t_B)/n(t_A)] \quad . \tag{5.51}$$

Using Equation (5.30) for $n(t_B)$ and Equation (5.36) for $n(t_A)$, Equation (5.51) becomes

$$\tau_r/\tau_d = [n_t(t=0)/n_t(t_{ss})] \; \{n_t(t_B) \cup S_n \; n_1(t_B) \; \tau_n \; [(1/\tau_n) + N_t(t=0) \cup S_n]\}/g_{op} \quad . \tag{5.52}$$

Since

$$n_t(t_B) \simeq n_t(t_{ss}) \quad ; \quad n_1(t_B) = n_1(t_{ss}) \quad , \tag{5.53}$$

we have

$$\tau_r/\tau_d = n_t(t=0) \cup S_n \, n_1(t_{ss}) \, \tau_n \, [(1/\tau_n) + N_t(t=0) \cup S_n] \, / \, g_{op} \, . \tag{5.54}$$

Substitution of Equation (5.36) into Equation (5.49) gives

$$\tau_r = n_t(t=0) \, [(1/\tau_n) + N_t(t=0) \cup S_n] \, \tau_n \, / \, g_{op} \quad . \tag{5.55}$$

Substitution of Equation (5.30) into Equation (5.50) yields

$$\begin{aligned} \tau_d &= n_t(t_{ss}) \, \tau_n \Big/ n_t(t_B) \cup S_n \, n_1(t_B) \, \tau_n \\ &= [\cup S_n \, n_1(t_{ss})]^{-1} \quad , \end{aligned} \tag{5.56}$$

since $n_t(t_B) \simeq n_t(t_{ss})$ and $n_1(t_B) = n_1(t_{ss})$.

5.4 PHOTOINJECTION

Photoinjection of electrons from an electode into a semiconductor can occur as shown in Figure 5.6. On the basis of the theory of photoinjection to an insulator [86], it is reasonable to assume that for low injection levels the field is uniform throughout the sample, since the amount of injected charge is too small to significantly modify the field and the injected charge carriers have the same energy distribution as the charge carriers moving in the insulator.

In calculating the yield we consider two factors. First we consider the concept of an escape cone. A photon of energy greater than the potential barrier may excite an electron over the interfacial barrier. In the simplest case, the momentum distribution of the photoexcited electron is isotopic ; thus only a fraction of the excited electrons enter the insulator. Only those electrons having a sufficiently large component of momentum directed into the insulator can overcome the barrier. This leads to a cone of momentum which the electrons must possess in order to enter the insulator. The probability for escape is given by [86]

$$F_e(hf) = 0.5\ [1 - (\Phi_B/hf)^{1/2}] \quad , \qquad (5.57)$$

where Φ_B is the potential barrier height for photoinjection and hf is the photon energy. This controls the number of photoexcited electrons entering the insulator.

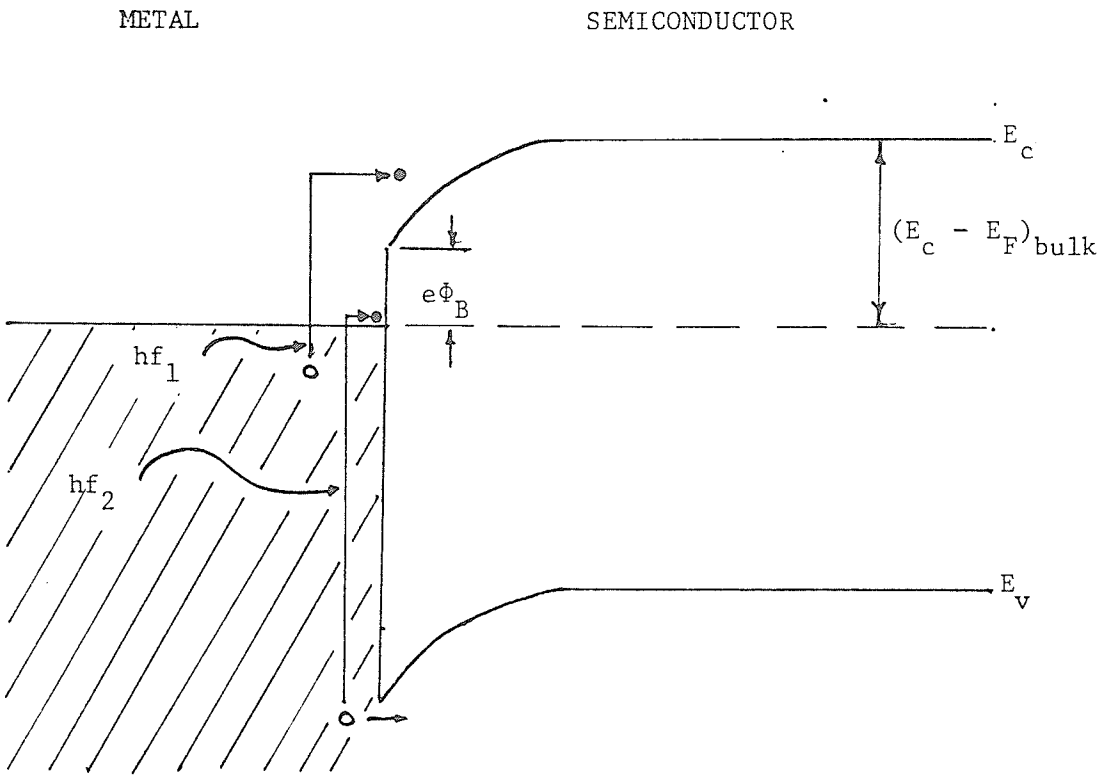

Figure 5.6: Photoinjection of electrons and holes from a metal into a semiconductor. Accumulation layer (ohmic contact) at the contact between the metal and a semiconductor.

A second consideration is how many electrons that enter the insulator, will remain in the insulator. This can be determined by the scattering and energy loss processes in the insulator. By asumming that the injected current, after taking the escape cone into consideration, is j_0, the yield determined by the scattering process is given by [86]

$$j/j_0 = 1 \; / \; 1 + [\upsilon/(6\pi)^{1/2} \; \mu \; F] \quad , \tag{5.58}$$

where υ is the average speed of the carriers (thermal velocity) and $j = e \; n_0 \; \mu \; F$. This case applies to only very low fields, where (a) $F\bar{\ell} \ll kT/e$ and (b) the energy of the electrons is comparable to kT ($\bar{\ell}$ is the mean free path for momentum exchange scattering.) When the energy of the injected electrons is large compared to kT, the velocity υ should have the value appopriate to the energy of the electrons rather than (3/2)kT.

Chapter VI

ANALYSIS AND DISCUSSION OF PHOTOCONDUCTION

We shall analyze our photoconductivity results based on the one dimensional treatment, that is any variation in carrier density or applied field normal to the incidence of the exciting light is ignored. We shall consider first the cases for illumination at λ = 632.8 nm and then the cases for illumination at λ = 940 nm. Photoconductivity at λ = 632.8 nm is due mainly to absorption of the radiation in the films, which generates carriers. Photoconductivity in both glow-discharge and evaporated a-Si(H) [82] has been interpreted as due mainly to electrons in extended states for temperatures greater than 250 K [9,87-89]. Anderson and Spear [8] have proposed that holes are quickly trapped due to a high density of tail states and electrons are the dominating carriers. Pawlewicz [56] has shown that a-Si films prepared by sputtering in Ar and H_2 are similiar to those produced by glow-discharge of silane. It is therefore reasonable to assume that most photogenerated holes are quickly trapped and immobilized, then the conduction is mainly unipolar, that is, the photoconductivity is due mainly to photogenerated electrons. Infrared absorption is mainly due to photoinjection of carriers (electrons only as we shall see

later) from the electrodes into the film. Thus we can apply the theory of Chapter V to our experimental results for sputtered a-$Si_{1-x}Ge_x$(H) films.

6.1 PHOTOGENERATED CARRIER TRANSPORT KINETICS

Photoconductivity measurements on a sandwich cell geometry may be expected to give rise to an excess electron distribution similiar to that shown in Figure 6.1. Strongly absorbed light is required for this type of excess carrier distribution (eg. λ = 632.8 nm, red). If the sample is illuminated at a certain moment with light of constant intensity through one electrode then the relaxation of the carrier density and of the current to a new steady state is governed by two processes;

(a) changes in the density due to electron transistions in the energy space (recombination, trapping, ionization, etc.)

(b) changes of the state due to the motion of carriers in coordinate space (diffusion and drift in an electric field).

Both processes occur simultaneously and are inter-dependent. An estimate of the infuence of each on the effective relaxtion time of the overall process can not be obtained from the time constants for each process alone. However, if one of these time constants, θ for the coordinate space, and τ for the energy space, is considerably larger than the oth-

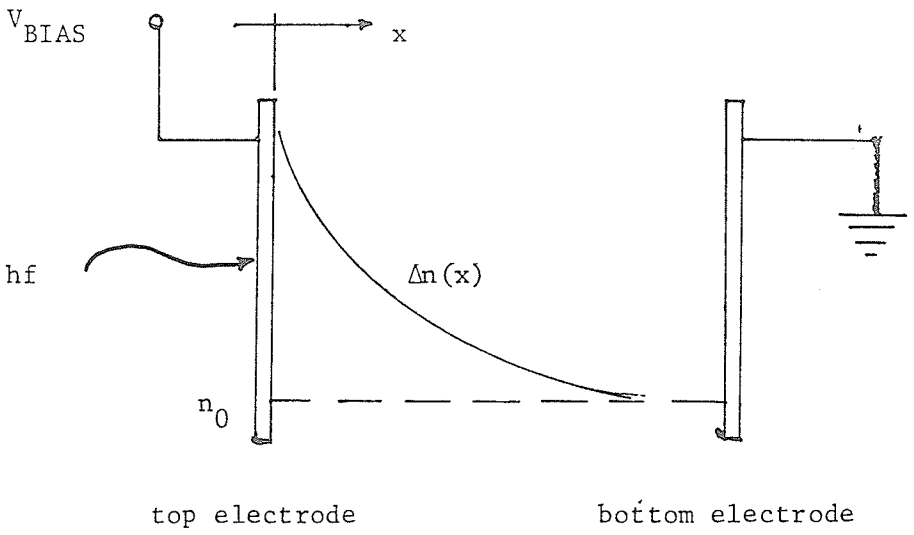

Figure 6.1: Excess carrier concentration distribution, n(x), for strongly absorbed light in a sandwich cell geometry.

er, then the larger time constant can be considered to govern the whole relaxation process.

The time for the establishment of a diffusion-drift equilibrium is governed by the electrical conductivity σ_0, and the permittivity ε. For our samples the room temperatue dark conductivity can be estimated to be about 10^{-9} $(\Omega\text{-cm})^{-1}$ [56]. Pawlewicz [56] has shown that films prepared by sputtering in Ar and H_2 gas mixtures have a resistivity, absorption coefficient and photoconductivity similiar to those prepared by glow-discharge of silane. For glow-discharge a-Si films, Spear and LeComber [9], give the room temperature defect controlled dark conductivity to be about 10^{-9} $(\Omega\text{-cm})^{-1}$. Apparently the incorporation of H_2 reduces the density of dangling bonds and hence localized states. A reduction of such localized states will reduce the room temperature dark conductivity, for sputtered films, from about 10^{-5} to 10^{-9} $(\Omega\text{-cm})^{-1}$ because the conductivity is contributed mainly by carriers hopping in localized states [56]. Therefore for $\sigma_0 = 10^{-9}$ $(\Omega\text{-cm})^{-1}$, typical of a-Si films, we have θ_m to be about 1.0 ms, based on Equation (5.7) by taking the relative permitivity, ε_r, to be about 10 for photon energies less than or equal to about 2 eV [37]. For low conductivity [σ_0 less than about 10^{-6} $(\Omega\text{-cm})^{-1}$] we would have to take in account the effects of impurity and/or defect states and therefore we would expect that for an impurity density as low as 10^{12} cm^{-3}, the screening length, ℓ_e,

as given by Equation (5.4) would be reduced considerably [84]. The reduced screening length is given by [84]

$$\ell_e' = [\varepsilon\, kT / e^2\, N_d]^{1/2} \quad , \tag{6.1}$$

where N_d is the density of acceptor-like impurity or defect states. By expressing the screening length as, $\ell_e' = (D\, \theta_m')^{1/2}$ and using $D = \mu kT/e$ we have

$$\theta_m' = \varepsilon / e\, \mu\, N_d \quad . \tag{6.2}$$

Taking $\mu_n = 10$ cm^2 /V-s [84], θ_m' has been estimated to be about 1.0 μs. The time constant θ_m has been reduced from about 1.0 ms to 1.0 μs for an impurity or defect density as low as 10^{12} cm^{-3}. For higher defect densities, θ_m is further reduced. Typical a-Si films have a defect density significantly in excess of 10^{12} cm^{-3}.

Since the lowest value of the photocurrent relaxation time constant is about 0.5 ms, we therefore can conclude that this relaxation process is not governed by the much faster diffusion-drift process. The relaxation of the photocurrent is due to changes in the carrier density due to transitions in energy space (eg. recombination, trapping, ionization, etc.) governed by an effective time constant τ. In addi-

tion, θ_m is in fact the rC time constant of the semiconductor. The rC time constant measured experimentally was less than 10 μs. (10 μs being the resolution of the measuring electronic system.).

It should be noted that in some cases the main component of the photocurrent relaxes in a time corresponding to the shorter of the time constants, and the residual photocurrent relaxes according to the longer time constant. Then the total photocurrent relaxation is not dominated simply by the component with the longer time constant.

However, this is not a problem encountered in our study. In fact the diffusion contribution to the photocurrent is negligibly small. Since the diffusion component relaxes relatively quickly, the photocurrent relaxation is dominated by transistions of carriers in energy space, where the photocurrent is mainly due to an excess number of carriers.

Figure 6.1 shows that there is an increase in current through the sample due to an increase in the number of carriers (drift term) and a carrier gradient (diffusion term). The ratio of the drift to diffusion components at any point x due to excess carriers is

$$R_{DD} = J_{drift} / J_{diffusion} = e\,\mu_n\,\Delta n(x)\,F(x) \Big/ e\,D\,[d\,\Delta n(x)/dx]$$
$$= (e/kT)\,(1/\alpha)\,F \quad , \qquad (6.3)$$

where F(x) = F the applied bias and the relation $D/\mu = kT/e$ was used. If we use $\alpha = 2 \times 10^4$ cm^{-1}, $kT/e = 0.026$ V and $F = 10^3$ v/cm, R_{DD} is about 2. $F = 10^3$ to 10^5 V/cm was the field used experimentally in measuring the photoconductivity, therefore R_{DD} is greater or at least equal 2. Thus, by considering that the measured photocurrent is due to the increase in the number of excess carriers in an applied field and the diffusion contriution can be neglected, Equation (5.22) is a good approximation for the photoconductance.

We have now established that the time for the establishment of diffusion equilibrium is much smaller than the time for the establishment of energy transition equilibrium. The contribution of diffusion current to the observed photocurrent is negligible, that is, the photocurrent is due to an excess concentration of carriers, brought about by optical transitions, drifting in an applied field. Thus the relaxation of the photocurrent can be considered to be due mainly to optical transitions, and the photoconductance is governed by Equation (5.22) and the diffusion component can be neglected.

6.2 PHOTOCONDUCTION - HIGH ABSORPTION REGION

6.2.1 Transient Photoconduction

A. Light intensity dependence of R_r and R_d

According to Equation (5.47), as g_{op} increases $g(t_{ss})/g_{op}$ decreases. This results in an increase in R_d [Equation

(5.34)] and R_r [Equation (5.39)]. This means that as the exciting light intensity increases, the ratio of the fast section on both the rise and the decay to the steady state photocurrent increases with increasing light intensity. This theoretical prediction is in good agreement with the experimental results shown in Figure 4.7. Using appropriate values for the various parameters, R_r and R_d can take on reasonable values. We can express K′ in Equation (5.34) as $K' = 1 + N_t(t_{ss})/N_r$, by using $\upsilon S_n = 1/N_r\tau_n$. From dark conductivity measurements the dark Fermi level is located above the midgap for all samples, therefore E_{Fn} should also always be above the midgap. Since the total number of localized states from E_{Fn} to E_c act as electron traps, and make up $N_t(t_{ss})$, and since the total number of localized states below E_{Fn} to E_v act as electron recombination centers, then $N_r > N_t(t_{ss})$ if the distribution of localized states density is somewhat symetric about the midgap.

Regarding the above arguement, K′ can be estimated to be roughly unity. Suppose also, that $N_A = 10^{19}$ cm^{-3} eV^{-1} (see Equation (5.41) and that the density distribution of localized states drops to 5×10^{14} cm^{-3} eV^{-1} at 0.1 eV below E_c, then we have estimated $kT_1 \simeq 10^{-2}$ eV from Equation (5.41). Using $N_A = 10^{19}$ cm^{-3} eV^{-1}, $\upsilon = 10^7$ cm/s, $S_n = 10^{-15}$ cm^2, $kT_1 = 10^{-2}$ eV, $N_M (E_P - E_{Fn}) = 10^{17}$ cm^{-3} and $\tau_n = 10^{-9}$ s as suggested by experimental data, we find $g(t_{ss})/g_{op} \simeq 2$ from Equation (5.47). With this value of $g(t_{ss})/g_{op}$ and K′, R_d

and R_r have been estimated to be about 0.33 from Equations (5.34) and (5.39). If E_{Fn} moves up with increasing intensity such that $(E_P - E_{Fn}) = 0$, then $g(t_{ss})/g_{op} \simeq 1$ and R_r and R_d increase to about 0.5.

B. Light intensity dependence of τ_r and τ_d

Experimentally we have found that τ_d seems to approach τ_r as the light intensity increases. Also an increase in intensity results in a decrease in both τ_r and τ_d as shown in Figure 4.3. These features can be explained as follows. The free electron density is given by

$$n = N_c \exp[-(E_c - E_{Fn})/kT] \quad , \qquad (6.4)$$

and the reduced density of states by

$$n_1 = N_c \exp[-(E_c - E_{te})/kT] \quad . \qquad (6.5)$$

By assuming that $E_{Fn} \simeq E_{te}$, $n_1/n \simeq 1$, Equation (5.54) becomes

$$\tau_r/\tau_d = n_t(t=0) \cup S_n \tau_n [(1/\tau_n) + N_t(t=0) \cup S_n] \tau_n \quad . \qquad (6.6)$$

Taking a value of $n_t(t=0) \simeq 10^{17}$ cm^{-3} as estimated from the ratio of response time to lifetime, and representative values of $\upsilon = 10^7$ cm/s, $S_n \simeq 10^{-15}$ cm^2, $N_t(t=0) \simeq 10^{18}$ cm^{-3} we have estimated τ_r/τ_d to be about 0.1 based on $\tau_n \simeq 10^{-10}$s deduced from the experimental results. Thus we can see that as experimentally observed, τ_r can be less than τ_d. Also as shown in Figure 4.9, τ_n increases with increasing intensity. If τ_n increases to about 3×10^{-10}s then $\tau_r/\tau_d \simeq 10^9 \tau_n^2 [\, 1/\tau_n + 10^{10}\,] = 1.0$. As the excitation intensity increases the two response times τ_r and τ_d tend to become approximately equal. The parameters $n_t(t=0)$, υ, S_n, and $N_t(t=0)$ obviously provide many degrees of freedom to adjust τ_r/τ_d to fit many possible qualities in the characteristics of τ_r and τ_d.

We can show the decrease in τ_r and τ_d with increasing intensity easily. Consider first τ_r as given by Equation (5.55) . Use as before representative values of $\upsilon \simeq 10^7$ cm/s, $S_n \simeq 10^{-15}$ cm^2, and as suggested by experimental results, a value of $N_t(t=0) \simeq 10^{18}$ cm^{-3} and $\tau_n \simeq 10^{-9}$ to 5×10^{-9} s. With these values, in Equation (5.55), the term $1/\tau_n + N_t(t=0)\upsilon S_n \simeq N_t(t=0)\upsilon S_n = 10^{10}$ s^{-1}. Since $n_t(t=0)$ is constant, Equation (5.55) simplifies to

$$\tau_r = K'' \tau_n / g_{op} \quad . \qquad (6.7)$$

Any change in τ_r is due to the variation of τ_n as compared to the variation of g_{op}. Experimental results in Figure 5.5 show that τ_n varies with g_{op} at some power smaller than unity so that we expect the value of τ_r to fall as g_{op} increases.

Now consider the decrease of τ_d with increasing excitation intensity. For a continuous distribution of localized states through the bandgap, as E_{Fn} moves toward E_c with increasing intensity we expect that the effective trap depth of the localized state distribution, E_{te}, will also move toward E_c since only the localized states above E_{Fn} act as traps and E_{Fn} is assumed to be close to the electron demarcation level. Therefore at $t = t_{ss}$ if the excitation, g_{op}, is made larger prior to cessation, $(E_c - E_{te})$ will become smaller and $n_1(t_{ss})$ increases. This results in, according to Equation (5.56) a decrease in τ_d. As the initial excitation prior to cessation increases, $n_1(t_{ss})$ increases resulting in a decrease in τ_d. From the photocurrent data, the electron carrier concentration can be estimated and it is about 2×10^{10} /cm^3 which also gives a value of 0.60 for $E_c - E_{Fn}$. Taking $E_c - E_{Fn} = 0.60$ eV, and $N_c = 10^{20}$ cm^{-3}, we have $n_1 = 10^{10}$ cm^{-3}. Using $\upsilon = 10^7$ cm/s, $\tau_d = 10^{-3}$ s (from experimental data), we have $S_n \simeq 1/\upsilon n_1 \tau_d = 10^{-14}$ cm^2 from Equation (5.56).

The physical interpretation for τ_r and τ_d is as follows. The term $N_t(t=0)\upsilon S_n$ in Equation (5.55) represents the speed

for removing electrons from the conduction band into trapping states. The larger this term the larger τ_r will be. Under steady light excitation the electron concentration will increase until an appropriate steady state value is reached. If, however, electrons are being removed by trapping, more time will be required for the electon concentration to reach its final value. Obviously, if this trapping rate is large (that is $N_t(t=0) \cup S_n$ is large) the net rate for the increase of the electron concentration in the conduction band (that is the rate at which electrons are excited into the conduction band by photogeneration minus the rate at which they are trapped in the trapping states) will be small and hence τ_r will be large.

Equation (5.56) indicates that τ_d is governed by the slow thermal release of electrons from traps. During the decay of the photocurrent, after the fast section is completed, time is required for trapped electrons to be thermalized into the conduction band. Once the electrons enter the conduction band they will quickly recombine. The time constant during this period will be determined by the slow thermal release of trapped electrons.

C. Field dependence of τ_r and τ_d

Figure 4.5 shows that the time constant τ_d decreases as the applied field F is increased. The behaviour for τ_r is quite similiar to that of τ_d. The effect of applied fields

can be interpreted as field-assisted detrapping or as a reduction in the possibility of retrapping [90]. Kallman and Mark [91] have found that the emptying of traps is accelerated by the presence of fields as low as 10^3 V/cm. For fields of 4×10^2 to 10^3 V/cm, Martini and McMath [92] have discussed field-assisted reemission of charge carriers from shallow impurity centers in Germanium based on the Poole-Frenkel theory.

The variation of the response times τ_r and τ_d with field can be explained by the movement of the dark Fermi level with field. At sufficiently high applied fields we can have a sudden increase in the density of free electrons injected from the cathode. This is shown in Figure 6.2. The number of electrons being captured in traps increases with time. Finally, a steady state is reached such that the rate of thermal excitation of electrons out of traps is equal to the rate of capture of free electrons by traps. That is, the Fermi level is raised to a new position consistent with a higher density of free electrons. The rise in the dark Fermi level with increasing field can now be used to explain the experimental behaviour of the response times with field.

Taking representative values of the following parameters: $N_t(t=0) \simeq 10^{18}$ cm^{-3}, $\upsilon \simeq 10^7$ cm/s, $S_n \simeq 10^{-15}$ cm^2 and $\tau_n \simeq 10^{-9}$ s, the term $1/\tau_n + N_t(t=0)\upsilon S_n \simeq N_t(t=0)\upsilon S_n$ in Equation (5.55). Since N_t is the total trap density from E_{Fn} to E_c for a quasi-continuous distribution of localized states

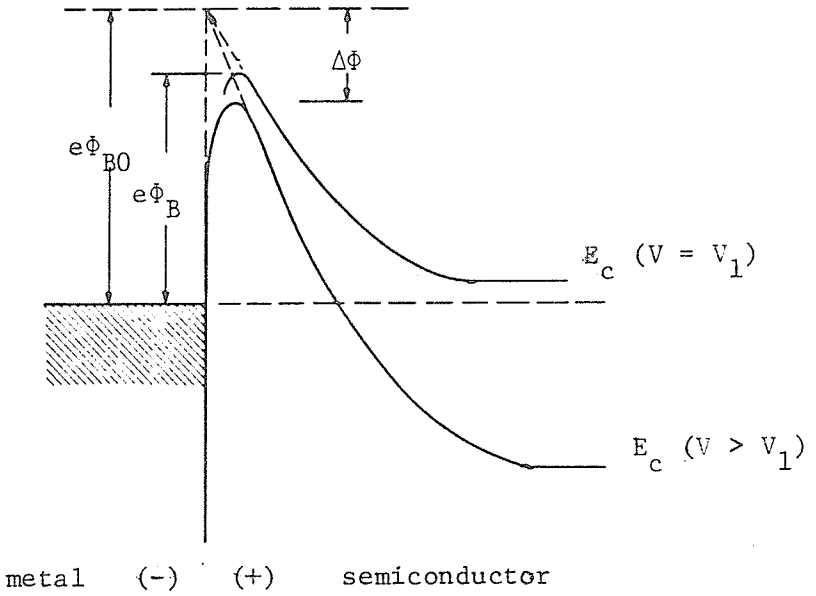

(a)

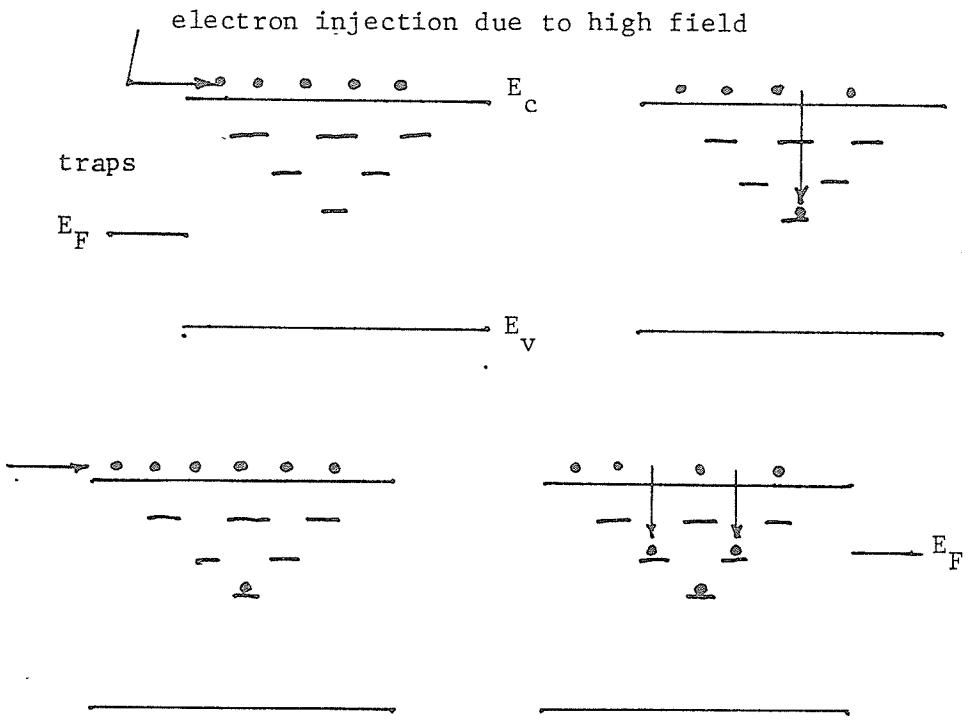

(b)

Figure 6.2: (a) Energy-band diagram for a metal-semiconductor contact under different baising conditions. Barrier lowering due to an increase in applied bias results in enhanced electron injection from the metal into the semiconductor. $e\Phi_{BO}$, intrinsic barrier height; $e\Phi_B$, barrier height at thermal equilibrium; $\Delta\Phi$, barrier lowering under applied bias. (b) Injection of electrons from electrodes due to a high field and subsequent rise of E_F.

throughout the bandgap, we would expect N_t to decrease since E_{Fn} moves toward E_c as the applied field is increased. This means that an increase in applied field will cause a decrease in τ_r since τ_r is dependent on $N_t(t=0)$ as given in Equation (5.55). Following the same arguement, an increase in applied field will increase n_1 given by Equation (6.5) since we assume E_{Fn} is close to E_{te}. According to Equation (5.56) the increase in n_1 with field will result in a decrease in τ_d.

D. Composition dependence of R_r, R_d, and τ_n

The effect of Germanium composition, x, on the photoconductive properties of the films is shown in Figure 4.7. Both R_r and R_d decrease as x increases. Also, Figure 4.9 indicates that increasing x enhances the electron lifetime τ_n.

By writing $\tau_n = 1/[N_r \upsilon S_n]$, then $g(t_{ss})/g_{op} \simeq [N_M(E_P-E_{Fn}) + N_A kT_1] / N_r$ in Equation (5.47). It can be seen from Equations (5.34) and (5.39) that R_d and R_r should decrease with increasing x. This implies that $g(t_{ss})/g_{op}$ increases with increasing x. This can be accounted for by changes in N_A, T_1, or N_r. If N_A is taken as approximately N_c, we would expect N_A and hence $g(t_{ss})/g_{op}$ to decrease with increasing x since N_c for Ge is less than that for Silicon. This would result in an increase in R_d and R_r with x. However, this expectation is contrary to what is observed. An

increase in T_1 and/or a decrease in N with increasing x will result in a reduction in R_d and R_r. Regarding the electron lifetime, a reduction of N_r and/or S_n with increasing x, will result in an increase of τ_n with x since $\tau_n = 1 / N_r \upsilon S_n$.

A reduction of the electron recombination center density caused by the change of x can occur simply because the number of such states may be reduced or spread in energy due to the change of x. Figure 6.3 shows how a spread in energy of the high density of localized states can lead to a reduction of N_r. In the first case there may be a narrow concentration of localized states, most of which can contribute to N_r since they lie below E_{Fn}. If this concentration of localized states remains the same in total number but becomes spread out in energy as in Figure 6.3b, N_r may be reduced due to some localized states now appearing above E_{Fn} and hence not contributing to N_r.

In Figure 4.3 we can see that τ_d is about 2×10^{-3} s for high illumination levels for every value of x. Thus from Equation (5.56), S_n can be calculated for each x. First from Equations (6.4) and (6.5) we see that if $E_{Fn} \simeq E_{te}$, $n_1 \simeq n$. From the measured photocurrent at $t = t_{ss}$ we have calculated n for each x at the illumination corresponding to $\tau_d = 2 \times 10^{-3}$ s and it is: 2.1×10^{10} cm^{-3} for x = 0, 1.6×10^{10} cm^{-3} for x = 0.10, and 7.7×10^{10} cm^{-3} for x = 0.25. With this appropriate value of n for

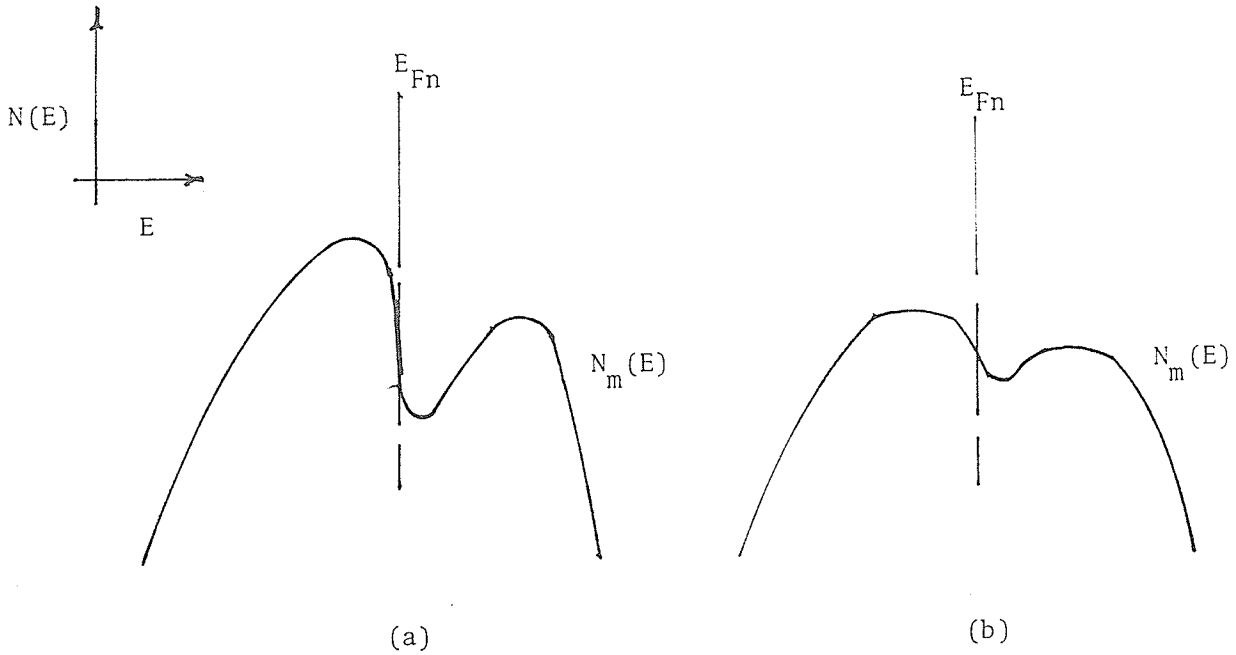

Figure 6.3: Change in shape of $N_m(E)$ (see Figure 5.4) which results in a decrease in the density of recombination centers for electrons (states below E_{Fn}), N_r due to the increase of x. (a) $x = 0$ (b) $x > 0$.

each x and $\upsilon = 10^7$ cm/s, we have, from Equation (5.56), $S_n \simeq 2.5 \times 10^{-15}$ cm^2 for x = 0, $S_n \simeq 3 \times 10^{-15}$ cm^2 for x = 0.10, and $S_n \simeq 6.5 \times 10^{-16}$ cm^2 for x = 0.25. It can be seen that a reduction in S_n is responsible for the increase in τ_n with x as shown in Figure 4.9. The calculated values for S_n for x = 0 and x = 0.10 are about equal while for x = 0.25, S_n decreases by a factor of about 5. The pattern is reflected by a approximately equal value for τ_n for x = 0 and x = 0.10 and an increase by about 5 for x = 0.25, as illustrated in Figure 4.9.

Using the computed values of S_n, we can estimate the total density of localized states acting as electron recombination centers, N_r, from the relation $\tau_n = 1 / N_r \upsilon S_n$. Using the appropriate value of τ_n we find $N_r \simeq 3 \times 10^{16}$ cm^{-3} for x = 0, $N_r \simeq 2.5 \times 10^{16}$ cm^{-3} for x = 0.10, and $N_r \simeq 1.5 \times 10^{16}$ cm^{-3} for x = 0.25. Thus the observed increase in τ_n can be attributed to the decrease of both N_r and S_n.

6.2.2 Steady State Photoconduction

A. Intensity dependence of J_{ph}

The photocurrent increases as some power greater than unity, of light intensity over a short range of light intensities as shown in Figure 4.9. An increase in intensity causes an increase in the electron lifetime, τ_n, over a small region. The increase of photocurrent as a high power

(greater than unity) of the light intensity is generally referred to as supralinearity [7].

In the region where the localized state density in the gap $N_m(E)$ decreases with decreasing E as shown in Figure 5.4, the movement of E_{Fn} due to light illumination will result in a rapid decrease in the rate of increase of the density of recombination centers, or in other words, in a rapid increase in electron lifetime τ_n and Δn. This reflects that there is a range of light intensities for which E_{Fn} moves towards the energy level for the dip of $N_m(E)$. In this range of light intensities the photoconductivity is supralinear, with $\nu > 1$, and the recombination is mainly monomolecular. From Figure 4.9 we see the supralinear dependence of photoconductivity σ_{ph}, on intensity. The intensity dependence can be described by

$$\sigma_{ph} = e \mu_n \Delta n \propto I^{\nu} \quad , \tag{6.8}$$

where for low intensities $\nu > 1$. However, as E_{Fn} moves toward the energy level E_D corresponding to the dip of $N_m(E)$, ν changes gradually to the values less than unity, and at E_D the recombination become the mixture of monomolecular and bimolecular recombinations with $\nu \simeq 0.75$. When E_{Fn} reaches E_D, the electron lifetime reaches the peak value. When E_{Fn} moves to levels lower than E_D, the localized state density

$N_m(E)$ starts to increase again. In the range of light intensities for this to occur, τ_n should start to decrease as shown in Figure 4.9. The dip in $N_m(E)$ obviously implies that there are two peaks in $N_m(E)$ and thus the modified Davis and Mott model for gap state distribution is an appropriate model for a-$Si_{1-x}Ge_x$(H) films. Vanier et al. [93], have observed supralinear photocurrent in plasma-deposited hydrogenated undoped a-Si films. Their explanation of the phenomenon follows the discussion given by Rose [7], based on electronic doping and sensitization.

B. Field dependence of J_{ph}

Figure 4.11 shows a rapid increase in the photocurrent, especially for x = 0.10 and 0.25, at fields of about 6×10^4 V/cm. There are many possible explanations for this behaiour. The rapid increase in the photocurrent with applied field may be caused by the following mechanisms:

(a) The barrier height for photoinjection from the electrodes may be reduced by the applied field. This mechanism is not likely to occur based on the fact that the photocurrent increased linearily with the applied field for the excitation with infrared light.

(b) The density of trapped electrons is decreased by impact ionization or by field extraction by tunneling [94]. Both of these mechanisms, however, require a field in the order of 10^5 to 10^6 V/cm [95]. In our experiments the fields are in the range from 10^3 to 10^5 V/cm.

(c) Field trapping parameters are changed by the applied field, as reported by Dussel and Bube [95] in CdS-CdSe crystals for fields of less than 3×10^3 V/cm.

(d) Field dependent carrier mobility.

(e) The electron lifetime and hence the photocurrent are increased by the applied field. We believe mechanism (e) is the major mechanism responsible for the field dependence of J_{ph}. At sufficiently high fields, n will be due to photogenerated electrons and electrons resulting from field injection from the electrodes. If the electron density due to injection is a significant component of the total electron density, the high applied field will result in movement of E_{Fn} toward E_c. In the previous section, we had shown how the movement of E_{Fn} toward E_c increases τ_n. When the field is of sufficient magnitude, we will see the beginning of a sharp increase in the photocurrent due to the increased movement of E_{Fn}. The ratio of the photogenerated electron density to the thermal equilibrium electron density is: 100 for x = 0, and 20 for x = 0.10 and 0.25; hence we would expect this field effect to be more prevalent in the films x = 0 and x = 0.25. This is the case as shown in Figure 4.11.

6.3 PHOTOCONDUCTION - LOW ABSORPTION REGION

The difference between excitation with infrared light (λ = 940 nm) and that with red light (λ = 632.8 nm) is that for infrared light an increase in carrier concentration would be expected to be due to photoinjection from the electrodes rather than creation of carriers inside the film. Figure 5.6 shows the process of electron and hole photoinjection from a metal electrode. For infared excitation, hf is about 1.32 eV, and thus photoinjection of holes is unlikely since 1.32 eV is less than the bandgap expected for our films (about 1.6 to 1.375 eV if the bandgap varies linearily with Germanium content as $E_g \simeq -0.9x + 1.6$ eV for $Si_{1-x}Ge_x$, x = 0 to 0.25). Thus just as was the case for excitation of λ = 632.8 nm, infrared excitation will result in photocurrent due to an increase in the electron concentration with few holes. Equation (5.28), given during discussion for red light excitation, still applies for infrared excitation where the generation of carriers is from the electrodes rather than in the bulk of the film.

The decrease in τ_r and τ_d with increasing excitation intensity, I, for λ = 940 nm (Figure 4.4) can be explained in the same way as for red light excitation (section 5.3.2). τ_r is proportional to $1/g_{op}$ (Equation 5.55) and the decrease in τ_d is as a result of the movement of E_{Fn} toward E_c with increasing n_1 or with increasing g_{op} [Equation (5.56)].

Figure 4.6 shows a decrease in τ_d with increasing applied field. The same behaviour is also observed for τ_r. Again the arguements for λ = 632.8 nm apply also for infrared excitation. An increase in the applied field will result in a rise in the dark Fermi level due to injection of electrons from the electrodes. This rise in E_F results in a decrease in N_t and an increase in n_1. This also results in a decrease in τ_r [Equation (5.55)] and in τ_d [Equation (5.56)].

From Figure 4.8 it can be seen that R_r is approximately constant with intensity for λ = 940 nm. Also, R_r seems to decrease with increasing x. As was the case for λ = 632.8 nm the decrease in R_r with increasing x may be interpreted as being due to an increase in T_1 and/or a reduction in N_r with increasing x. The mechanism behind a relatively constant R_r with intensity is not clear.

Figure 4.10 and 4.11 show a linear increase of the photocurrent with excitation intensity and applied field. A linear variation of photocurrent with intensity indicates that the electron lifetime, τ_n, is constant. Figure 4.10 indicates that as for red illumination, an increase in Germanium content, x, increases τ_n since the photocurrent increases with increasing x. That the photocurrent increases linearily with applied field as shown in Figure 4.12 implies that the applied field does not alter the barrier height for photoinjection.

Using the following expression for electron mobility [96]

$$\mu_n \equiv e\,\bar{t} \,/\, m_n^* \quad . \tag{6.9}$$

we can estimate the relaxation time (mean time) between collisions $\bar{t}$. Taking μ_n = 1 cm /V-s and $m_n^* = m_0 = 9.11 \times 10^{-31}$ kg, we have $\bar{t} = 5.7 \times 10^{-16}$ s. m_n^* is the electron effective mass. We can also estimate the electron mean free path, $\bar{\ell}$, from the following equation

$$D = \bar{\ell}^2 \,/\, 2\bar{t} \quad . \tag{6.10}$$

Taking $D = 0.026$ cm^2 based on μ_n = 1 cm^2/V-s and $\bar{t} = 5.7 \times 10^{-16}$ s, the value of $\bar{\ell}$ has been estimated to be 5.4×10^{-9} cm. The above estimated values for $\bar{t}$ and $\bar{\ell}$ imply that (a) $F\bar{\ell} \ll kT/e$ for the field 10^3 - 10^5 V/cm (see section 5.4). Also we expect that (b) the energy of the injected electron is large compared to kT since the photon energy of the infrared light is 1.32 eV which is much larger than the expected Φ_B. Thus $0.5mv^2$ should be to 1.32 eV. The velocity v, can be estimated from

$$0.5\, m_0\, v^2 = (hf - \Phi_B) \simeq hf \quad . \tag{6.11}$$

Thus $\upsilon \simeq 4.8 \times 10^{7}$ cm/s which is slightly higher than the thermal velocity. By assuming $\Phi_B/hf \ll 1$, and taking $\upsilon = 4.8 \times 10^{7}$ cm/s, $\mu_n = 1$ cm^2/V-s, and $F = 10^4$ V/cm, the ratio j/j_0 is estimated to be about 10^{-3} from Equation (5.58). The net yield based on Equation (5.57) is about 50% of the ration j/j_0, that is about 5×10^{-4}.

From the measured power of the infrared light and reflectivity of the top Al electrode, we can estimate the total photon flux absorbed by the top and/or bottom electrodes. By assuming that all the radiation that is not reflected is completely absorbed by the electrodes, none being absorbed by the $Si_{1-x}Ge_x$ film; the net number of electrons photoinjected into the film per cm^2 per second is equal to the net yield times the total incident photon flux, that is $5 \times 10^{-4} \times 10^{17} \simeq 5 \times 10^{13}$ electrons/cm^2-s. For simplicity we assume a uniform concentration of photoinjected electrons throughout the film and a uniform applied electric field. For the sample, x = 0, the film thickness is about 2.5×10^{-4} cm which is equivalent to an effective volume generation rate, $g_{op} \simeq 5 \times 10^{13} / 2.5 \times 10^{-4} = 2 \times 10^{17}$ electrons/cm -s. From Figure 4.12 at an applied field of 10^4 V/cm the photocurrent for x = 0 is about 10^{-8} A, or the photocurrent density is about $10^{-8} / 3.14 \times 10^{-2} \simeq 3 \times 10^{-7}$ A/cm . We can also estimate the electron concentration from the following relation

$$J_{ph} = \sigma_{ph} F = e \Delta n \mu_n F \quad . \qquad (6.12)$$

For μ_n = 1 cm /V-s, $F = 10^4$ V/cm and $J_{ph} = 3 \times 10^{-7}$ A/cm , Δn is about 1.9×10^8 cm^{-3}. The electron lifetime can be estimated from $\tau_n = \Delta n / g_{op}$, which gives 10^{-9} s. This agrees very well with the value estimated for red light excitation and x = 0 as shown in Figure 4.9. It can be concluded that the theory, based on which the yield for photoinjection and other parameters have been calculated, agrees well with the experimental results.

Chapter VII

CONCLUSIONS

(1) Experimental data for the steady state and transient photocurrent in r.f. sputter deposited a-$Si_{1-x}Ge_x$(H) films can be interpreted in terms of a distribution of states similiar to that of the modified Davis and Mott model.

(2) For excitation of these films with red light, the photocurrent is mainly due to photogenerated electrons with the photogenerated holes being rapidily trapped by deep centers. For infrared light excitation, absorption is as a result of photoinjection of electrons from the metal electrode into the film.

(3) The transient photocurrent consists of a fast section, or trap-free behaviour, and a slow section, or trap-controlled behaviour.

(4) The ratio of the fast section of the photocurrent to the total photocurrent for the rising transient and decaying transient is denoted as R_r and R_d, respectively. The increase in R_r and R_d is as a result of the decrease of $g(t_{ss})/g_{op}$ with increasing illuminating light intensity, where $g(t_{ss})/g_{op}$ is the ratio of the electron generation rate from traps to the electron photogeneration rate.

(5) Both the photoresponse times during the rising and decaying transient, τ_r and τ_d respectively, decrease with increasing illuminating light intensity. The change in τ_r is due to the variation of the electron lifetime τ_n, as compared to the variation of g_{op}, with light intensity. For τ_d, the increase of the reduced density of states at steady state $n_1(t_{ss})$, with increasing light intensity results in the observed decrease of τ_d.

(6) τ_r and τ_d are directly dependent on electron trapping and detrapping, respectively.

(7) The decrease in τ_r and τ_d with increasing applied field is due to the decrease in the total density of trapping centers $N_t(t=0)$, and increase in $n_1(t_{ss})$ with applied field.

(8) The capture cross section for an unoccupied center for an electron S_n, for these films is about 3×10^{-15} cm^2 for $x = 0$ and $x = 0.10$ and decreases to 6.5×10^{-16} cm^2 for $x = 0.25$. This decrease in S_n with x results in an increase in τ_n.

(9) The decrease in R_r and R_d with x is as a result of a decrease in the total density of recombination centers N_r, with x.

(10) At steady state for red light excitation, a supralinear dependence of photocurrent on illuminating light intensity is observed for all x, where the power dependence constant ν, increases as x increases.

(11) For red light excitation, the supralinear increase of the steady state photocurrent with applied field is due to an enhancement of τ_n. The increase in τ_n is attributed to the movement of the dark Fermi level with applied field.

(12) The behaviour of these films for infrared light excitation is basically the same as that for red light excitation.

REFERENCES

1. A. Onton, H. Wieder, J. Chevallier, and R.C. Guarnieri, Proc. of the 7th Int. Conf. on Amorphous and Liquid Semiconductors, Edinburgh, p. 357, (1977).

2. N. Van Dong, T.H. Danh, and J.Y. Leny, J. Appl. Phys. 52(1), 338, (1981).

3. T. Suzuki, M Hirose, S. Ogose, and Y. Osaka, Phys. Stat. Sol. (a) 42, 337, (1977).

4. R.J. Loveland, W.E. Spear, and A. Al-Snarbaty, J. Non-Cryst. Solids 13, 55, (1973/74).

5. P.J. Zanzucchi, C.R. Wronski, and D.E. Carlson, J. Appl. Phys. 48(12), 5227, (1977).

6. W. Fuhs, M. Milleville, and J. Stuke, Phys. Stat. Sol.(b) 89, 495, (1978).

7. A. Rose, Concepts in Photoconductivity and Allied Problems, (Interscience, New York, 1963).

8. D.A. Anderson and W.E. Spear, Phil. Mag. 36(3), 695, (1977).

9. W.E. Spear and P.G. LeComber, Phil. Mag. 33(b), 935, (1976).

10. W. Rehm, R. Fischer, J. Stuke, and H. Wagner, Phys. Stat. Sol. (b) 79, 539, (1977).

11. P.G. LeComber and W.E. Spear, Phys. Rev. Letters 25, 509, (1970).

12. D.L. Staebler and C.R. Wronski, Appl. Phys. Letters 31, 292, (1977).

13. R. Fischer and D. Vornholz, Phys. Stat. Sol.(b) 68, 561, (1975).

14. P.G. LeComber, A. Madan, and W.E. Spear, J. Non-Cryst. Solids 11, 219, (1972).

15. D.L. Dexter, C.C. Klick, and C.A. Russell, Phys. Rev. 100, 603, (1955).

16. N.F. Mott, E.A. Davis, and R.A. Street, Phil. Mag. 32, 961, (1975).

17. R.A. Street, Phys. Rev. B 17(10), 3984, (1978).

18. N.F. Mott, Phil. Mag. 36(2), 413, (1977).

19. E.A. Davis, J. Non-Cryst. Solids 4, 107, (1970).

20. J.C. Knights and E.A. Davis, J. Phys. Chem. Solids 35, 543, (1974).

21. L. Onsager, Phys. Rev. 54, 554, (1938).

22. T.S. Nashashibi, I.G. Austin and T.M. Searle, Phil. Mag.

35(3), 831, (1977).

23. W.E. Spear, Amorphous and Liguid Semiconductors, edited by J. Stuke and W. Brenig (Taylor and Francis, London, 1974), p. 1.

24. W.E. Spear and P.G. LeComber, Proceedings of the 7th Int. Conf. on Amorphous and Liquid Semiconductors, edited by W.E. Spear (Edinburgh University, 1977) p. 309.

25. J.I. Pankove and D.E. Carlson, Appl. Phys. Letters 29(9), 620, (1976).

26. D. Engemann and R. Fischer, Phys. Stat. Sol.(b) 79, 195, (1977).

27. J.C. Knights, AIP Conf. Proc. 31, 296, (1976).

28. R.A. Street, J.C. Knights, and D.K. Biegelsen, Phys. Rev. B 18(4), 1880. (1978).

29. D. Engemann and R. Fischer, Amorphous and Liguid Semiconductors, edited by J. Stuke and W. Brenig (London, Taylor and Francis Ltd.) 1974, p. 947; Proc. of the 12th Int. Conf. on the Physics of Semiconductors, edited by M.H. Pilkuhn (Stuttgart, Tuebner), 1976, p. 1042.

30. D. Engemann and R. Fischer, AIP Conf. Proc. 31, 37, (1976).

31. D. Engemann, R. Fischer, F.W. Richter, and H. Wagner, Structure and Properties of Non-Crystalline Semiconductors, edited by B.T. Kolomiets (Lennigrad, 1976) p. 217.

32. M.H. Brodsky, J.J. Cuomo, and F. Evangelist, Proc. of the 7th Int. Conf. on Amorphous and Liquid Semiconductors, edited by W.E. Spear (University of Edingburgh, 1977) p. 397.

33. D. Engemann and R. Fischer, Structure and Excitations of Amorphous Solids, edited by G. Lucovsky and F.L. Galaener, (American Insitute of Physics, Williamburg).

34. C.W. Peterson, J.H. Dinan, and T.E. Fischer, Phys. Rev. Letters 25(13), 861, (1970).

35. T.E. Fischer and M. Erbudak, Phys. Rev. Letters 27(18), 1220, (1971).

36. D.T. Pierce and W.E. Spicer, Phys. Rev. Letters 27(18), 1217, (1971).

37. D.T. Spicer and W.E Spicer, Phys, Rev. B 5(8), 3017, (1972).

38. L. Ley, S. Kowalczyk, R. Pollack, and D.A. Shirley, Phys. Rev. Letters 29(16), 1088, (1972).

39. R. Grigorovici, N. Croitoru, and A. Devenyi, Phys. Stat. Sol. 23, 621, (1967).

40. P.A. Wiley, Thin Solid Films 2, 327, (1968).

41. M.H. Brodsky and R.J. Gambino, J. Non-Cryst. Solids 8-10, 739, (1972).

42. A. Lewis, Phys. Rev. Letters 29, 1555, (1972).

43. W. Beyer and J. Stuke, Proc. of the 5th Int. Conf. on Amorphous and Liquid Semiconductors, Edited by J. Stuke and W. Brenig, (Taylor and Francis, London, 1974) p. 251.

44. S.K. Bahl and S.M. Bhagat, J. Non-Cryst. Solids 17, 409, (1975).

45. A. Madan, P.G. LeComber, and W.E. Spear, J. Non-Cryst. Solids 20, 239, (1976).

46. M.H. Brodsky, R.S. Title, K. Weiser, and G.D. Pettit, Phys. Rev. B 1, 2632, (1970).

47. D.K. Paul and S.S. Mitra, Phys. Rev. Letters 31, 1000, (1973).

48. A.J. Lewis, Phys. Rev. B 13, 2565, (1976).

49. W.E. Spear and P.G. LeComber, J. Non-Cryst. Solids 8-10, 727, (1972).

50. W.E. Spear, R.J. Loveland, and Al-Sharbaty, J. Non-Cryst. Solids 15, 410, (1974).

51. M.H. Brodsky, M.A. Frisach, J.F. Ziegler, and W.A. Lanford, Appl. Phys. Letters 30, 561, (1977).

52. C.R. Wronski, D.E. Carlson, and R.E. Daniel, Appl. Phys. Letters 29, 602, (1976).

53. R.C. Chittick, J.H. Alexander, and H.F. Sterling, J. Electrochem. Soc. 116, 77, (1969).

54. W.E. Spear, Fifth Int. Conf. Proc., Garmisch- Partenkirchen, Germany, Edited by J. Stuke and W. Brenig (Taylor and Francis, London, 1974) p. 1.

55. J.J. Hauser, Solid State Commum. 19, 1049, (1976).

56. W.T. Pawiewicz, J. Appl. Phys. 49(11), 5595, (1978).

57. W. Paul, Thin Solid Films 33, 381, (1976).

58. R.J. Temkin, W. Paul, and G.A.N. Connel, Adv. Phys. 22, 581, (1973).

59. M.H. Brodsky, R.S. Title, K. Wiesier, and G.D. Petit, Phys. Rev. B 1, 2632, (1970).

60. W. Paul, G.A.N. Connel and R.J. Temkin, Adv. Phys. 22, 529, (1973).

61. A.J. Lewis, Phys. Rev. B 14, 658, (1976).

62. G.A.N. Connel and J.R. Pawlik, Phys. Rev. B 13, 787, (1976).

63. T.D. Moustakas and W. Paul, Phys. Rev. B 16, 1564, (1977).

64. T.M. Donovan, M.L. Knotek, and J.E. Fischer, Proc. of the 5th Int. Conf. on Amorphous and Liquid Semiconductors, edited by J. Stuke and W. Brenig. (Taylor and Francis, London, 1974) p. 549.

65. R. Fischer and D. Vornholz, Phys. Status Solidi B 68, 561, (1975).

66. T.D. Moustakas, C.A.N. Connel, and W. Paul, Electonic Phenomena in Non-Crystalline Semiconductors, edited by B.T. Kolomiets (Academy of Sciences of the USSR, 1976) p. 310.

67. L. Vescan and N. Croitoru in Ref. 64 p. 244.

68. M. Hirose, I. Ohe, and Y. Osada in Ref. 64 p. 255.

69. J.E. Fischer, Thin Film Solids 17, 223, (1973).

70. J.E. Fischer and T.M. Donvan, Opt. Commun. 3, 116, (1971).

71. M.L. Knotek and T.M. Donovan, Phys. Rev. Letters 30, 652, (1973).

72. N.F. Mott and E.A. Davis, Electronic Processes in Non-Crystalline Materials, Clarendon Press, Oxford, 1977, p. 378.

73. L. Vescan and N. Croitoru, Conf. on Amorphous Semiconductors, 1974, Reinhardsbrunn, East Germany, Akad. Wiss der DDR.

74. G. Jungk, Phys. Stat. Sol.(b) 46, 603, (1971).

75. G.A.N. Connell, R.J. Temkin, W. Paul, Adv. Phys. 22, 643, (1973).

76. G.A.N. Connel, Topics in Appl. Physics 30, Amorphous Semiconductors, M.H. Brodsky Editor, New York 1979, p. 95.

77. B. Kramer, Phys. Stat. Sol.(b) 47, 501, (1971).

78. J.D. Joanopoulos and M.L. Cohen, Solid State Commum. 13, 1115, (1973).

79. Y.F. Tsay and D.K. Paul, Phys. Rev. B 8(6), 2827, (1977).

80. J. Szczyrbowski, Phys. Stat. Sol.(b) 79, K43, (1977).

81. W.E. Spear and P.G. LeComber, Photoconductivity and Related Phenomena, Edited by J. Mort and D.M. Pai, Elsevier Scientific Publishing Co., New York, 1976, p. 187.

82. C.R. Wronski and R.E. Daniel, Phys. Rev. B 23(2), 794, (1981).

83. A. Rose, RCA Rev. 12, 362, (1951).

84. S.M. Ryvkin, Photoelectric Effects in Semiconductors, Consultants Bureau, New York, 1964.

85. p. 188 in ref. 81.

86. M. Silver and M.P. Shaw in ref. 81, p. 10-12.

87. T.D. Moustakas, Solid State Commum. 35(10), 745, (1980).

88. p. 189 in ref. 81.

89. p. 207 in ref. 81.

90. R.H. Bube, Photoconductivity of Solids, John Wiley and Sons, New York, 1960, p. 292.

91. H. Kallman and P. Mark, Phys Rev. 105, 1445, (1957).

92. M. Martini and T.A. McMath, Appl. Phys. Letters 17(9), 362, (1970).

93. P.E. Vanier, A.E. Delahoy and R.W. Griffith, J. Appl. Phys. 52(8), 5235, (1981).

94. W. Ruppel, J. Phys. Chem. Solids 22, 199, (1961).

95. C.A. Dussel and R.H. Bube, J. Appl. Phys. 37(7), 2797, (1966).

96. B.G. Streetman, Solid State Electronic Devices, Prentice-Hall, New Jersey, 1980, Editor N. Holonyak Jr.

97. T. Makino and H. Nakamura, Japan J. Appl. Phys. 17(10), 1897, (1978).

98. P.G. LeComber, W.E, Spear, and D. Allan, J. Non-Cryst. Solids 32, 1, (1979).

99. I.G. Austin, T.S. Nashashibi, T.M. Searle, P.G. LeComber, and W.E. Spear, J. Non-Cryst. Solids 32, 373, (1978).

100. M.H. Brodsky and D. Kaplan, J. Non-Cryst. Solids 32, 431, (1979).

101. T. Mizrah and D. Adler, J. Non-Cryst. Solids 22, 37, (1976).

102. B. Welber and M.H. Brodsky, Phys. Rev. B 16(8), 3660, (1977).

103. G.P. Srivastava, Phys. Stat Sol.(b) 85, K121, (1978).

104. N.J. Harrick, Phys. Rev. 103(5), 1173, (1956).

105. D.M. Bielle-Daspet, A.M. Johan, and F. Espioussas, Revue Phys. Appl. 15, 219 (1980).

106. H. Oheda, Solid State Commum. 33, 203, (1980).

107. N.G. Zhdanova, M.S. Kagan, S.G. Kalashnikov, R.A. Suris, and B.I. Fuks, Sov. Phys. Semicond. 13(12), 1387, (1979).

108. T.D. Moustakas, Phys. Rev. B 12(6), 2448, (1975).

109. R.H. Bube, G.A. Dussel, C. Ho, and L.D. Miller, J. Appl. Phys. 37(1), 21, (1966).

110. M. Martini and T.A. McMath, Nucl. Instr. and Methods 79, 259, (1970).

111. R.H. Bube, J. Phys. Chem. Solids 1, 234, (1957).

112. A.G. Milnes, Deep Inpurities in Semiconductors, John Wiley and Sons, New York, 1973.

113. W. Schockley, Electrons and Holes in Semiconductors, D. Van Nostrand Co., New Jersey, 1950.

114. E.M. Pell editor, Proc. of the 3rd Int. Conf. on Photoconductivity, Stanford Aug. 12-15, 1969, Pergamon Press, New York, 1971.

115. D. Dascalu, Electronic Processes in Unipolar Solid-State Devices, Abacus Press, Tunbridge Wells, Kent England, 1977.